

William Hughes

University of Birmingham



School of Biosciences

Cryptococcus neoformans phospholipase B and its influence on fungal cell morphology and a study into proteins proposed to be involved in C-di-GMP signalling and predation from *Bdellovibrio bacteriovorus* – Bd1483, Bd1996, Bd2538 and Bd3100

A research thesis submitted by:

William S. Hughes

As part of the requirement for the degree of
M.Res. in Molecular and Cellular Biology

Supervisors:

Prof. R.C. May

And

Dr. A.L. Lovering

UNIVERSITY OF
BIRMINGHAM

University of Birmingham Research Archive

e-theses repository

This unpublished thesis/dissertation is copyright of the author and/or third parties. The intellectual property rights of the author or third parties in respect of this work are as defined by The Copyright Designs and Patents Act 1988 or as modified by any successor legislation.

Any use made of information contained in this thesis/dissertation must be in accordance with that legislation and must be properly acknowledged. Further distribution or reproduction in any format is prohibited without the permission of the copyright holder.

William Hughes

Summary

The two following projects reported were undertaken as part of the masters of research in molecular and cellular biology. The first project takes a look at the emerging fungal pathogen *Cryptococcus neoformans* and how one of its known virulence factors, phospholipase B, controls cell morphology. We investigated the knockout strain and their changes in cell size and nuclear content, after phagocytosis by murine macrophages, along with other stresses, to investigate whether phospholipase B may be involved in the regulation of titan cells. Results from the study showed that during infection both nuclear content and whole cell size of the phospholipase B knockout *C. neoformans* strain increased over 18 hours, but further study will need to be undertaken to conclusively prove this observation. The second project changes kingdom and investigates bacterial cell signalling. *Bdellovibrio bacteriovorus* is a predatory bacterium, which is known to predate other Gram-negative bacteria. The molecular basis of how this bacterium goes from 'bite' to invasion has been shown to require Cyclic-di-guanosine monophosphate signalling. In this study we have attempted purification and structural analysis of 4 proteins that are believed to be involved in the initial bite and downstream signalling within *B. bacteriovorus* and have documented the outcome within.

William Hughes

Acknowledgements

Firstly, I would like to thank both of my supervisors for these projects, Robin and Andy. I am very lucky to have chosen two brilliantly happy, intelligent and caring supervisors who both have a passion for science and fun! As well as tolerance for my, sometimes, disjointed speech and appalling grammar (thanks for the help with that!).

I would also like to thank everyone in the HAPI and Lovering labs for all their support and kindness, once again I am so lucky to have worked with people as brilliant as my supervisors! This is followed by a special thanks to the people who looked after me during my time in the, Robbie and Ian. Cheers Robbie for getting me off to a running start on the Plb project and for being one of the most genuinely nice people I have ever met! Ian, the funniest and most vocally talented (not) post doc I have ever worked with. I hope we can grab some fishing trips and a few (many) more ales in the future! I have been so lucky (as I have previously mentioned many times) to meet all these amazing friends, who I will most definitely carry on annoying for the foreseeable future!

Next, I would like to thank all my mates, especially Dave, Sarah and Barlow for keeping me sane and in good spirits during the stressful write-up!

Of course I thank my entire family, especially my Mum, for all the support and help throughout all of my studies, trials and tribulations, and for my future studies. Without them, especially my Nan and Granddad buying me the great 'How your body works' series of books I would not be studying biology!

William Hughes

I would like to thank my partner and love of my life Hannah for her support as well, especially when I wake up with stress dreams about choking felt tip pen lids (need to cut down on the late night cheese I think)!

I cannot wait to carry on learning and loving what I do, for at least another 4 years but I am aiming for a few more years after that!

William Hughes

Abstract Project 1- *Cryptococcus neoformans* phospholipase B and its influence on fungal cell morphology

Cryptococcus neoformans is an opportunistic intracellular fungal pathogen and is a causative agent of Cryptococcal meningitis, which kills more than 500,000 a year. Phospholipase B (Plb1) has been implicated in host survival as well as resistance to macrophage uptake and particle killing. Plb1 knockout cells have been observed increasing in size once phagocytosed, these cells may possibly be precursors to titan cells, which are involved in modulating the host immune system. The aim of the project was to determine whether these enlarged Plb1 knockout cells are indeed precursors of titan cells through observations of certain markers specific for titan cells, such as increased nuclear content. Wild type, mutant and reconstituted cells were measured for cell size increase and for nuclear content in J774.1 macrophages and macrophage lysate. After 18 hours of infection within macrophages a greater proportion of the Plb1 knockouts showed an enlarged cell size and an increased amount of nuclear content, greater than that of the wild type and reconstituted strains. While it is not conclusive proof that these larger cells are true representatives of different morphologies it poses interesting questions about how Plb1 is involved in fungal cell morphology.

Keywords: *Cryptococcus neoformans*, Titan cells, Phospholipase B, Cell morphology, Flow cytometry

William Hughes

Abstract Project 2 - A study into proteins proposed to be involved in C-di-GMP

signalling and predation from *Bdellovibrio bacteriovorus* – Bd1483, Bd1996, Bd2538 and Bd3100.

Bdellovibrio bacteriovorus is a predatory Gram negative bacterium of the δ -proteobacteria, and known to predate on other Gram negative bacteria. It has been suggested that this could one day be used as a 'living antibiotic' but much of the underpinning biology of the bacterium remains to be uncovered. A pathway yet to be defined is the signal pathway from the initial 'bite' to invasion into the prey periplasm. This study attempts to uncover information regarding the mediators of the cyclic-di-guanosine monophosphate (C-di-GMP) signal that is required for invasion, as well as possible prey recognition proteins. The proteins studied were Bd1483, a von willebrand type A domain containing protein, Bd2538, a predicted lipid binding protein and Bd1996 and Bd3100, both of which contain PilZ domains, known to bind C-di-GMP, and domains that are predicted glycine-tyrosine-phenylalanine (GYF) domains, which are known to bind polyproline sequences. With the initial aim of expressing these proteins in *E. coli* and purifying them for structural and biochemical characterisation, we have shown that Bd1483 is soluble upon overexpression, and crystalizes readily. Bd1996 is soluble, but unstable when crystallization was attempted. Bd3100 is insoluble upon expression and Bd2538 remains to be cloned successfully.

Keywords: *Bdellovibrio bacteriovorus*, Cyclic-di-GMP, Invasion, Predation, Protein purification

William Hughes

William Hughes

Contents-Project 1

1. Introduction	1
1.1 The biology of <i>Cryptococcus</i> spp.....	2
1.1.1 <i>C. neoformans</i> reproduction.....	3
1.2 Epidemiology of <i>C. neoformans</i>	5
1.3 Host-pathogen interaction.....	5
1.3.1 Life with the macrophage.....	6
1.4 The treatment of cryptococcal infections.....	8
1.5 Virulence factors.....	9
1.5.1 Melanin	9
1.5.2 The cryptococcal polysaccharide capsule.....	10
1.6 Phospholipase B and its role in Cryptococcal virulence.....	11
1.7 Titan cells and their role in pathogenesis.....	15
1.8 Project aims	18
2. Materials and Methods	19
2.1 Strains, media and cultivation	19
2.2 Freezing down and thawing of J774 macrophage stocks.....	20
2.2.1 Freezing.....	20
2.2.2 Thawing of J774.1 cells.....	20
2.3 Preparation of coverslips.....	20
2.3.1 Immunostaining of coverslips.....	21
2.4 Infection of J774 macrophages with <i>C. neoformans</i>	21
2.4.1 Preparation of <i>C. neoformans</i> for infection.....	21
2.4.2 Macrophage preparation.....	22
2.4.3 Infection.....	22
2.4.4 Fixation of <i>C. neoformans</i> cells.....	22
2.4.5 Preparation of slides for imaging	23
2.4.6 Clumping of macrophage debris.....	23
2.5 Preparation of macrophage lysate.....	23
2.5.1 Measuring cell growth in macrophage lysate.....	24
2.6 Staining of the Cryptococcal cells.....	24
2.7 Imaging of Cryptococcal cells and measuring of cell diameter.....	25

William Hughes

2.8 Measuring cell growth and cell size under nutrient deficient conditions.	25
2.9 Data analysis of Cryptococcal cell diameter.	26
2.10 Flow cytometry of Cryptococcal cells after infection.	26
3. Results	27
3.1 Staining of the nuclear content of macrophage incubated cryptococci to observe whether larger cells were polyploidy.	27
3.1.1 After fixing and washing, cryptococcal cells recovered from macrophages were limited and often co-localized with macrophage debris.	27
3.1.2 The addition of poly-L-lysine to the lysate improved the amount of cells per coverslip but fungal cells co-localized with debris.	29
3.2 Does macrophage lysate induce an altered phenotype in Plb1 knockout <i>C. neoformans</i> ?	32
3.2.1 Plb1 knockout cells did not show a change in cell diameter after a 7 day incubation in SF-DMEM or macrophage lysate.	32
3.2.2 Over 7 days of incubation in macrophage lysate a significant number of Plb1 knockout cells were shown to have an altered cell morphologies.	33
3.2.3 Attempts at trying to determine whether the absence of extracellular Plb1 was responsible for the altered cell morphology in the Plb1 knockout strain were unsuccessful.	34
3.2.4 Plb1 knockout cells do not survive as well as wildtype/reconstituted Cryptococci in SF-DMEM and essence of macrophage.	40
3.3 Measuring cell growth and cell size in nutrient deficient conditions to investigate whether nutrient deficiency induces the large cell phenotype.	43
3.3.1 There is no increase in cell diameter in <i>C. neoformans</i> cells over 48 hours of nutrient deficiency.	43
3.4 Using flow cytometry to measure the fluorescence of nuclear content in cryptococcal cells after macrophage incubation.	47
3.4.1 After 18 hours of infection within J774 macrophages there is an increase in the proportion of cells with a greater diameter and more nuclear material in the Δ PLB1 strain.	47
4.0 Discussion	50
4.1 Hoechst staining of <i>C. neoformans</i> cells after infecting into macrophages	50
4.2 Macrophage lysate incubations.	52
4.3 Nutrient starvation	54
4.4 Flow cytometry.	54
5.0 Conclusions.	56
6.1 Supplementary figure 1	58

William Hughes

Bibliography	60
7.0 Introduction	71
7.1 Possible uses of <i>Bdellovibrio</i> spp.	72
7.2 The lifecycle of host dependent <i>B. bacteriovorus</i>	73
7.2.1 Host independent strains	76
7.3 Cyclic di-GMP signalling	79
7.3.1 A brief introduction	79
7.3.2 What is known of C-di-GMP signalling in <i>B. bacteriovorus</i> ?	81
7.4 Proteins of interest for the project.....	87
7.5 Project aims	93
8.0 Methods	93
8.1 Constructs used in the study	93
8.2 Preparation and storage of cell lines	94
8.2.1 The making of competent cells	94
8.3 Cloning of genes of interest.....	95
8.3.1 Primers and restriction free cloning.....	95
8.3.2 Transformation of competent bacterial strains	96
8.3.3 Colony PCR and sequencing	96
8.4 Expression of the genes of interest	97
8.4.1 Small scale expression test.....	97
8.4.3 Purification of over expressed protein.....	99
8.4.4 Buffer exchange and concentrating of target protein.....	100
8.4.5 Initial screening of target protein for crystallization	100
8.4.6 Custom screening of initial hits	101
8.4.6 Cryoprotection of Bd1483 crystals	102
9.0 Results	103
9.1 Expression and refolding of the suspected c-di-GMP binding protein, Bd3100.....	103
9.1.1 Test expression of Bd3100 showed it to be insoluble across all tested conditions.	103
9.1.2 On-column refolding of Bd3100 was unsuccessful.....	108
9.1.3 Shock refolding of Bd3100 proved more successful but the protein was not pure.	108
9.2 Expression, purification and crystallization of the predicted binding protein, Bd1483.	112

William Hughes

9.2.1 Cloning of bd1483 was successful.	112
9.2.2 Bd1483 was shown expresses and remain soluble in all expression conditions tested.	114
9.2.3 Scale up expression of Bd1483 was successful but purification was found to be difficult due to the protein binding weakly to the nickel loaded column.	117
9.2.4 Screening of conditions for Bd1483 crystallisation.	120
9.3 Cloning, expression, expression and crystallization studies of the suspected c-di-GMP binding protein, Bd1996.	129
9.3.1 Cloning of bd1996 proved successful.	129
9.3.2 Test expression of Bd1996 showed that Bd1996 was possibly insoluble upon overexpression.	131
9.3.3 Bd1996 expresses as a soluble protein upon scale up, but the stability of Bd1996 is dependant upon the buffer.	134
9.3.4 Crystallisation screens of Bd1996 yielded conditions that showed the beginnings of crystal formation, but these conditions could not be optimised.	139
9.4 Cloning of the suspected lipid binding protein, Bd2538.	141
9.4.1 Cloning and transformation of <i>bd2538</i> plasmids proved difficult with no plasmid constructs being produced.	141
10.0 Discussion.	146
10.1 Bd3100.	146
10.1.1 Bd3100 expression is insoluble even when expression is optimised.	146
10.1.2 Shock refolding of Bd3100 yields soluble, but unstable, protein.	147
10.1.3 Further work with Bd3100.	148
10.2 Bd1996.	149
10.2.1 Bd1996 expression is soluble but relatively unstable in the presence of imidazole.	149
10.2.2 Crystallization of Bd1996 gave hits but could not be optimised to give diffractable crystals and further study.	150
10.3 Bd2538.	150
10.3.1 Initial primers for <i>bd2538</i> hampered initial efforts at cloning but altered primers remedied this.	150
10.3.2 Cloning of <i>bd2538</i> could not be carried on past the initial plasmid.	151
10.4 Bd1483.	151
10.4.1 Bd1483 expression is soluble and it crystalizes readily with non-diffracting crystals.	151

William Hughes

10.4.2 Altering the initial screening conditions of Bd1483 in JCSG+ led to interesting results.	152
10.4.3 0.2M magnesium formate with 20% PEG 3350 gave geometric crystals but these could not be repeated, nor did they diffract.....	153
10.4.4 Further study of Bd1483	154
11.0 Conclusion	155
Bibliography	156

William Hughes

Abbreviations

Project one

5-FUTP – 5-fluorouracil triphosphate

5-FU – 5-fluorouracil

AmB – Amphotericin B

AIDS – Acquired immunodeficiency syndrome

BBB – Blood brain barrier

cAMP – Cyclic adenosine monophosphate

CD4 – Cluster of differentiation 4

CFU – Colony forming unit

CnPLB – *Cryptococcus neoformans* phospholipase B

CNS – Central nervous system

CSF – Cerebrospinal fluid

DAPI – 4',6-diamidino-2-phenylindole

DMEM – Dulbecco's Modified Eagle's Media

DMSO – Dimethyl sulfoxide

DNA – Deoxyribonucleic acid

EoM – Essence of Macrophage (Macrophage lysate)

William Hughes

FACS - Fluorescence-activated cell sorting

FSC – Forward scatter

GFP – Green fluorescent protein

GPI – Glycosylphosphatidylinositol

GXM – Galactoxylomannan

HIV – Human immunodeficiency virus

H99 – *Cryptococcus neoformans* wild type strain (serotype A)

LPL – Lysophospholipase

LPTA – lysophospholipase transacylase

MAb – Monoclonal antibody

MAT – Mating type locus

MOI – Multiplicity of infection

PBS – Phosphate buffered saline

PFA – Paraformaldehyde

PKA – Protein kinase A

PKC – Protein kinase C

Plb1 – Phospholipase B

Δ PLB1 – *Cryptococcus neoformans* Plb1 knockout – H99 parental strain

William Hughes

PLB1^{rec} – *Cryptococcus neoformans* Plb1 reconstituted – ΔPLB1 parental strain

PLL – Poly-L-lysine

PMA – Phorbol-12-myristate-13-acetate

PMBC - Peripheral blood mononuclear cells

RNA – Ribonucleic acid

SF-DMEM – Serum free - Dulbecco's modified Eagle's media

SDS – Sodium dodecyl sulphate

TNF-α – Tumour necrosis factor α

WHO – World health organization

YPD – Yeast peptone dextrose media

Project two

β-ME – β-mercaptoethanol

Arg – Arginine

Asp – Aspartate

C-di-GMP – Bis-(3'5')-cyclic dimeric guanosine monophosphate

CSP – Cold shock protein

Dgc – Diguanylyl cyclase

ER – Endoplasmic reticulum

William Hughes

FPLC – Fast protein liquid chromatography

Gln – Glutamine

Glu - Glutamate

GMP – Guanidine monophosphate

GndHCl – Guanidine hydrochloride

GST – Glutathione S-transferase

HD – Host dependent

HI – Host independent

hit – Host independent locus

IMAC – Immobilised metal affinity chromatography

IPTG – Isopropyl β -D-1-thiogalactopyranoside

Iso – Isoleucine

LB – Luria-Bertani media

Leu – Leucine

mRNA – Messenger ribonucleic acid

MWCO – Molecular weight cut off

NDSB – Non-Detergents Sulfobetaines

PBP4 – Penicillin binding protein 4

William Hughes

PCR – Polymerase chain reaction

PEG – Polyethylene glycol

PG – Peptidoglycan

pGpG - 5' – phosphoguanyl – (3'-5')- guanosine

PRS – Poly-proline rich sequences

PY – Peptone-yeast media

OD – Optical density

SDS-PAGE - Sodium dodecyl sulphate polyacrylamide gel electrophoresis

Thr – Threonine

TULIP – Tubular lipid binding domain

Tyr - Tyrosine

T4P – Type 4 pili

vWA – von Willebrand type A domain

William Hughes

Project 1

***Cryptococcus neoformans* phospholipase B** **and its influence on fungal cell morphology**

1. Introduction

Cryptococcus neoformans is an opportunistic fungal pathogen, and it is the primary cause of cryptococcosis in immunocompromised patients, which often leads to meningioencephalitis and death (figure 1) (Lin and Heitman 2006, Voelz and May 2010, Johnston and May 2013, Cogliati 2013). While normally a soil dwelling organism associated with guano and wooded areas, contact with the fungi is common. A study by Goldman *et al.*, 2001 found that a majority of children over the age of two tested seropositive for *C. neoformans* (Lin and Heitman 2006, Voelz and May 2010, Johnston and May 2013). While it is known that melanin and the polysaccharide capsule produced by the fungi contribute heavily to its virulence, there has been a recent surge in interest around the secreted lipid modifying enzyme phospholipase B (Plb) and how it influences the interaction between *C. neoformans* and the host's immune system (Ghannoum 2000, Steenbergen and Casadevall 2003, Santangelo *et al.*, 2004, Jones *et al.*, 2007 Wright *et al.*, 2007). Plb has been shown to be required for full virulence in *C. neoformans*, as well as normal cell function (Cox *et al.*, 2001). Deletion of the gene lowers the virulence of the pathogen in the murine model and reduces adhesion to cultured lung epithelium (Cox *et al.*, 2001, Ganendren *et al.*, 2006). Due to the relatively recent surge in HIV-infected individuals the amount of cryptococcosis cases have increased dramatically, leading to more deaths a year being attributed to cryptococcal meningitis than tuberculosis (WHO 2011, Park *et al.*, 2009). Due to this, there is a need to understand how this pathogen's virulence factors contribute to host interactions and disease. With the hopes of one day targeting these virulence factors to aid treatment of this disease.

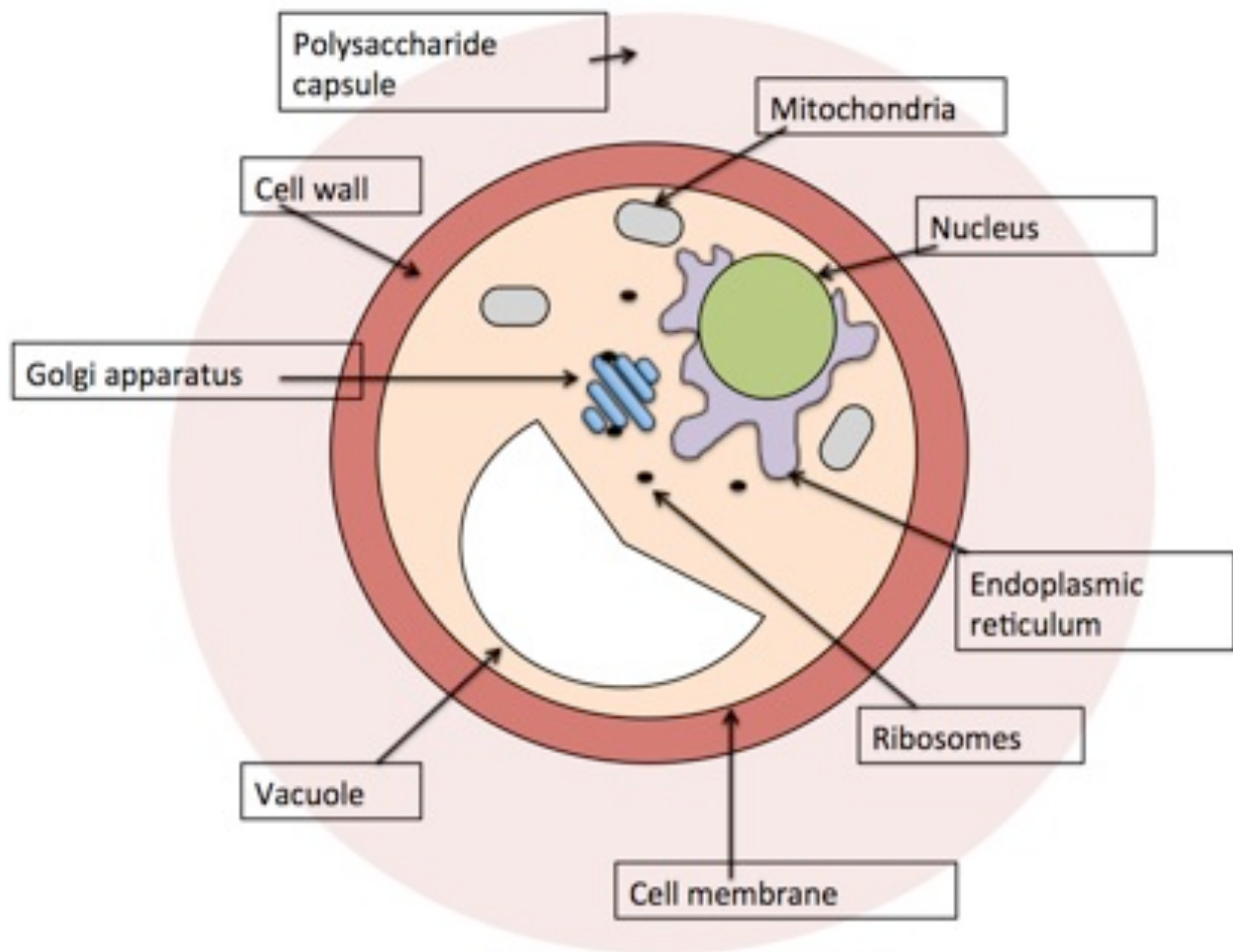


Figure 1. A cartoon diagram of a cryptococcal cell.

Adapted from Simmer, M., 2003.

1.1 The biology of *Cryptococcus* spp.

C. neoformans, shown in figure 1, is a yeast belonging to the basidiomycetes family of fungi. While it is a saprophyte, normally, it has the ability to infect humans whose immune systems are compromised (Ruiz *et al.*, 1989, Voelz *et al.*, 2010, Johnston and May 2013). While it has not evolved to be a pathogen of mammals it is believed to have evolved the ability to survive within predatory amoebas, which have similarities to mammalian phagocytic cells (Steenbergen and Casadevall 2001, Steenbergen and Casadevall 2003 Chrisman *et al.*, 2010 Chrisman *et al* 2011).

Historically, cryptococcosis was thought to be caused by a single agent, *C. neoformans*, but recently 5 serotypes have been identified through capsular agglutination to differentiate between the causative agents (Dromer *et al.*, 1993, Lin and Heitman 2006, Voelz and May 2010). Of these strains A, D and A/D belong to the species *C. neoformans*, while B and C (once thought to be of the *C. neoformans* species) have been accepted as a different species *C. gattii*, which is associated with infection of immunocompetent patients (Lin and Heitman 2006, Byrnes *et al.*, 2010, Voelz and May 2010).

1.1.1 *C. neoformans* reproduction

C. neoformans mating types are defined by the mating type locus (MAT), which is found in many fungi (Metin *et al.*, 2010). In clinical isolates the α sex of *C. neoformans* predominates, and undergoes asexual budding, rather than sexual reproduction with the 'a' sex, both *in vitro* and in the host (Lin *et al.*, 2005, Metin *et al.*, 2010). *C. neoformans* contains a second mating type **a**. When nutrients become limiting and starvation occurs the two mating types secrete pheromones then fuse and sexual reproduction occurs (figure 2) (Lin *et al.* 2006). The nuclei of the fused cells do not yet recombine and a dikaryon filament then grows. Basidia form at the tips and this is where nuclear fusion between the two mating type nuclei occurs (figure 2) (Nielsen *et al.*, 2003, Lin *et al.*, 2006, Kronstad *et al.*, 2011.). Meiosis and mitosis occur at the basidia forming many haploid basidiospores along 4 distinctive chains (Lin *et al.*, 2005) (figure 2). These basidiospores are then released into the environment, and are thought to be the main route of infection in humans (Nielsen *et al.*, 2003, Lin *et al.*, 2005). Spores then germinate into haploid yeast cells. Although this mating has been observed under laboratory conditions there have been

questions on how a population that has a unisexual majority could maintain a sexual reproduction cycle in nature. Lin *et al.*, 2005 put forward a mechanism, where-by two cells of the same mating type (α) could sexually reproduce by 'fruiting'. So, when under nutrient starvation the fusion of *C. neoformans* of the same mating type, monokaryotic diploid hyphae form (figure 2) (Lin *et al.*, 2005). This leads to basidia formation, sporulation and release of spores, similar to the sexual reproduction cycle between different mating types (Lin *et al* 2005, Metin *et al* 2010).

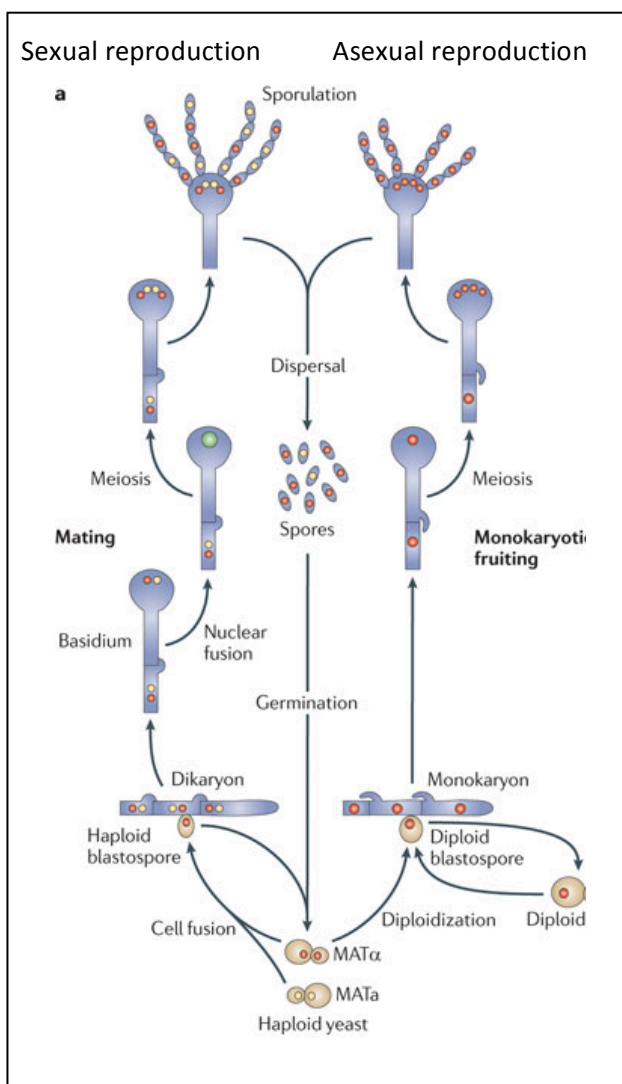


Figure 2. Sexual and asexual reproduction in *C. neoformans*

In sexual reproduction spores cell of different mating types fuse to form a dikaryon filament. At the tip of the filament, basidium, nuclear fusion and meiosis occur. Haploid basidiospores form along 4 chains, which are then dispersed into the environment to germinate into haploid cells.

Asexual reproduction, monokaryotic mating, occurs in a similar mechanism but with a diploid monokaryon filament forming which leads to meiosis in the basidium and sporulation, similar to sexual reproduction.

Reproduced from Kronstad *et al.*, 2011.

1.2 Epidemiology of *C. neoformans*

Along with other infections related to HIV immunocompromisation, *C. neoformans* has had a recent emergence as a major pathogen of immunocompromised patients (Park *et al.*, 2009). Due to its association with patients infected with HIV/AIDS it is not surprising that sub-Saharan Africa (SSA) shows a high incidence of cryptococcosis, but what may seem more surprising is that in 2006 deaths attributed to cryptococcal meningitis were greater than that of tuberculosis (Park *et al* 2009). In 2011 the world health organization (WHO) attributed 500,000 deaths per year to cryptococcal meningitis in SSA. While in SSA, up to 65% of HIV related fatalities belong to cryptococcal infection, which is staggeringly high when compared to other areas of the world where it causes around 20% of HIV-related deaths (Park *et al.*, 2009).

While *C. neoformans* is associated with regions of high HIV-related burden, the recently defined species, *C. gattii*, is not. *C. gattii* is an emerging pathogen of immunocompetent patients, with most cases occurring around Papua New Guinea and Australia; typically tropical and sub-tropical regions and the fungi are found to be associated with eucalyptus trees (Voelz *et al.*, 2010). In 1999, there was an outbreak of a hyper-virulent strain, known to replicate within macrophages. Since the outbreak in 1999 over 400 people across north western Canada and America have been infected with this virulent *C. gattii* strain (Byrnes *et al.*, 2003, Voelz *et al.*, 2013).

1.3 Host-pathogen interaction

Infection with *C. neoformans* normally occurs through inhalation of spores from the environment, leading to an initial interaction with the host immune system in the lungs (Goldman *et al.*, 1994, Eisenmann *et al.*, 2007). In the lungs the primary interaction with the host immune system is with the alveolar macrophages, which are

recruited when infection is detected (Eisenmann *et al.*, 2007, Kechichian *et al.*, 2007). Normally, pathogens are detected by the macrophages through opsonic and non-opsonic receptors found on the macrophage surface, but *C. neoformans* generally avoids detection by non-opsonic receptors and is detected by opsonic receptors, including Fc receptor and CR3 receptors, which bind to opsonins deposited on the surface of the pathogen and enhance phagocytic uptake (Voelz and May 2010, Johnston and May 2013). The capsule has been implicated in preventing uptake, by masking the fungal cell wall from macrophage mannose receptors, as well as inactivating C3b, an opsonin deposited on the fungal surface (Kozel and Pfrommer 1986, Voelz and May 2010). Along with the capsule, anti-phagocytic protein 1 (App1) blocks complement receptor mediated phagocytosis by binding directly with the CR3 and CR2 receptors preventing them from binding to the deposited opsonins (Stano *et al.*, 2009).

1.3.1 Life with the macrophage

Once a particle (or pathogen) has been phagocytosed, a series of events leads to the degradation of the particle in the phagosome. This normally occurs through a sequential maturation of the phagosome, with active compounds being sequestered to the phagosome, which are involved in killing and degrading foreign objects. *C. neoformans*, as well as other intracellular pathogens, have evolved ways of subverting this maturation process (Tucker and Casadevall 2002, May and Johnston 2013, Smith and May 2013). Certain pathogens, namely *Mycobacterium tuberculosis*, have evolved ways to subvert phagosome maturation by evolving with humans over millennia; *C. neoformans* (and related species) appear to have not evolved this trait through co-evolution with humans. It is believed that this ability to subvert

phagosome maturation has come about through evolutionary interactions with soil amoeba (Steenbergen *et al.*, 2001, Hershkovitz *et al.*, 2009, Chrismann *et al.*, 2010, Chrismann *et al.*, 2011). Acanthamoeba are known to predate bacteria and fungi in the soil, and it has been shown that *C. neoformans* has strategies to prevent degradation and escape after being engulfed (Chrismann *et al.*, 2010). This predation has also been implicated in maintenance of pathogenicity in the environment, with exposure to the predatory amoeba *Dictyoselium discoideum* enhancing virulence in a mammalian host (Steenbergen *et al.*, 2003).

As with *M. tuberculosis*, if the infection cannot be handled at the initial site of infection, the immune system changes from destruction of the pathogen to containment, leading to latent cryptococcal disease (Shibuya *et al.*, 2005). This containment is similar to tubercular containment and is also orchestrated by CD4+ T-helper cells and requires alveolar macrophages (Hill *et al.*, 1992). When the immune system becomes compromised and weakened this containment breaks down leading to reactivation and possible dissemination of disease to the CNS (Shibuya *et al.*, 2005).

Dissemination of the cryptococci to the CNS is believed to be due to its ability to persist and replicate within host macrophages (Eisenmann *et al.*, 2007, Johnston and May 2013, Smith and May 2013). TNF- α has been implicated in prevention of dissemination of cryptococci, and *C. neoformans* is known to modulate host TNF- α (Chaka *et al.*, 1997, Eisenmann *et al.*, 2007). The 'Trojan horse model' of cryptococcal dissemination describes a scenario whereby survival within the macrophage allows cryptococci to evade the immune system and non-lytically expel (vomocytosis) from the circulating macrophages, once they pass near the brain (Ma

et al., 2006, Eisenmann *et al.*, 2007). The reason and mechanism of this neurotropism has yet to be discovered, but it is suggested that *C. neoformans*' ability to use neuronal transmitters, such as epinephrine to produce melanin, may be a reason for this tropism to the CNS, but this still remains unproven (Casadevall *et al.*, 2000, Steenbergen and Casadevall 2003, Casadevall 2010). *C. neoformans* must first cross the blood brain barrier (BBB) to infect the brain. It has been proposed that while it is hidden within the circulating macrophage, when the macrophage passes through the BBB cryptococci can expel from the macrophage and enter the brain, but *in vitro* data suggests *C. neoformans* can pass through the BBB without the assistance of macrophages, via transcytosis (Casadevall 2010, Johnston and May 2013, Eisenmann *et al* 2007, Chang *et al* 2004).

1.4 The treatment of cryptococcal infections

Treatment of cryptococcosis depends upon various factors that are dependent on the patient's specific circumstances (Perfect *et al.*, 2010). Recent guidelines suggest that for patients with a HIV co-infection, or other immunosuppressive conditions, a combinational drug approach should be taken, similar to that of the combinational therapy used in the treatment of tuberculosis (Perfect *et al.*, 2010). An induction therapy of amphotericin B and flucytosine is then followed by a consolidation therapy with fluconazole. Therapy can up to 12 months, but this is dependent upon the patients' personal circumstances (Perfect *et al.*, 2010). Amphotericin B is known to interact with fungal ergosterol and is believed to introduce pores into the fungal cell membrane, although this mechanism of action had been disputed (Ghannoum and Rice 1999). Flucytosine is a pro-drug and requires being taken up by susceptible

fungal cells (Vermes *et al.*, 2000). Once deaminated into 5-fluorouracil (5-FU), the nucleotide analogue 5-fluorouracil triphosphate (5-FUTP) is incorporated into fungal RNA in the place of uracil and inhibits protein synthesis (Vermes *et al.*, 2000). One metabolite of 5-FU also inhibits thymine production halting DNA synthesis as well (Vermes *et al.*, 2000). Fluconazole, along with other azoles, are believed to affect ergosterol production in fungi, by inhibiting the heme-protein responsible for the demethylation of ergosterol precursors (Ghannoum and Rice 1999). In *C. neoformans* it has also been found that fluconazole inhibits reduction of obtusifolinone. This lack of ergosterol and variation in other related sterols leads to a loss in membrane stability and changing the overall membrane structure (Ghannoum and Rice 1999). Drug resistance has not been a major problem, but relapse during maintenance therapy has been shown to be due to fluconazole resistance in the cryptococci. This resistance has been associated with a disomy of chromosome 1, containing the ERG11 gene (Sionov *et al* 2010, Sionov *et al* 2013). Resistance to amphotericin B is associated with melanin production, possibly depositing it in the cell wall away from the membrane (Ikeda *et al* 2003).

1.5 Virulence factors

1.5.1 Melanin

Melanin-like pigments are used by many organisms as protective compounds; in humans it is involved in protecting the skin from ultraviolet radiation, while in cryptococci it is known to factor into virulence (Casadevall *et al.*, 2000, Ikeda *et al.*, 2003). In *C. neoformans* melanin has been shown to be produced *in vivo* and has association with a resistance to immune function, as well as melanised cells being found in human brain tissue, giving possible reasoning for *C. neoformans*

neurotropism (Williamson *et al.*, 1998, Steenbergen and Casadevall, 2003). Melanin is produced by the cell wall associated laccase enzyme and requires exogenous substrate such as the catecholamines (dopamine), unlike other fungi that can produce these pigments without external substrate (Steenbergen and Casadevall, 2003). Melanised cryptococci show reduced susceptibility to oxidative stress and antimicrobial peptides produced by alveolar macrophages (Doering *et al.*, 1999, Ikeda *et al.*, 2003). Melanin is also implicated in a resistance to antifungal agents, such as amphotericin B (Wang *et al.*, 1994). It has been suggested that the laccase enzyme, required for the polymerization of melanin, may be involved in reduction of hydroxyl free radicals, employed by alveolar macrophages in oxidative bursts (Williamson *et al* 1998, Casadevall *et al* 2000, Steenbergen and Casadevall 2003).

1.5.2 The cryptococcal polysaccharide capsule

The capsule of *C. neoformans* has been shown to be one of the most important virulence factors for the pathogen and as such it has been researched extensively. It is composed of glucuronoxylomannan (GXM), galactoxylomannan, and dispersed with mannoproteins. Deletion of one of the 4 capsular genes CAP10, CAP59, CAP60 and CAP64, leads to abolishment of capsular production and abolition of virulence in the murine model (Kwon-Chung 1998, Steenbergen and Casadevall 2003, O'Meara and Alspaugh 2012). *In vitro*, the diameter of the capsule is relatively modest (4-8um) but upon infection this capsule increases in diameter. This has led to the conclusion that the capsule is required *in vivo* for virulence, the fact that unencapsulated strains of *C. neoformans* are avirulent proves this (O'Meara and Alspaugh 2012). The capsule prevents phagocytosis by preventing recognition of fungal cell wall components by phagocytic receptors, such as dectin-1 receptor and mannose

receptor, whose ligands (beta-glucans and mannose respectively) are found on the fungal cell wall (Johnston and May 2013). Once the fungi have crossed the BBB, GXM found in the cerebrospinal fluid has been associated with increasing cranial pressure, by disturbing water balance, leading to the tell tale symptoms such as blurred vision and headaches associated with fungal meningitis (Eisenmann *et al.*, 2007).

1.6 Phospholipase B and its role in Cryptococcal virulence.

Phospholipase B is part of a large family of phospholipases that are found ubiquitously, and function from initiators of lipid signalling to virulence factors for pathogens, such as *Pseudomonas aeruginosa* and *Candida albicans* (Ghannoum 2000, Steenbergen and Casadevall 2003). Phospholipases act upon glycerolphospholipids, and have distinct activities. The phospholipase B enzyme is characterised by hydrolase activity against the sn-1 and sn-2 linkages found on glycerolphospholipids, the main component of plasma membranes (phospholipase A and lysophospholipase) (figure 3A) (Chen *et al.*, 1997, Cox *et al.*, 2001, Jones *et al.*, 2007). While *C. neoformans* Plb (CnPlb) maintains this characterised activity, a third activity is observed, lysophospholipase transacylase (LPTA) (Chen *et al.*, 1997, Cox *et al.*, 2001). Whereby the enzyme can catalyse the acylation of free fatty acids to lysophospholipids, allowing PLB to degrade and build phospholipids (figure 3A) (Chen *et al.*, 1997, Cox *et al.*, 2001). While it has been suggested that Plb1 contains 2 active sites that facilitate the wide range of activities it possesses, Jones *et al.*, 2007 showed that CnPlb1 contains one active site within a single domain (PLAC2) that can accommodate all three activities, possibly due to the loss of an occluding

cap region involved in substrate specificity in the catalytically similar phospholipase A₂, found in *C. albicans* (Jones *et al.*, 2007) (figure 3b).

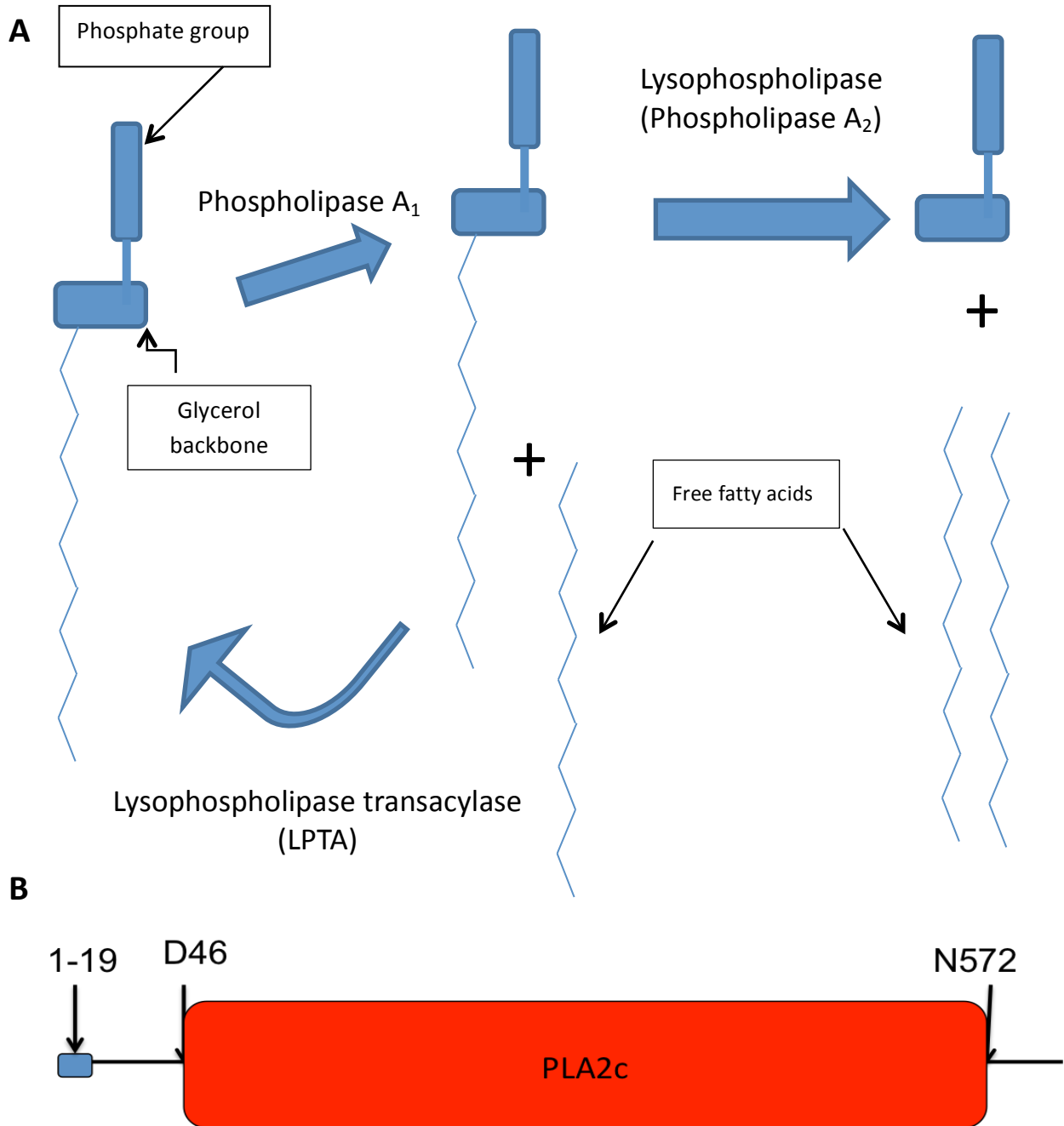


Figure 3. A schematic diagram of *C. neoformans* Phospholipase B activity.

A) Phospholipase B has three activities. Its first activity is its phospholipase A₁ activity where one on the fatty acid chains is cleaved from the phospholipid at the ester linkage (sn1/2) to the glycerol backbone to form a lysophospholipid. This lysophospholipid can then have the remaining fatty acid chain cleaved at the sn-2 ester linkage by the Plb1 lysophospholipase activity (phospholipase A₂). A third activity has been characterised, in *C. neoformans* phospholipase, lysophospholipase transacylase (LPTA). The LPTA activity of Plb1 catalyses the acylation of free fatty acids, to lysophospholipids.

B) The domain diagram of *C. neoformans* phospholipase B. The region found between amino acid 1-19 contains a signal sequence required for its transport and subsequent lipidation. The PLA_{2c} domain of Plb1 is responsible for all 3 activities that Plb1 has been attributed to it, phospholipase A, lysophospholipase and lysophospholipase transacylase and is found between aspartate 46 and asparagine 572.

Phospholipase B has recently been implicated in the virulence of certain fungal pathogens, such as *Candida albicans* and *C. neoformans*. In *C. neoformans* Plb1 has been implicated in host survival, adhesion to the host, dissemination across the BBB, tissue invasion, lipid metabolism within the host, and maintaining membrane stability and cell wall integrity in the fungi (Ganendren *et al.*, 2006, Siafakas *et al* 2007, Wright *et al* 2007, Cheyakulkeeree *et al.*, 2011, Maruvada *et al.*, 2012). Plb1 is sequestered to the cell wall by a glycosylphosphatidylinositol anchor and this anchor is required for its secretion through the Sec pathway via the phosphatidylinositol transfer protein Sec14-1 (Djordjevic *et al.*, 2005, Siafakis *et al.*, 2007,

Cheyakulkeeree *et al.*, 2011). Knockout strains of Sec14-1 are not deleterious to *C. neoformans*, unlike other fungi; they do show a decreased virulence that is similar to the Plb1 knockouts and also lack extracellular phospholipase B activity (Cheyakulkeeree *et al.*, 2011). In strains shown to produce larger amounts of extracellular phospholipase activity the converse is seen, showing increased virulence and quicker mortality in the murine model of infection, pointing toward an extracellular function of Plb1 being responsible for virulence *in vivo*. CnPlb has been shown to be covalently bound to the β -1,6-linked glucans of the cell wall, and release of CnPlb1 is mediated by β -1,6 glucanases encoded by *C. neoformans* (Siafakas *et al.*, 2007). At increased temperatures Plb1 activity increases and the amount of Plb1 associated with the cell wall also increases (Siafakas *et al* 2007).

Knockout studies on Plb1 show a decrease in virulence associated with an increase in clearance by the macrophage, reduced vomocytosis, and a decrease in dissemination to the brain in the mouse model (Cheyakulkeeree *et al.*, 2011). This has led to speculation that exported CnPlb is involved in survival within the macrophage, possibly due to degradation of the host phagolysosomal membrane, or by providing lipids to the cryptococcal cells for metabolism (Wright *et al.*, 2007). Plb1 knockout strains have been associated with a decrease in cell wall integrity, showing a lower capability to withstand stresses from detergents, such as SDS, that disrupt the membrane and interfere with protein folding (Siafakas *et al.*, 2007). CnPlb has been shown to have a high affinity for dipalmitoyl phosphatidylcholine, a constituent of lung surfactant (involved in alveolar maintenance), phosphoglycerolipids, involved in preventing injury and infection in the lungs, and dioleoyl phosphatidylcholine, a component of macrophage membranes. (Griese 1999, Wright *et al.*, 2007). *C.*

neoformans Plb1 has been associated with utilisation of host lipids. A report by Wright *et al.*, 2007 showed that Plb1 is required for metabolism of radiolabelled host macrophage lipids, these fatty acids are then utilised in eicosanoid production, which is associated with melanin production. Plb1 was also implicated in subverting the macrophages' response to *C. neoformans*, by utilising macrophage derived arachidonate, which is involved in activation of antimicrobial killing mechanisms in the macrophage, such as nitric oxide production (Ryoyama *et al.*, 1993).

Recent data (unpublished) from collaborators appears to show that a GFP tagged CnPLB1 is sequestered to the membrane, and localises at foci that could be lipids rafts, which Plb1 has been suggested to localize within (Siafakas *et al.*, 2006). As well as localising in foci across the cell membrane, the tagged Plb1 appears to localise at the site of budding, possibly implicating Plb1 in cell division.

1.7 Titan cells and their role in pathogenesis.

One of the striking features about Cryptococcal infection is the increase in cell size of a sub-population of fungal cells during infection (Okagaki *et al.*, 2010, Okagaki and Nielsen, 2012). Normally, *C. neoformans* has a diameter of 4-8um, but 24 hours after the initial infection event roughly 10-20% of cells have been found to reach up to 900 times larger in volume than normal (figure 4) (Zaragoza *et al.*, 2010). While *C. neoformans* has been shown to increase the size of the polysaccharide capsule during infection, so called titans cells have tell tale traits that differentiates them from *C. neoformans* cells with increased capsule thickness (figure 4). They exhibit a highly cross linked polysaccharide capsule, which is both resistant to DMSO treatment and γ -radiation, both of which strip the capsule off of normal sized cells grown *in vitro* (Zaragoza *et al.*, 2010). To add to this the cell wall of the cells increases in thickness

from 50-100nm to 2-3µm. The appearances of vesicles that stain with the vacuole specific marker MDY-64 have been seen in titan cells, either as a single large vesicle or many small ones (Zaragoza *et al.*, 2010). Titan cells have also been shown to have an increase in nuclear content, roughly reaching around 16 times the amount of DNA found in cells grown *in vitro*, while other studies have found this to range from 4-64 polyploidy (Zaragoza *et al.*, 2010). This increase in DNA content has been suggested to be required for the maintenance of the modified cell wall found in titan cells (Zaragoza *et al.*, 2010). These characteristics of an increased cell size and polyploidy have been associated with defects in cell cycle, causing endoreduplication in *Saccharomyces cerevisiae* (Okagaki *et al.*, 2011). In *C. neoformans* titan cells produce normal sized and presumptively haploid offspring (Okagaki and Nielsen, 2012).

The production of titan cells have been shown to increase virulence in the mouse infection model, with mice infected with FACS purified titan cells showing a higher fungal burden when compared to the wild-type (Crabtree *et al.*, 2012). As well as this, *C. neoformans* strains that have titan cell production knocked out show decreased virulence and mortality in the mouse model, when compared to the wild-type strains (Okagaki and Nielsen, 2012). Virulence is restored in the knockout cells when they are reconstituted with gpr4/gpr5 receptors (Okagaki and Nielsen, 2012). Titan cells have been implicated in promoting early pulmonary survival as well as increasing dissemination to the CNS and inhibiting phagocytosis of normal size cells (Zaragoza *et al.*, 2010, Okagaki and Nielsen, 2012). This protection against phagocytosis is not solely due to the size of the titan cells conferring resistance, as latex beads of a similar size to titan cells, 30 µm, do not provide a protection to phagocytosis of normal sized *C. neoformans*. This immunomodulatory function against the host

immune system is linked with the large vesicular compartments seen in titan cells that have been shown to contain immunomodulatory compounds that affect phagocyte function and may be responsible for this protective effect (Oliviera *et al* 2010, Okagaki and Nielsen, 2012).

While there is no conclusive evidence as to how titan cells form, formation has been shown to require specific cellular signalling. Two receptors found on the cryptococcal surface, GPR5 and Ste3a, modulate titan cell formation, both acting on the PKA/cAMP pathways (which controls other *C. neoformans* virulence factors), and activate the transcription factor, RIM101. RIM101 homologues play important roles in virulence in pathogenic fungi (Okagaki *et al* 2011, Okagaki and Nielsen 2012, Zaragoza and Nielsen 2013). While the ligand for GPR5 has not been discovered, Ste3a, the pheromone receptor, has been shown to enhance titan cell formation in the less virulent MATa sex, with up to 40% of cells being of titan cell morphology in co-infections with both cryptococcal mating types (Okagaki *et al* 2011). Although other receptors have not been ruled out in affecting the production of titan cells, the two discussed receptors, in particular GPR5, play important roles (Okagaki and Nielsen 2012, Okagaki *et al* 2011).

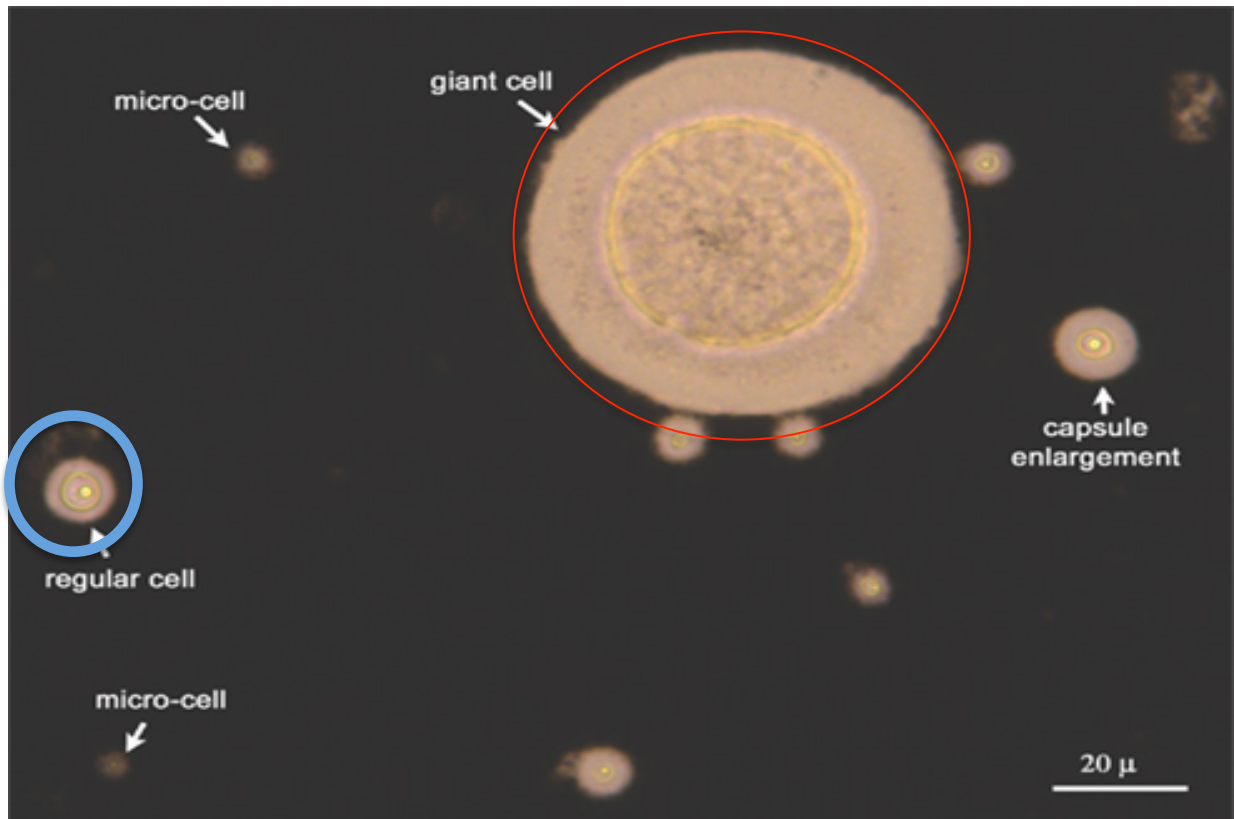


Figure 4. An India Ink stained imaged of cryptococci from an infected mouse lung.

As the image shows it can be seen that the 'giant cells' (another term for titan cell) (circled red), are massive when compared to other 'regular' cryptococci (circled blue) and have a large increase in polysaccharide capsule which does not stain with India Ink.

Figure reproduced from Zaragoza, 2011.

1.8 Project aims

Previous studies within the group have shown that cell diameter, and therefore cell size, increases in Plb1 knockout cells, when phagocytosed by J774.1 macrophages. These cells do not appear to reach the same size as titan cells do *in vivo*, but they may be precursors of titan cells. To study whether these large cells are the beginning

of titan cell formation, we intended to use the known markers of titan cells, cell size and nuclear content, to study this distinct morphology. From this we would hopefully be able to determine whether these cells carry markers for titan cells and implicate Plb1 in titan cell formation and fungal cell morphology.

2. Materials and Methods

2.1 Strains, media and cultivation

During the study *C. neoformans* var. *grubii* strains H99, Δ Plb1, Δ Plb1:Plb1 reconstituted, referenced as PLB1^{rec}, were used. Both mutant strains came from a H99 parent, and produced through methods described by Cox *et al.*, 2001. *C. neoformans* stocks were stored at -80°C, thawed and streaked onto yeast extract/peptone/D-glucose (YPD) agar (1% yeast extract, 2% peptone and 2% D-glucose) and incubated at 25°C for 48 hours. Plates were then stored at 4°C until required. Overnight cultures of 2mL YPD broth were seeded with colonies picked from the stored YPD plates, incubated at 25°C and rotated 25 rpm. J774.1 macrophage cells were used throughout the experiment; cells were cultured in Dulbecco's Modified Eagle's Media (DMEM), which had been supplemented with 10% (50mL) live foetal bovine serum (FBS), 1% (5mL, 2mM) 200mM L-glutamine and 1% (5mL) 10,000 units penicillin/ 10 mg streptomycin. J774.1's were maintained in an incubator at 37°C in 5% CO₂ during the study.

2.2 Freezing down and thawing of J774 macrophage stocks.

2.2.1 Freezing

Media for freezing down stocks of J774 cells consisted of 50% FBS, 40% complete DMEM and 10% dimethyl sulfoxide (DMSO). This was filter sterilised (0.2µm) to remove possible contaminants. 8 flasks of confluent J774 cells were scraped into fresh complete DMEM. The cells were spun at 1000xg for 7 minutes to sediment cells. The supernatant was discarded, and cells resuspended in the freezing media (5ml for every flask). The suspension was aliquoted into 1mL cryovials, frozen at -80°C for 24 hours, and then moved into liquid nitrogen for prolonged storage.

2.2.2 Thawing of J774.1 cells

Once removed from liquid nitrogen storage, cells were defrosted in a water bath at 37°C. Once defrosted, the 1mL aliquots were added to 9mL complete DMEM and centrifuged at 1000xg for 7 minutes. Pellets were resuspended in 15mL of DMEM and incubated in T75 culture flasks overnight at 37°C. 24 hours after thawing DMEM was replaced with fresh media, or passaged if needed.

2.3 Preparation of coverslips

Coverslips were treated with 20mL of nitric acid, and left for 10 minutes at room temperature. Nitric acid was poured off and coverslips dowsed in dH₂O. Coverslips were then washed with dH₂O three times. Ethanol was used to wash the coverslips a further 2 times, and then coverslips stored in ethanol at room temperature until needed.

2.3.1 Immunostaining of coverslips

Prepared coverslips were removed from the ethanol and allowed to dry for 30 minutes. Dried coverslips were incubated in 200 μ L 0.1% (w/v) Poly-L-lysine (PLL) (Sigma Aldrich) for 1 hour at room temperature. Coverslips were then washed with dH₂O to remove non-bound poly-L-lysine. Aliquots of the GXM specific monoclonal antibody 18B7 (kindly provided by Arturo Casadevall) were diluted 1 in 5000 and 15 μ L pipetted on to parafilm. Poly-L-lysine treated coverslips were placed poly-L-lysine treated side down, in contact with the 15 μ L of 18B7. The coverslips were then incubated at room temperature for 1 hour. After incubation PLL-18B7 treated coverslips were washed 3 times in dH₂O, covered in phosphate buffered saline (PBS) and stored at 4°C.

2.4 Infection of J774.1 macrophages with *C. neoformans*

2.4.1 Preparation of *C. neoformans* for infection

One day prior to infection, overnight cultures of *C. neoformans* strains H99, Δ PLB1, PLB1^{rec}, were cultured as previously described (2.1). On the day of infection overnight cultures were vortexed to ensure the cells were evenly suspended and 1mL of culture was removed from each culture tube. The 1mL samples were spun at 8000xg for 3 minutes. The supernatant was discarded and pellets resuspended in 1mL PBS. This was repeated 3 times and *C. neoformans* cells resuspended in a final volume of 1mL of PBS. 1 in 10 dilutions of *C. neoformans* cells were counted on a haemocytometer and dilutions of 1x10⁶/100 μ L were made. *C. neoformans* cells were then opsonised with 0.1uL/100 μ L of 18B7 monoclonal antibodies, and incubated at room temperature for an hour on a rotator.

2.4.2 Macrophage preparation

Macrophages were also prepared on the day prior to the infection. J774.1 cells were scraped from a confluent flask and the number of cells was counted with a haemocytometer. J774.1 cells were then diluted to 1×10^5 cells/mL into complete DMEM. 1mL of the diluted culture was used to seed wells of a 24 well plate (each well was seeded with 1×10^5 cells) and incubated overnight at 37°C, 5% CO₂. 133ng/mL of phorbol-12-myristate-13-acetate (PMA) was used to activate J774.1 cells via the PKC pathway, increasing the phagocytic activity. Complete DMEM was removed from J774.1 cells plated the previous day, and replaced with 1mL of serum-free DMEM (SF-DMEM) and 15µL of the 10µg/L PMA dilution. The cells were incubated at 37°C for 45 minutes and the SF-DMEM removed and replaced with 1mL SF-DMEM.

2.4.3 Infection of J774.1 macrophages

J774.1 cells were infected *C. neoformans* at a multiplicity of infection (MOI) of 10 and incubated for 2 hours at 37°C, 5% CO₂ to allow for phagocytosis. After 2 hours, media was removed from each well, and then washed and agitated 3 times with 1ml PBS to remove PMA and non-phagocytosed *C. neoformans*. After the washes 1mL of SF-DMEM was added and cells incubated for a further 18 hours.

2.4.4 Fixation of *C. neoformans* cells

0 hour wells were washed and then the macrophages were lysed with 200µL dH₂O for 20 minutes. *C. neoformans* cells and J774.1 debris was scraped off the plate bottom and aliquoted into microcentrifuge tubes. Wells were washed with 200µL PBS and aliquoted into the 200µL dH₂O. *C. neoformans* cells were centrifuged at 8000xg for 3 minutes, the supernatant was discarded and cells were resuspended in 400µL

paraformaldehyde (PFA) to fix the cells. Cells were incubated for 10 minutes in PFA and then washed 3 times in 400 μ L PBS, centrifuging at 8000xg for 3 minutes in between washes. Cells were finally resuspended in 400 μ L PBS. At the 18 hour time point, cells were treated in the same manner and fixed as described previously. If cells were not imaged on the day of fixing they were stored at 4°C until imaging.

2.4.5 Preparation of slides for imaging

For initial imaging, 15 μ L of sample was pipetted onto a glass slide and a coverslip placed on top. When using immunostained coverslips, fixed lysates were pipetted onto the immunostained side of the coverslip and centrifuged at 1000xg for 10 minutes and incubated for 1 hour. When lysates have not been fixed, samples are placed upon the immunostained coverslip and centrifuged as before. After centrifugation, lysates are fixed to the coverslip with 400 μ L PFA and incubated for 15 minutes before washing with PBS.

2.4.6 Clumping of macrophage debris

To remove macrophage debris from the lysate 0.1% PLL was added to the lysate, to increase clumping. Lysates were placed upon immunostained coverslips and were fixed and treated as before (2.4.5).

2.5 Preparation of macrophage lysate

Non-activated macrophage lysate (referred as essence of macrophage (EoM) in results) was collected as so. J774.1 cells were scraped from a confluent culture in 10mL SF-DMEM. For activated macrophage lysate J774.1 cells were activated with SF-DMEM supplemented 133ng/mL PMA in the culture flasks for 45 minutes prior to lysis. Cells were lysed through sonication, with 15 seconds pulsing and 15 seconds

rest, for 2 minutes or until all cells were lysed, whichever was the longest (cells never took greater than a total of 4 minutes to lyse through sonication). During sonication cells were kept on ice to prevent the lysate becoming excessively hot.

2.5.1 Measuring cell growth in macrophage lysate

Once lysed, the macrophage lysate was plated on a 24 well plate, 1mL per well and inoculated with 5×10^5 *C. neoformans*. As a control SF-DMEM was inoculated with 5×10^5 *C. neoformans* cells. Lysate experiments were carried out with H99, Δ PLB1 and PLB1^{rec} strains over a 7 day period. Where by, every 24 hours cells would be resuspended and a dilution of the suspension would be removed and plated onto YPD agar and incubated for 48 hours at 25°C. After the incubation, colonies were counted and colony-forming units (CFU) per 0.5 μ L calculated.

2.6 Staining of the Cryptococcal cells

To visualise the nucleic acids of cryptococcal cells during the project, both Hoechst 33342 and 4',6-diamidino-2-phenylindole (DAPI) fluorescent stains were used. Both Hoechst and DAPI bind preferentially to A-T rich sequences in double stranded DNA. Once cells had been fixed, they were stained with 0.5 μ g/ml of Hoechst 33342 and incubated at room temperature for 30 minutes. After incubation cells were spun at 17000xg for 0.5-5 minutes, depending on the amount of macrophage debris then washed with 400 μ L of PBS to remove unbound dye. This process was repeated 2-3 times depending on the amount of cells recovered after the infection. Cells were finally re-suspended in 200 μ L of PBS.

400 μ L of *C. neoformans* cells, from infections or washed overnight cultures, were added onto the coverslip and centrifuged at 500xg for 5 minutes to force the *C.*

neoformans cells to contact the surface of the coverslip. Coverslips were incubated at room temperature for 15 minutes. Supernatants were discarded, taking care not to disturb the coverslips and cells were fixed to the coverslip with 4% PFA at room temperature for 10 minutes, and then washed 3 times in PBS.

2.7 Imaging of Cryptococcal cells and measuring of cell diameter

All microscopy was undertaken on a Nikon Eclipse Ti microscope, mounted with a QImaging QICAM-B mono camera. All images, brightfield and fluorescent, were viewed through a Nikon Plan APO VC 60x Oil DIC N2 objective lens. All images of Hoechst fluorescence were imaged with an exposure time of 700ms, while all Brightfield images were given a 70ms exposure time.

Cell sizes were measured using the 'circle drawing' function on Nikon NIS Element Advanced research imaging software. The software was able to determine the diameter of cells due to a function whereby each pixel is representative of a set length. All images were taken on the 60x lens and each pixel measured was 0.11 μ m.

2.8 Measuring cell growth and cell size under nutrient deficient conditions

To determine whether nutrient deficiency affected the proportion of Δ PLB1 cells that grew beyond 8 μ m, 24 well plates were set up with a decreasing concentration of YPD broth, diluted out with PBS to a final volume of 1mL, ranging 100% YPD, 50% YPD, 25% YPD, 12.5% YPD and 1% YPD. Wells were then inoculated with 100 μ L of a 1 in 10 dilution from overnight cultures, prepared in the same manner as 2.4.1. Stains tested were H99, Δ PLB1, and PLB1^{rec}, they were incubated at 37°C for 48 hours and the optical density at 600nm was measured every 30 minutes.

2.9 Data analysis of Cryptococcal cell diameter

For each condition, the diameter of up to 100 cells was measured. To check whether the cell diameter distribution had significantly changed over the course of the experiment a non-parametric Mann-Whitney U test was performed to compare the means of each condition. The z-values, an output of the significance, were calculated using an online tool (<http://elegans.som.vcu.edu/~leon/stats/utest.cgi>). Due to the α -value being 0.05, significant results would be found with Z value outside of -1.95 to 1.95.

2.10 Flow cytometry of Cryptococcal cells after infection

To test for an increase in cell size after infection in the Plb1 mutant *C. neoformans* cells H99, Δ PLB1 and PLB1^{rec} were used in an infection assay (same protocol as stated in section 2.4). After the 18-hour infection, lysates were stained with Hoechst 33342 as previously. Controls consisted of Hoechst 33342 stained non-infected macrophage debris that had been treated in the exact manner infected macrophage, pre-infection *C. neoformans* (all 3 strains) and non-stained *C. neoformans* post-infection H99. Samples were measured for forward scatter and fluorescence on a BD biosciences FACS Aria II cell sorter. Flow cytometry data was analysed using FlowJo flow cytometry analysis software (TreeStar Inc).

3. Results

3.1 Staining of the nuclear content of macrophage incubated cryptococci to observe whether larger cells were polyploidy

3.1.1 After fixing and washing, cryptococcal cells recovered from macrophages were limited and often co-localized with macrophage debris

To semi-quantitatively determine the nuclear content of cryptococcal cells after infecting and incubating within mouse macrophages we attempted to extract the fungal cells and stain specifically for the nucleic acids. This would allow us to semi-quantitatively determine whether Plb1 knockout cells have an increased amount of nucleic acids, a titan cell marker. To image the nuclei of *C. neoformans* cells after infection, macrophages were lysed in water. This was to allow for the imaging of the fungal nuclei without interference from the stained macrophage nuclei. The lysates were fixed with PFA and washed 3 times in PBS. Lysates were stained with 0.5µg/mL Hoechst 33342. When cells were imaged, it was apparent that *C. neoformans* cells were sparse on the coverslip, and were found to co-localize with macrophage debris (figure 5). The macrophage debris stained strongly with the Hoechst 33342 and made analysing the nuclei of cryptococci impossible (figure 5). This was seen with all 3 strains at 0 hours and 18 hours post infection. As well as co-localizing with the macrophage debris, a large amount of background fluorescence was observed. Suggesting that nuclear material, lysed from macrophages, was also binding with Hoechst 33342 in the lysate.

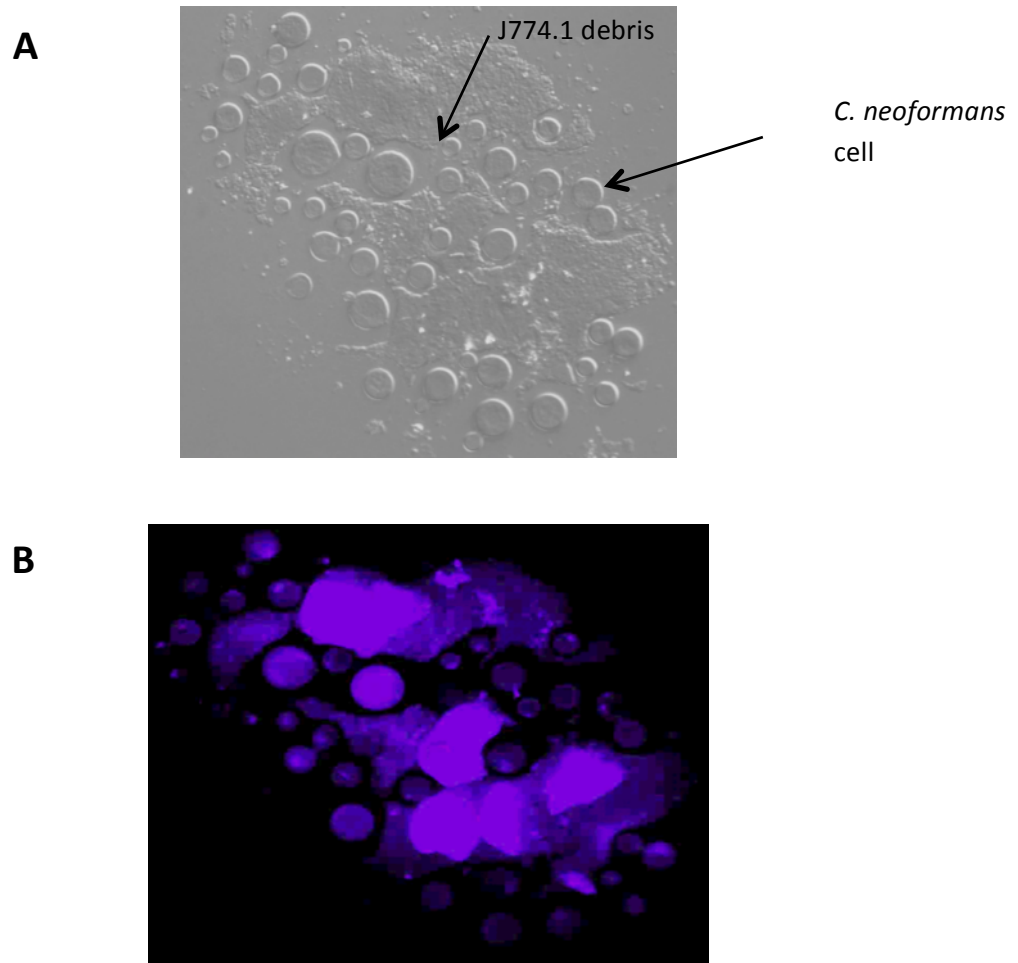


Figure 5: Co-localization of *C. neoformans* cells with J774 macrophage debris after lysis.

To study the nuclear content of *C. neoformans* cells after J774 macrophages were lysed 18 hours after being infected with an MOI of 10 of *C. neoformans*. The lysate was then stained with 0.5 μ g/mL of Hoechst 33342. Cells were imaged with QImaging QICAM-B mono camera attached to a Nikon Ti eclipse microscope, viewed on a Plan APO VC 60x Oil DIC N2 objective lens. Figure 5A shows the Brightfield image. Figure 5B shows the same imaged when fluoresced under UV light to excite the Hoechst 33342 stain. As it shows fungal cells localize with J774.1 debris, making imaging of the nucleus impossible.

3.1.2 The addition of poly-L-lysine to the lysate improved the amount of cells per coverslip but fungal cells co-localized with debris

In an attempt to improve the yield of fungal cells found on the coverslip, coverslips were treated with poly-L-lysine (PLL) and immunostained with the GXM specific monoclonal antibody, 18B7. This would hopefully help reduce the loss of cells on the coverslip to washing, due to fungal cells directly binding to the monoclonal antibody. 18B7 immunostained coverslips showed an improvement in the amount of fungal cells visible. Unfortunately, as with the untreated coverslips, cryptococci co-localized with macrophage debris, leading to analysis the size of the cryptococci nuclei impossible, similar to figure 5 (data not shown).

Because Matsui *et al.*, 1983, showed that PLL acts as a non-physiological opsonin, and may have been a factor causing macrophage debris binding to the PLL treated coverslips, PLL was added to the lysate during washing to clump the macrophage debris together. Hopefully, preventing its dispersion across the coverslip. Imaging showed that macrophage debris had clumped together (Figure 6), but macrophage debris was bound to the *C. neoformans* cells (Figure 7). This prevented analysis of the size of the *C. neoformans* nuclei. This was found in all strains at 0 hours and 18 hours post infection. DAPI infused vector shield was found not to penetrate cryptococcal cells, but did stain nuclear material in the lysate (data not shown).

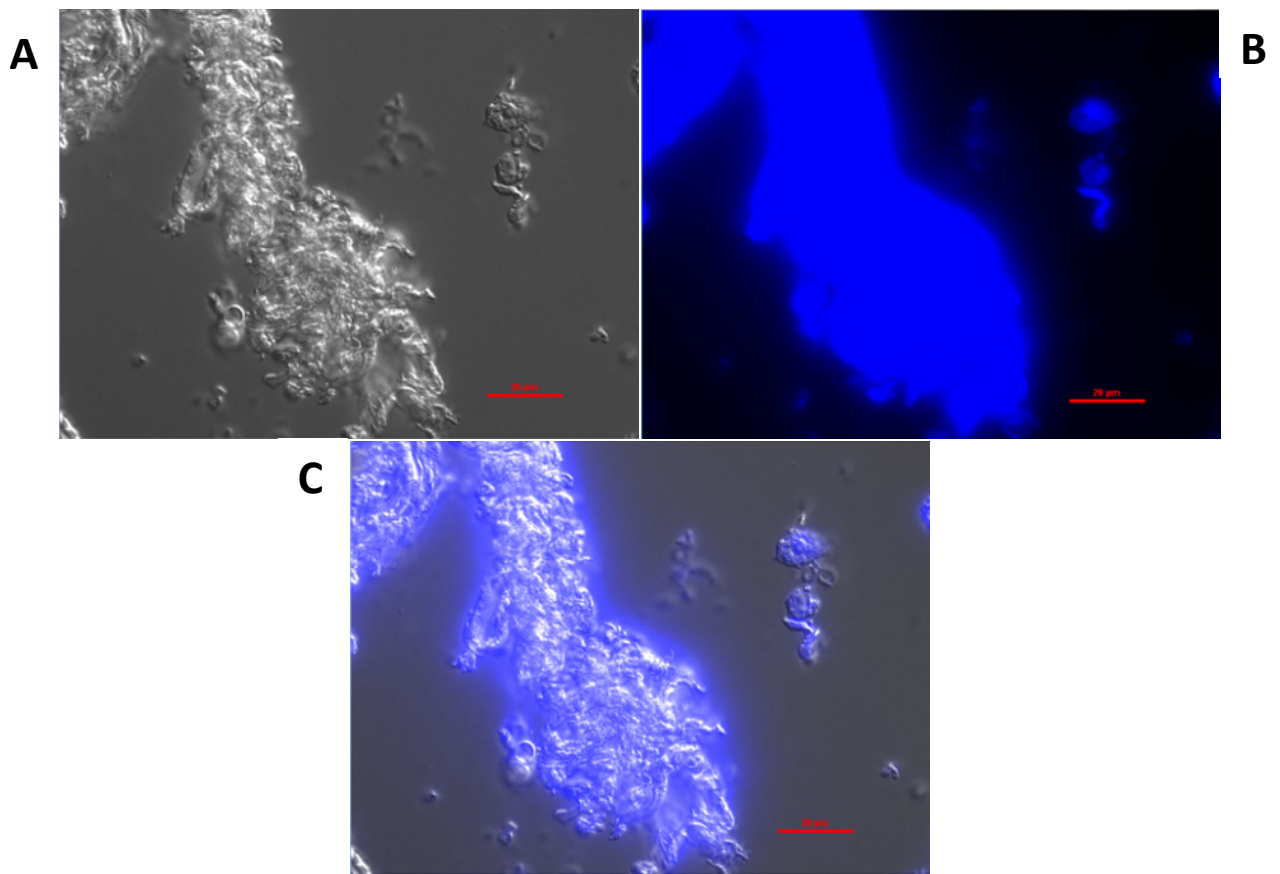


Figure 6: Using Poly-L-Lysine to clump together J774 macrophage debris.

To try and prevent J774.1 macrophage debris from interfering with analysis of *C. neoformans* nuclear content, 0.1% poly-L-lysine was added to the lysate prior to imaging. Images were taken with QImaging QICAM-B mono camera attached to a Nikon Ti eclipse microscope, viewed on a Plan APO VC 60x Oil DIC N2 objective lens. Figure 6A is the brightfield image of debris, 6B Hoechst stained nuclear content and 6C is the composite image. The addition of PLL to the lysate helps clump the debris together.

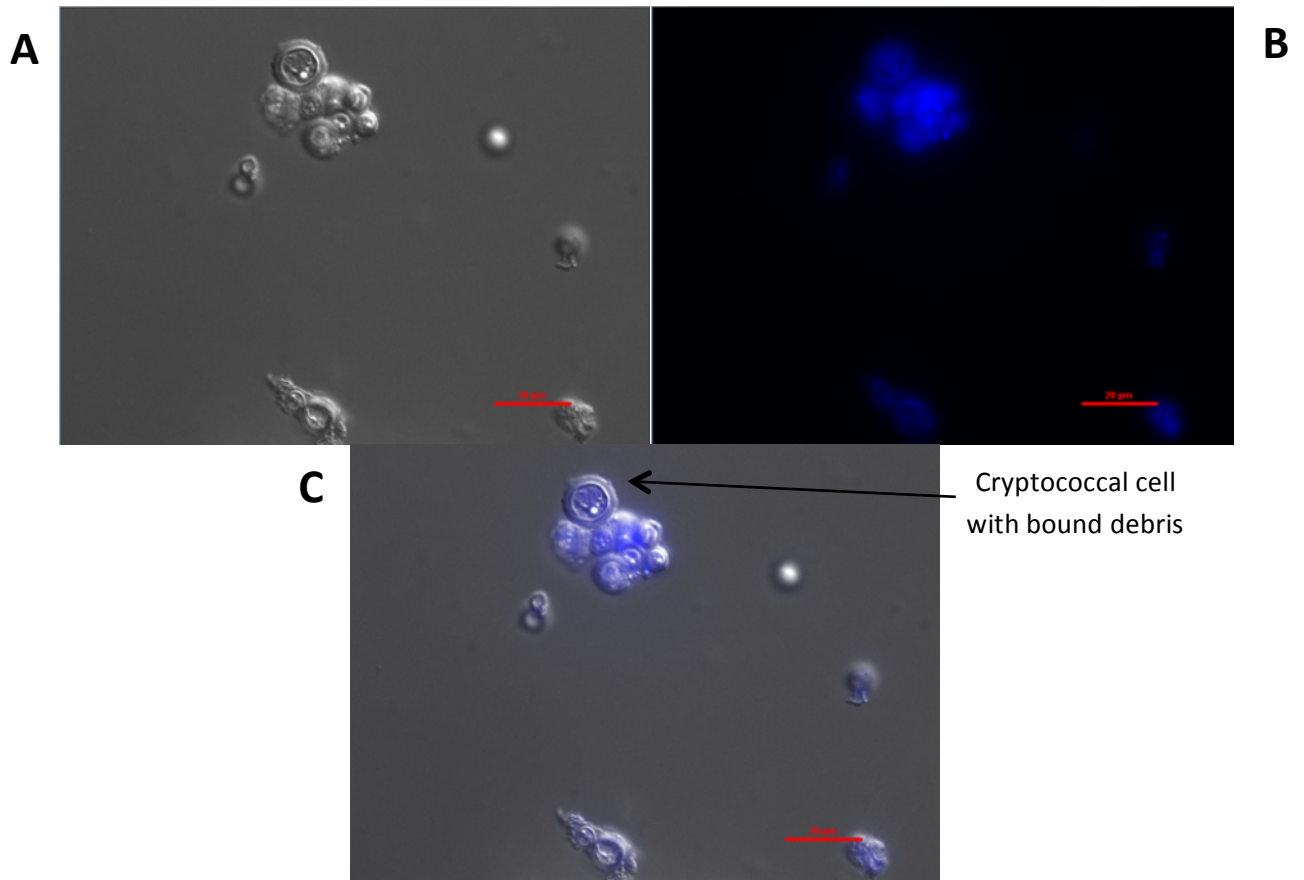


Figure 7: Using Poly-L-Lysine to clump together J774 macrophage debris causes macrophage debris to bind to fungal cells.

To try and prevent J774.1 macrophage debris from interfering with analysis of *C. neoformans* nuclear content 0.1% Poly-L-Lysine was added to the lysate prior to imaging. Images were taken with QImaging QICAM-B mono camera attached to a Nikon Ti eclipse microscope. Figure 7A is the Brightfield image of debris, 7B is the imaged when excited with UV light to image the nuclear content and 7C is the composite image. The addition of PLL to the lysate clumps macrophage debris together but also causes debris to bind to the fungal cells. This prevents any sort of reliable imaging of *C. neoformans* nuclei.

3.2 Does macrophage lysate induce an altered phenotype in Plb1 knockout *C. neoformans*?

3.2.1 Plb1 knockout cells did not show a change in cell diameter after a 7 day incubation in SF-DMEM or macrophage lysate

During this portion of the study we chose to investigate the cell diameter, and therefore cell size (another known marker of titan cell), of Plb1 knockout cells due to the difficulties of measuring nuclear content, as described previously. Every 24 hours, during the experiment, cultures in SF-DMEM and macrophage lysate were sampled and imaged under the microscope. Cell diameter, cell morphology and relative growth (measured in colony forming units) were measured over a 7 day period. All *C. neoformans* strains were incubated in SF-DMEM and EoM. Cell diameter was measured and plotted onto box whisker plots (Figure 8). H99 showed significant decrease in cell diameter between the day 0 measurement and day 7 measurements ($Z=5.09$, $P<0.001$). A significant decrease in cell diameter was also observed between the start point and day 7 measurement of the H99 strain in EoM ($z=7.1818$, $P<0.001$). Unfortunately, at the 6/7-day stage the H99 in the EoM appeared to lyse in the culture, limiting the amount of cells countable on those days (Figure 9). Neither of the Δ PLB1 conditions, in SF-DMEM or EoM showed a significant difference in cell diameter after 7 days incubation ($z=0.603$, $P>=0.05$ and $z=0.765$, $P>=0.05$, respectively). The diameter of PLB1^{rec} cells in SF-DMEM also decreased significantly over the incubation ($z=6.98$, $P<0.001$). Similarly, a significant decrease in cell diameter was also seen in the PLB1^{rec} cells that had been incubated in EoM ($z=9.42$, $P<0.001$). The PLB1^{rec} cells incubated in EoM, began to lyse after 6-7 days, the same as the H99 (Figure 9). These results suggest that it is not a

component of the macrophage lysate that induces large cells. What is interesting to note is that when the wild-type H99 and reconstituted PLB1^{rec} strains were incubated in EoM they both appeared to begin to lyse at days 6 and 7, while Δ PLB1 cells did not. This would suggest that EoM affects the wild type and reconstituted strains, during prolonged incubation. While the Δ PLB1 knockout has a protective effect. Δ PLB1 cells at 10 days did not begin to show the lysed phenotype, suggesting that it is not related to the speed of growth between the wild type and mutant.

3.2.2 Over 7 days of incubation in macrophage lysate a significant number of Plb1 knockout cells were shown to have an altered cell morphologies

During the course of the incubation it was noted that certain cells appeared to have morphology very distant from the 'normal' round morphology of *C. neoformans*. These cells appeared to have projections stemming from the surface, taking on an appearance similar to that of pseudohyphae (Figure 10). To measure this, 100 fungal cells were counted and the amount of cells with this phenotype was recorded. As shown in figure 11, this morphological phenotype appeared more so in the cells incubated at 37°C in EoM. In the EoM, the Δ PLB1 strain showed a greatest amount of fungal cells with this morphology than any other strain, with the greatest amount being seen on day 5. The Δ PLB1 mutant in SF-DMEM and the H99 in EoM appear to have similar amounts of cells with this morphology. H99 cells in SF-DMEM showed only 1 cell with this morphology over the whole 7 day incubation (N=2). On days 2 (P<0.05, 0.0022), 5 (P<0.05, 0.0035), 6 (P<0.05, 0.0061) and 7 (P<0.05, 0.012) there was a significant increase in cells with an altered morphology in the population of Plb1 knockout cells grown in macrophage lysate when compared to wild type cells grown in the same media. A significant difference was not seen between the

morphologies the H99 strain and Plb1 knockout when incubated in SF-DMEM. These results indicate that the knockout of Plb1 affects cell morphology in cells incubated in macrophage lysate when compared to the wild type strain.

3.2.3 Attempts at trying to determine whether the absence of extracellular Plb1 was responsible for the altered cell morphology in the Plb1 knockout strain were unsuccessful

To observe whether the effect of Plb1 on cell morphology was due to internal or secreted phospholipase activity, a H99/ Δ PLB1 co-infection was attempted. Transwells were used to 'house' the H99 cells while Δ PLB1 cells were outside the transwell on the plate base. The transwell would allow for the diffusion of Plb1 across the membrane. Even though this proved promising, after 2 days contamination was found in all conditions and proved to bring an end to this avenue of investigation.

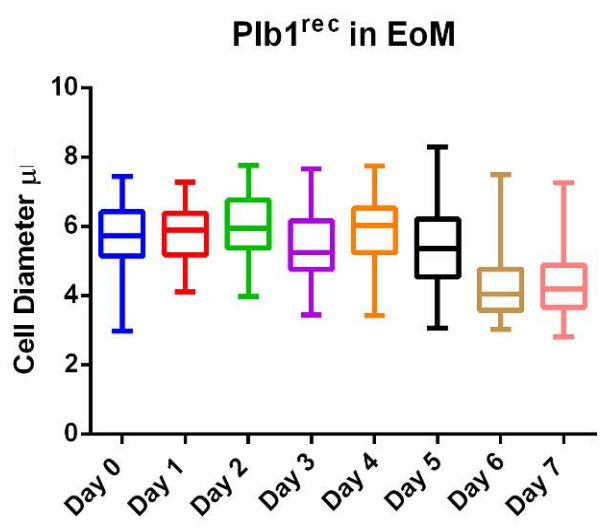
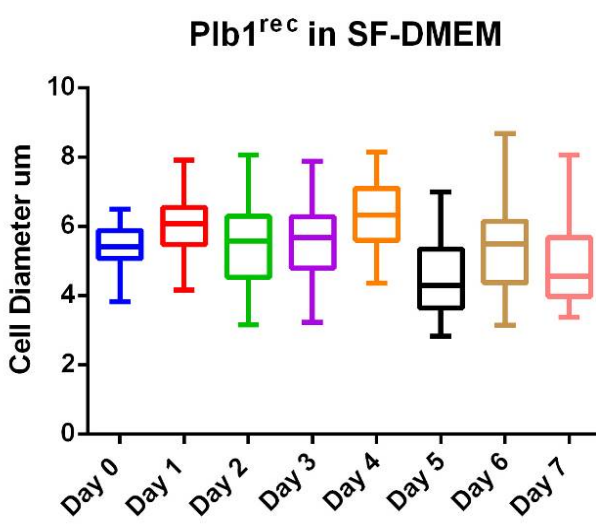
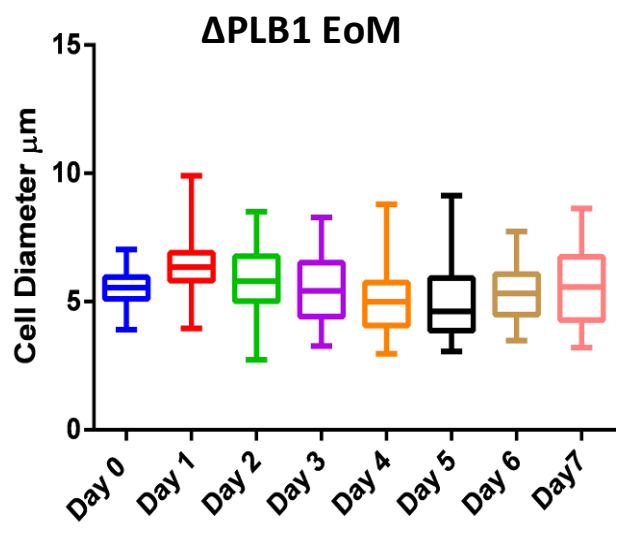
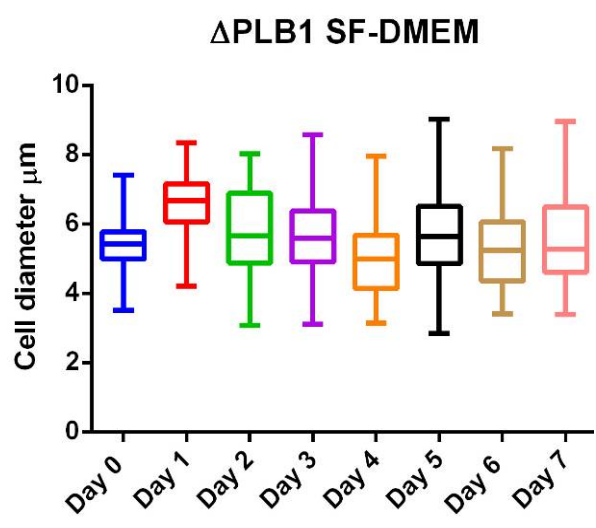
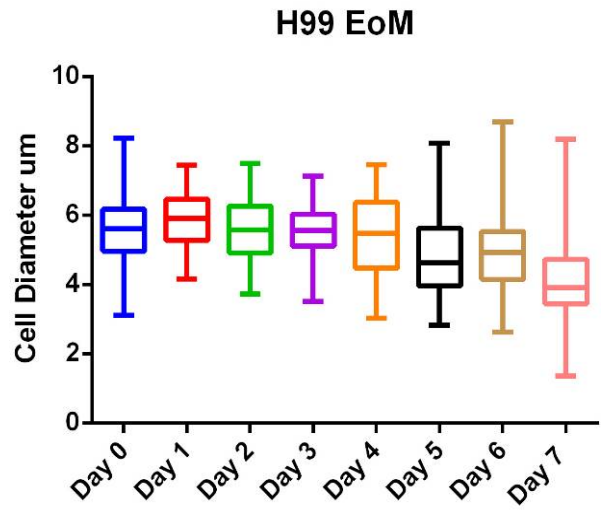
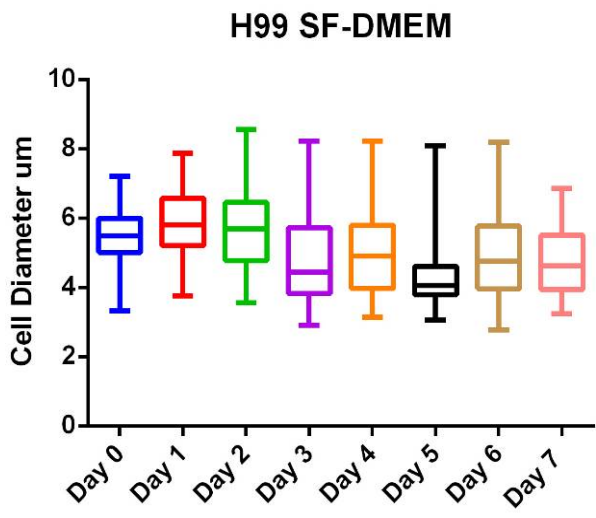


Figure 8: Box and whisker plots *C. neoformans* cell diameter over 7 days incubation in SF-DMEM and J774 macrophage lysate.

Every day during of the lysate experiment the diameter of 100 fungal was measured for each strain and range and distribution plotted. All 3 strains were incubated in SF-DMEM as a control and J774 macrophage lysate (EoM). The whiskers of the boxes represent the range of the diameters. While the centre line of the box represents the mean and upper and lower lines of the box represent the upper and lower interquartile ranges respectively. Between day 0 and day 7 of incubation a significant decrease in cell diameter was found in H99 cells incubated in SF-DMEM and macrophage essence (EoM) ($Z=5.09$, $P<0.001$ and $Z=7.1818$, $P<0.001$, respectively). A significant decrease in cell diameter was also seen in the Plb1 reconstituted cells when grown in SF-DMEM ($Z=6.98$, $P<0.001$) and macrophage essence (EoM) ($Z=9.42$, $P<0.001$), after 7 days in incubation. Plb1 knockout cells did not show a significant change in cell diameter over the 7-day incubation.

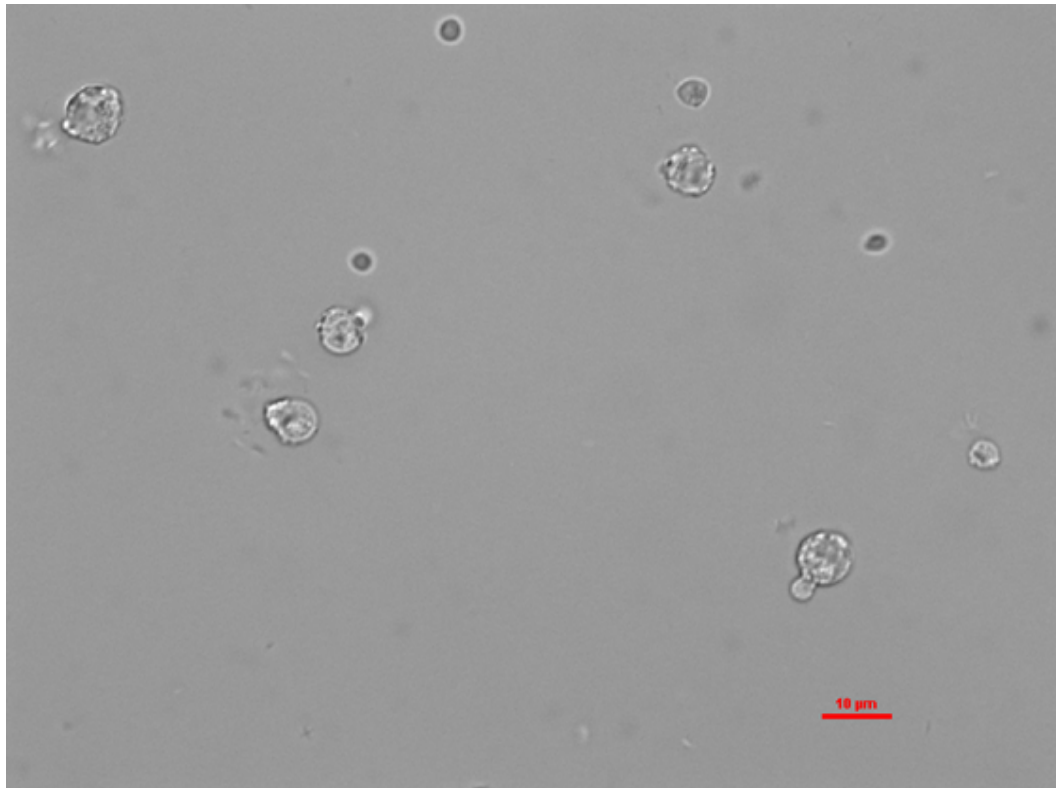


Figure 9: After 7 days incubation in J774 macrophage lysate H99 cells and PLB1^{rec} cells appear stressed.

Images were taken with QImaging QICAM-B mono camera attached to a Nikon Ti eclipse microscope, viewed on a Plan APO VC 60x Oil DIC N2 objective lens. During the incubation in the macrophage lysate H99 and PLB1^{rec} appeared to stress and lyse at the 7 day period. The image is a brightfield image of PLB1^{rec} cells on day 7 of incubation.

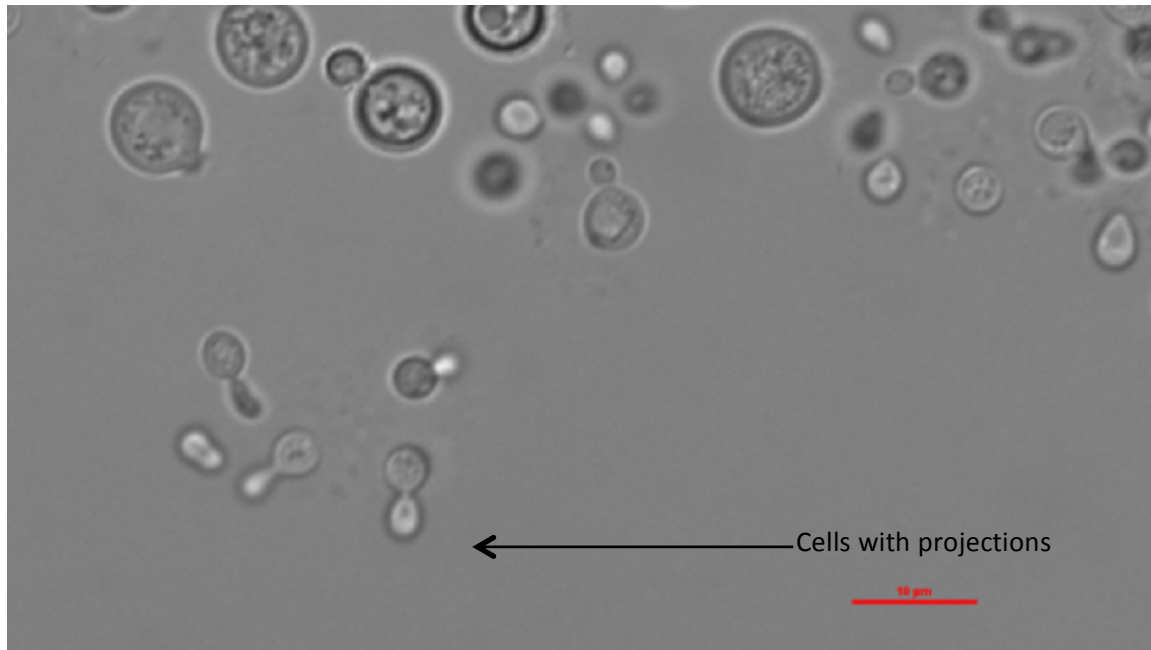


Figure 10: During incubation in macrophage lysate Δ Plb1 cells had different morphologies.

Images were taken with QImaging QICAM-B mono camera attached to a Nikon Ti eclipse microscope, viewed on a Plan APO VC 60x Oil DIC N2 objective lens. During the incubation in the macrophage lysate Δ PLB1 cell morphology changed with what appears to be projections coming from some cells. These appear to be similar to pseudohyphae, as described by others.

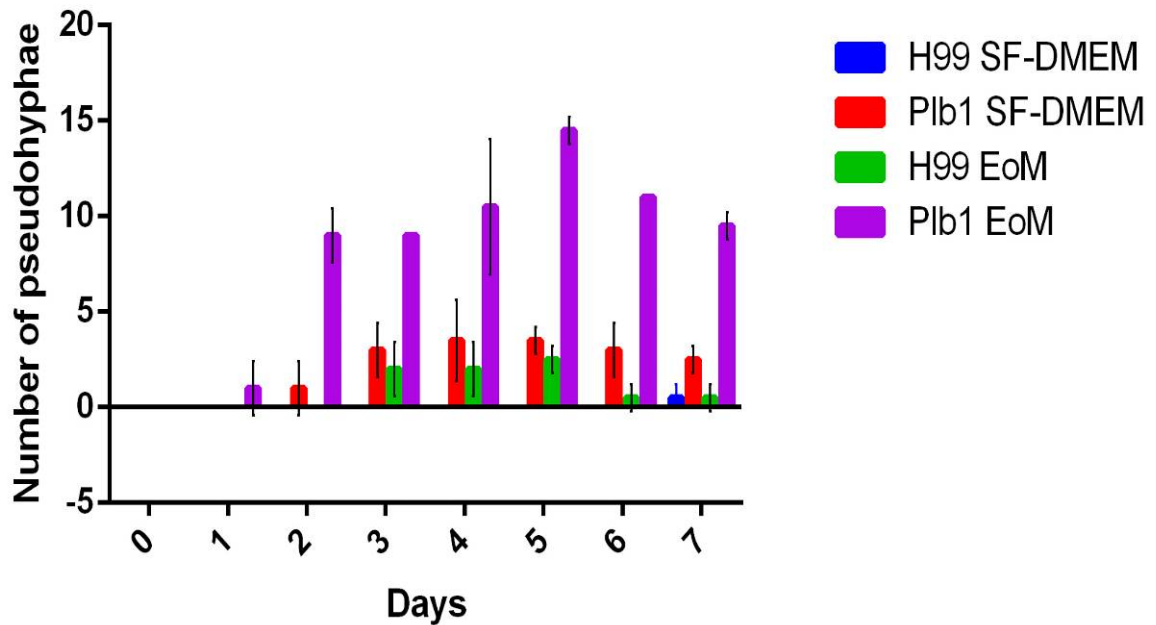


Figure 11: The proportion of fungal cells, out of 100 counted, with altered cell morphology, similar to pseudohyphae, observed during incubation of H99 and Plb1 knockout strains in macrophage lysate and SF-DMEM.

The number of cells with projections coming away from the *C. neoformans* cells were counted every day (per every 100 cells) and plotted. While all strain in all media showed this altered morphology during the incubation, Δ PLB1 cells showed a greater amount of cells with this altered morphology in macrophage lysate, than any other condition. On day 2 ($P < 0.05$, 0.0022), 5 ($P < 0.05$, 0.0035), 6 ($P < 0.05$, 0.0061) and 7 ($P < 0.05$, 0.012) the amount of cells with an altered morphology was significantly different in the Plb1 knockout cells when compared to H99 cells grown in macrophage essence. A significant difference was not seen when comparing Plb1 against the H99 wild type when grown in SF-DMEM at any day.

3.2.4 Plb1 knockout cells do not survive as well as wild type/reconstituted Cryptococci in SF-DMEM and essence of macrophage

To determine whether the ability to survive in stress inducing conditions was different in the Plb1 knockout strain, cell viability was measured in SF-DMEM and macrophage lysate over 7 days using colony forming units (CFU). CFUs were measured daily by plating out a dilution of the culture onto YPD plates and incubating for 48 hours at 25°C. After this, colonies were counted and CFUs/0.5µL calculated. In all three conditions the Δ PLB1 mutant fared worse than the H99 and PLB1^{rec} strains, as shown in figure 12 but only Plb1 cells grown in SF-DMEM showing a significant difference comparative to the wild type and Plb1^{rec} strains at days 4 ($P < 0.05$, 0.042), 5 ($P < 0.05$, 0.023) and 7 ($P < 0.05$, 0.026). Strains incubated in EoM showed a similar pattern with Δ PLB1 fared worse than the other two strains. But in EoM, Δ PLB1 fared better in CFU count, at day 7, of 2632 CFUs/0.5uL averaged over 2 repeats. While both the H99 and PLB1^{rec} had CFUs of 4616 and 5816 respectively at day 7 but this found not to be statistically significant when compared to the wild type and Plb1 reconstituted strains. Plb1 knockout cells fared better in EoM than those in SF-DMEM, which is expected, as macrophage lysate would contain potential metabolites for *C. neoformans*. Although, it is unknown how long these may last in the lysate before degrading. This is in conflict with microscopy observations, where at day 7 both the H99 and PLB1^{rec} strains appeared fewer in numbers, with many cells being stressed and immeasurable. This could be due to the cells observed under the microscope being less tolerant to the protocol used to fix the cells. Or, it could suggest that the lysed cells observed before were not dead, and were indeed viable. Even though the Δ Plb1 strain was slightly less viable in YPD all three strains fared

similarly over the course of the experiment with no significant difference between CFU counts (figure 12).

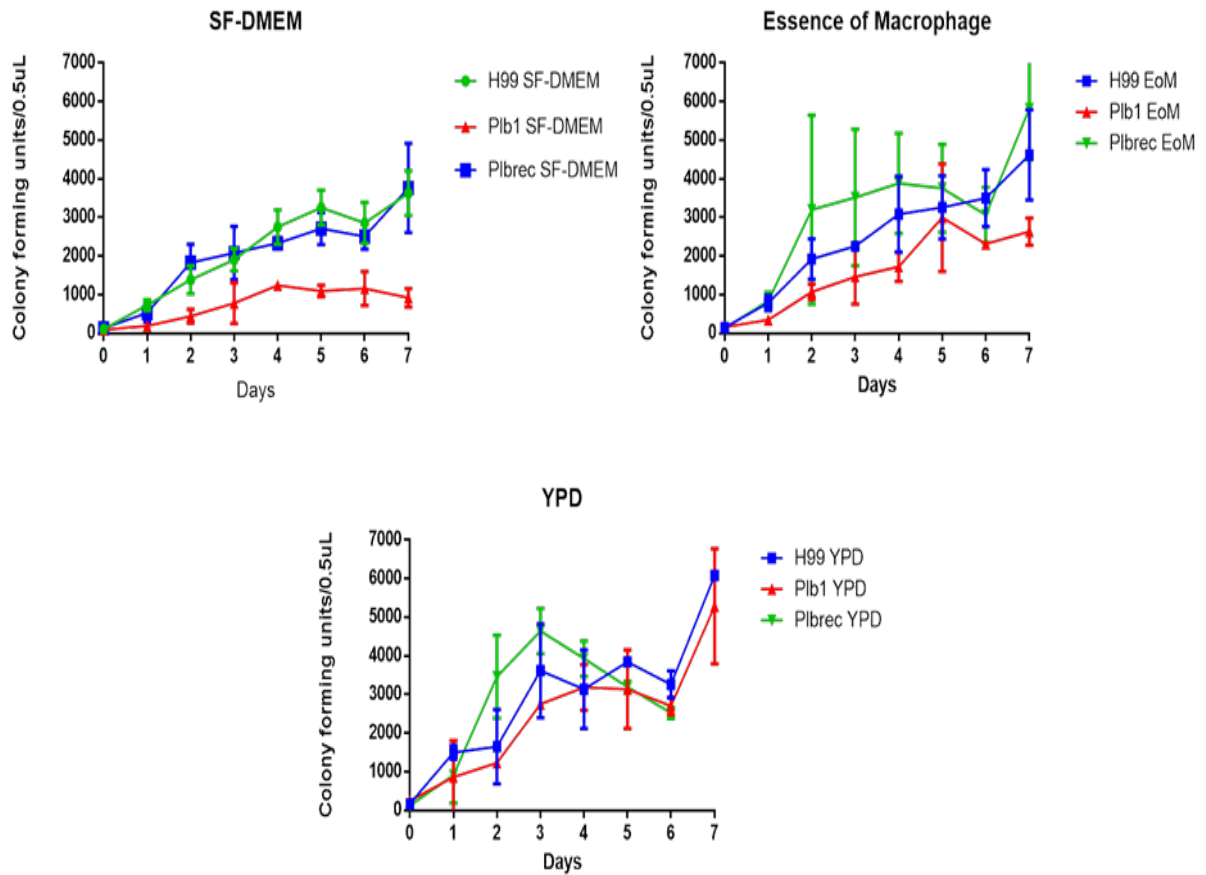


Figure 12: Cell viability and growth as measured by colony forming units per 0.5µL of culture (CFUs/0.5µL) during the macrophage lysate experiment.

Everyday, growth and viability was measured by counting colonies on YPD agar plates after dilution of the cultures were plated out. Plates were incubated at 25°C for 48 hours. CFUs were measured for *C. neoformans* grown in SF-DMEM, EoM and YPD broth. Across all 3 conditions the Δ PLB1 strain fared worse than every other strain, although in EoM and YPD this was not found to be significantly different to the wild type or reconstituted strain. In SF-DMEM the Plb1 mutant had significantly fewer colonies on days 4 ($P < 0.05$, 0.042), 5 ($P < 0.05$, 0.023) and 7 ($P < 0.05$, 0.026) when compared to the H99 strain.

3.3 Measuring cell growth and cell size in nutrient deficient conditions to investigate whether nutrient deficiency induces the large cell phenotype

3.3.1 There is no increase in cell diameter in *C. neoformans* cells over 48 hours of nutrient deficiency

To determine whether nutrient deficiency, specifically, was the cause of the increase in cell diameter, H99 and Δ PLB1 cells were incubated for 48 hours at 37°C in gradually decreasing amounts of YPD. After the incubation cells were imaged as previous, and the diameters of 100 cells were measured and plotted. Growth of each strain in each condition was measured by optical density at 600nm (OD₆₀₀) every 30 minutes. In this experiment cell diameter was measured twice, while growth at OD₆₀₀ was measured once. Cells grown in 100% YPD reached an average maximum OD of 0.130 and 0.1394, for H99 and Δ PLB1 respectively (Figure 13). Surprisingly, cells in both 50% and 25% YPD grew better than their counterparts in 100% YPD (Figure 13). H99 cells grown at 50% YPD reached a maximum OD₆₀₀ of 1.603, the Δ PLB1 cells grew to 1.696, and H99 and Δ PLB1 cells grown at 25% YPD attained an OD₆₀₀ of 1.643 and 1.703. *C. neoformans* cells grown in 12.5% YPD were only marginally worse reaching an average peak OD of 1.25 and 1.144, in the H99 and Δ PLB1 respectively (Figure 13). Both H99 and Δ PLB1 cells performed worse in 1% YPD, as expected, most probably due to the very limited amount of nutrients available to them for active growth and proliferation.

As well as the growth curve data, cell diameter was measured before and 48 hours after incubation, for each condition. There was a significant decrease in cell diameter between the *C. neoformans* H99 at 0 hours and at 1% YPD (z=1356, P<0.001) (Figure 14). There was also a significant decrease in cell size for *C. neoformans* H99

grown in 12.5% ($z=14.038$, $P<0.001$) (Figure 14). In Δ PLB1 the same trend was seen with cells grown in 1% YPD significantly decreasing in diameter over the 48 hours ($z=10.17$, $P<0.001$), but different to the H99 there was no significant difference between 0 hours and 12.5% after 48 hours (Figure 14). While in the PLB1 mutant there was a significant increase in cell diameter between the 0 hour and 100% YPD after 48 hours ($z=8.953$, $P<0.001$), which seems odd as cells were grown in 100% prior to inoculating the conditions so no change would be expected (Figure 14).

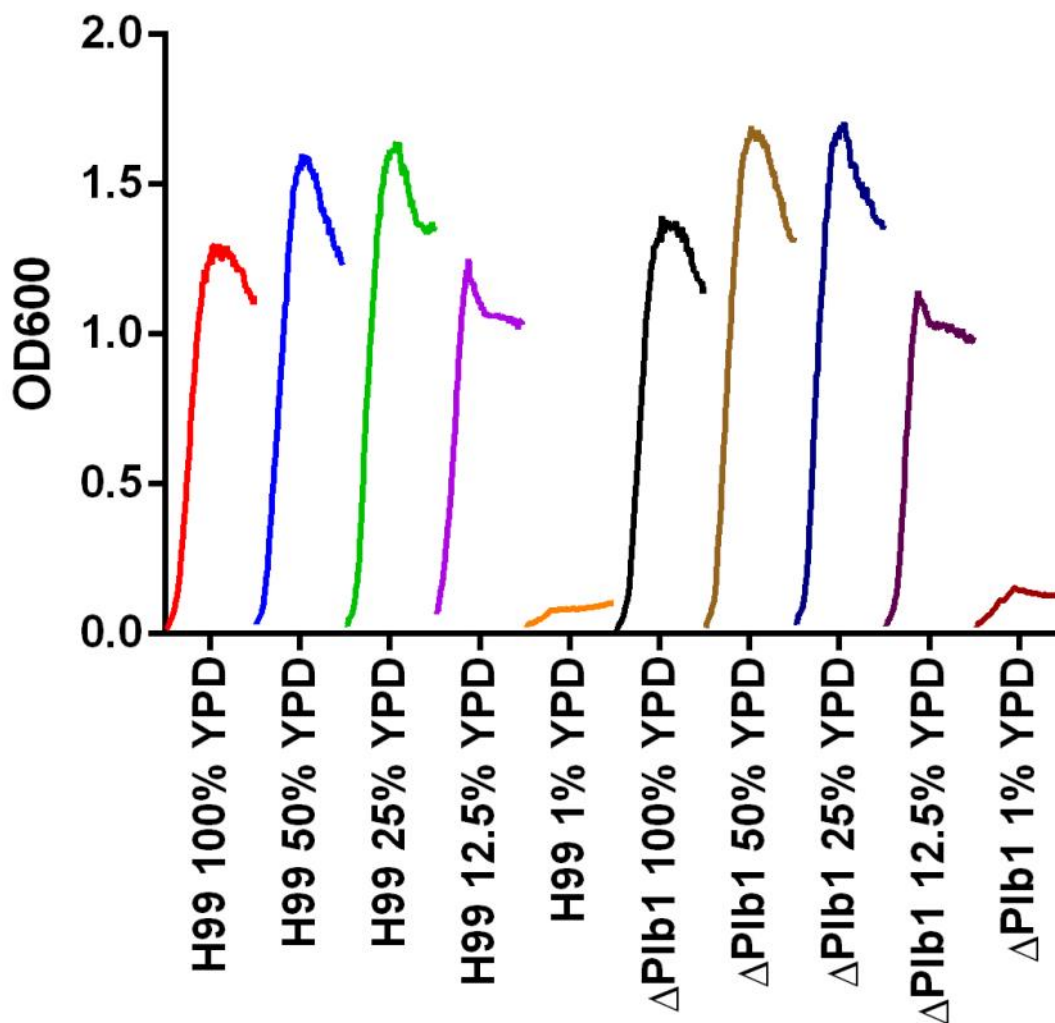


Figure 13: Growth curves of *C. neoformans* subjected to varying amounts of nutrient starvation during incubation at 37°C for 48 hours.

To look at how nutrient starvation affected growth of cells *C. neoformans* cells were grown in decreasing amounts of YPD broth to mimic nutrient starvation. Growth was measured every 30 minutes and determined by optical density at 600nm (OD₆₀₀). Cells grown in 100%, 50% and 25% YPD appeared to have no detrimental effects on growth over 48 hours in both strains. While in 12.5% and 1% YPD both strains appear to growth less than the 100% YPD counterpart.

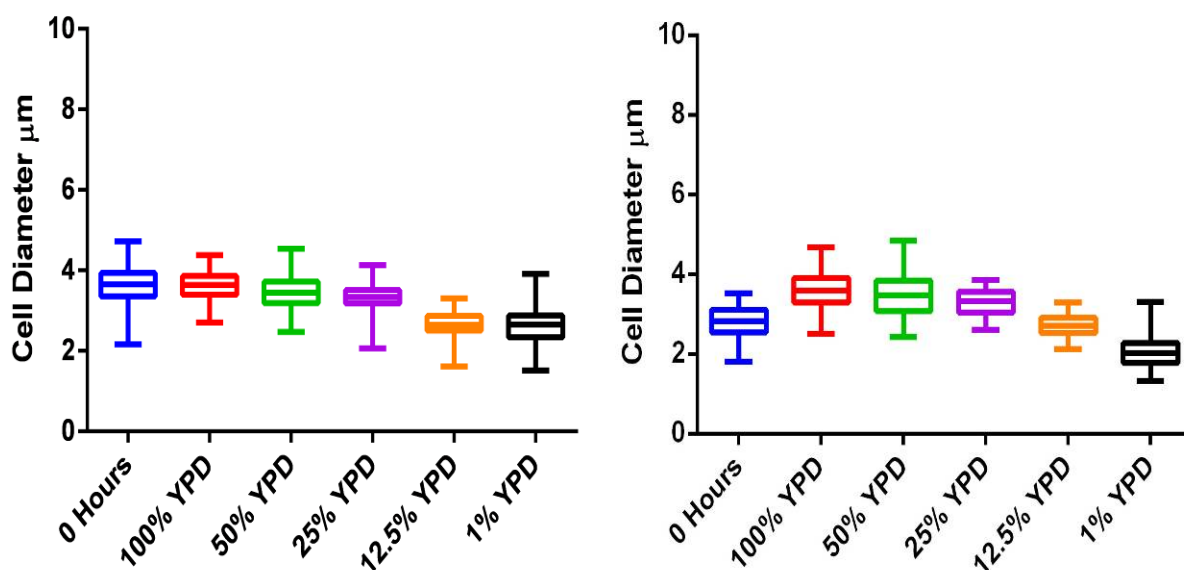


Figure 14: Cell diameter of *C. neoformans* in varying degrees of nutrient starvation after 48 hours of incubation at 37°C

To determine whether nutrient deficiency may cause the increase in cell diameter during infection or causes the altered morphology, *C. neoformans* H99 and Δ PLB1 were incubated in lower concentrations of YPD for 48 hours to mimic nutrient starvation. The whiskers of the boxes represent the range of the diameters. While the centre line of the box represents the mean and upper and lower lines of the box represent the upper and lower interquartile ranges respectively. In the H99 strain, comparative to the cell diameter of 0 hour cells those grown in 12.5% YPD and 1% YPD ($z=13.56$, $P<0.001$ and $z=14.038$, $P<0.001$, respectively). Plb1 mutants showed a significant decrease in cell diameter over 48 hours when grown in 1% YPD ($z=10.17$, $P<0.001$), but oddly show a significant increase in cell diameter when grown in 100% YPD ($z=8.953$, $P<0.001$).

3.4 Using flow cytometry to measure the fluorescence of nuclear content in cryptococcal cells after macrophage incubation

3.4.1 After 18 hours of infection within J774 macrophages there is an increase in the proportion of cells with a greater diameter and more nuclear material in the Δ PLB1 strain

Flow cytometry was employed to differentiate between cell size and nuclear content of *C. neoformans* cells, pre-infection and 18 hours post infection. This was chosen as a quicker, more precise method at measuring both of these parameters, which had been difficult to do under the microscope. Forward scatter (FSC) would measure fungal cell size, while the fluorescence, due to DNA binding stain Hoechst 33342, would be measured as a semi-quantitative measurement of the amount of nuclear material in each cell. The results from the flow cytometry data were gated against the fluorescence of the macrophage debris to remove this debris from the results (Supplementary figure 1). Unstained post-infection H99 cells were used as controls, proving that fluorescence was solely due to Hoechst 33342 staining and not auto-fluorescent (Figure S2). As shown in figure 15, all populations of pre-infection cells were similarly sized and had similar nuclear content. What is interesting is that there appeared to be sub-populations within the sample. This could be attributed to cells, which are undergoing budding or in different phases of cell cycle (Figure 15).

After 18 hours within the macrophages *C. neoformans* cells were lysed with dH₂O. Post infection, all 3 strains showed an overall increase in forward scatter, indicating an increase in cell size. To determine whether cells were getting larger post-infection

a gate was placed on cells with a forward scatter of 400 or above. A forward scatter of 400 was chosen as the cut off for larger cells, because in all 3 strains tested 99% of the population was found to be below a forward scatter of 400. A gate based on the fluorescence was also applied to the data. The gate was applied on particles which fluoresced greater than 10^3 . This gate was chosen due to less than 2% of cells, in all strains, having fluoresced above this point prior to infection. All 3 strains after the 18-hour infection showed an increase in the population above the 400 FSC unit gate. 7.99% of H99 cells reached over the 400 FSC unit gate, while Δ PLB1 cells and PLB1^{rec} cells had 19.7% and 4.25% of cells above 400 FSC units, respectively. After 18 hours of infection the proportion of cells with nuclear fluorescence above 10^3 increases, indicating an increase in nuclear content. Both H99 and PLB1^{rec} cells have 17.7% and 16.4% of the population above 10^3 , while in Δ PLB1 cells 50.5% of cells have nuclear content above 10^3 . When both gates are placed on top of each other, the percentage of cells with a FSC above 400 and fluorescence greater than 10^3 is different between all three strains. 5.17% of H99 cells, 3.86% of Plb^{rec} and 17.8% of Δ Plb1 cells showed greater size and nuclear fluorescence (figure 15). While it is not quantitative, the data does show that knocking out Plb1 affects nuclear content during infection along with an increase in cells size. Although this is not conclusive proof that these are titan cells, it is interesting that as the cells increase in size so does the nuclear content, which is a known marker of the titan cell morphology.

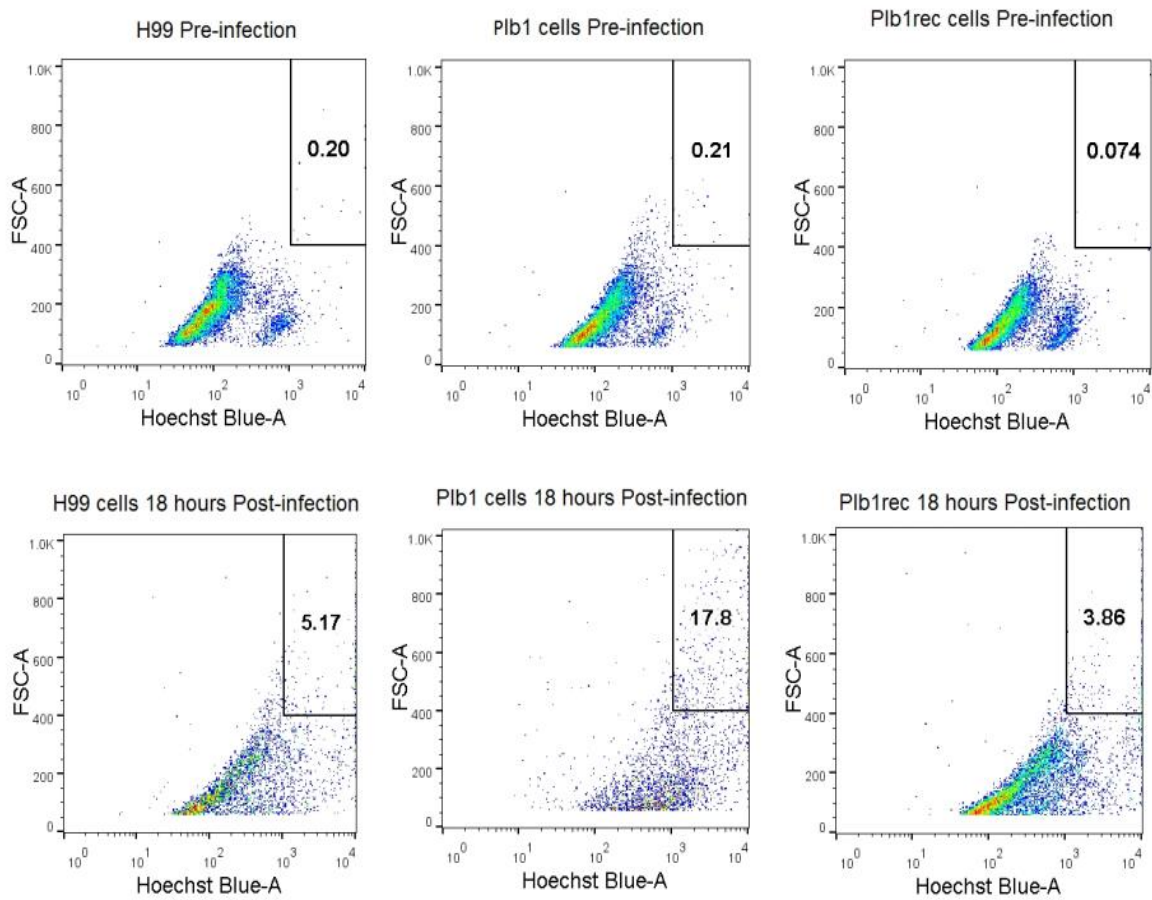


Figure 15: Cryptococcal cell size and nuclear content measured by forward scatter (FSC-A) and Hoechst fluorescence, before and after 18 hours incubation in J774 macrophages.

Flow cytometry was employed to determine cell size and nuclear content of H99, Δ PLB1 and PLB1^{rec} cells after infecting J774 macrophages for 18 hours. Samples were stained with 0.5 μ g/ml Hoechst 33342 after fixing. Plots were gated on stained macrophage debris to remove the majority of macrophage debris from the infected samples. While all strains increase in both size and nuclear content, there is a greater amount of cells, which are above these gates in the Δ PLB1 mutant (17.8% in the Δ PLB1 strain when compared to the 5.17% in H99 and 3.86 % in Plb^{rec}.)

4.0 Discussion

Even though imaging of cryptococcal nuclear content, to semi quantitatively determine overall nuclear content, was not achieved during the study, we were able to observe an increase in overall nuclear content through flow cytometry with the use of DNA-specific fluorescent stains. This experiment leads to possible suggestion that in the Plb1 knockout cells that have been recovered from infection of macrophages have an increase in both cell size and nuclear content, both markers of titan cells. While this is not conclusive it proposes a new route of investigation to answer this question. As well as the observation of increased nuclear content, Plb1 knockout cells showed altered cell morphology, similar to clinically relevant pseudohyphae, when grown for 7 days in macrophage lysate.

4.1 Hoechst staining of *C. neoformans* cells after infecting into macrophages

The first obstacle during the investigation was the lack of observable cells in 10uL of fixed, post infection, lysate on coverslips. This could be attributed to the relatively few cells up taken by macrophages, even after opsonisation, described previously to be as low as 10%. As well as the relatively low amount of particle uptake, the process of centrifugation, washing and re-suspending the lysate pellets (to remove SF-DMEM and PFA after infection and fixation) will compound the loss of cells in the samples. The few cells that were observable upon microscopy were mostly co-localized with macrophage debris, which meant analysis of the fungal nuclei impossible. To try and combat this various methods were employed. Firstly, coverslips were treated with poly-L-lysine (PLL) and immunostained with the mouse IgG1 antibody, 18B7, to bind fungal cells directly to the coverslip. 18B7 has a variable region that binds specifically, and with high affinity, to glucuronoxylomannan found in cryptococcal

polysaccharide capsule (Casadevall *et al.* 1998). Coverslips were treated with PLL and then incubated with 18B7 to allow for binding of the MAb to the poly-L-lysine matrix. The lysates were placed on top of coverslips and centrifuged to force the *C. neoformans* cells upon the coverslips, where they would hopefully bind specifically with PLL-bound 18B7. Coverslips were then fixed to secure the binding between the antibodies and their ligand on the Cryptococcal cell surface. While this did work and many more *C. neoformans* cells were visible during imaging, the same problem was observed, colocalization of *C. neoformans* with macrophage debris. To try and separate *C. neoformans* from debris, the lysates were vortexed vigorously for 5 minutes. Then lysates were centrifuged, to attempt to pellet *C. neoformans* without pelleting macrophage debris. This proved unfruitful as debris and fungal cells pelleted at the same time, likely due to them both being of similar size after lysis.

One reason for the increased amount of debris binding to the immunostained coverslips could be due to macrophage debris binding the poly-L-lysine on the coverslip. Poly-L-lysine has been shown to act as non-physiological opsonins, and Matsui *et al.*, 1983, claim this to be due to non-specific ionic interactions, due to poly-L-lysine's charge. Whether this still occurs once cells have been lysed is debatable, but this offers a possible reason why macrophage debris appeared bound to the coverslip, which should be specifically binding GXM in the Cryptococcal capsule.

Another method of preventing dispersed clumping was treating the lysate with poly-L-lysine prior to fixing, to clump the macrophage debris together. This proved effective in clumping debris together and allowing more cells to disperse across the coverslip. But unfortunately it seemed that small portions of macrophage debris bound to the

surface of the cryptococcal cells making the whole cell fluoresce, it also appeared to make the capsule partially visible (Figure 7).

One possible way to get round this excess fluorescence would be to treat the lysate with a low concentration of DNase to remove background fluorescence. Although caution would have to be taken to not affect the nuclear material in *C. neoformans* cells. To determine this, one could undertake an experiment where the concentration of DNase required to effect *C. neoformans* nuclear material, prior to infection, is determined. Then the use of a concentration of DNase lower than determined amount could be applied to the lysates to remove background fluorescence without effecting fungal cells.

Vector shield infused DAPI unfortunately failed to stain cryptococci under normal conditions, but did stain the macrophage debris in the fixed lysate. While it is disappointing, this could be attributed to the DAPI vector shield being out of date. This would be interesting to use in future studies.

4.2 Macrophage lysate incubations

While the enlarged cell morphology was not observed in the SF-DMEM or macrophage lysate in any of the strains examined, all strains showed altered cell morphologies after prolonged incubation in the macrophage lysate. After 6-7 days both the H99 and PLB1^{rec} cells appeared stressed in the lysate and looked like they may be lysing (Figure 9), but this was not observed in Δ PLB1 cells incubated in macrophage lysate, nor in strains incubated in SF-DMEM. To look at whether this persistence was due to a slower growth of Δ PLB1 cells, they were observed after 10 days of incubation, and Δ Plb1 cells did not have the same stressed morphology as

H99 cells in EoM. This suggests that the knockout of Δ PLB1 may have a beneficial effect when incubating in macrophage lysate. While this is interesting, cell viability was not measured directly, and it is unknown whether these cells apparently lysing cells were dead or viable. Viability could be tested directly with trypan blue exclusion, which has been used previously to check cryptococcal cell viability (Byrnes III *et al.*, 2010).

To indirectly measure cell viability CFUs were measured every day during the incubation. This appeared to show that on day 7, CFUs reached their highest levels for almost all strains in all conditions, which would suggest that these stressed cells are still viable. During the measurement of cell diameter it was surprising to observe that Δ PLB1 knockout cells, in macrophage lysate predominantly, had with projections jutting from the surface that do not appear to be buds (Figure 10). These cells appear to be similar to previously described pseudohyphae (Lee *et al.*, 2012). Pseudohyphae have been observed in human lung tissue, and when incubated in the presence of amoeba. The pseudohyphal morphology has been associated with a survival strategy for host survival and escape (Bava *et al.*, 2008, Gazzoni *et al.*, 2010, Lee *et al.*, 2012). What is interesting to see is that this morphology is regulated, along with other factors implicated in host survival (like titan cells), via the cAMP/PKA pathway. Nutrient starvation, specifically limited ammonium, has been shown to influence a reversible switch between normal and pseudohyphal morphologies (Lee *et al.*, 2012). Even though these cells appear to look similar to pseudohyphal cells, the fact that Δ PLB1 cells have irregular cell shapes during incubation, such as ovoid cells, shrouds doubt that these may be true pseudohyphal cells. This is especially true when GFP-tagged Plb1 appears to localise near buds

(unpublished data). But if these are indeed pseudohyphae it is interesting that they are seen when incubated in macrophage lysate. This could possibly indicate that there may be compounds within macrophages that induce this morphology, and that Plb1 is involved in regulating this.

4.3 Nutrient starvation

To observe whether any of the phenotypes described were due to nutrient starvation, cells were grown in decreasing amounts of YPD broth for 48 hours. The cell diameter was measured before and after the incubation, and optical density at 600nm was measured during the incubation to observe the growth. From the 100% YPD to 1% YPD the mean cell diameter decreases. This can be attributed to cells dividing but then not increasing in size, as they get older due to the lack of nutrients available. As well as the decrease in mean cell diameter, no larger cells (above 8µm) were observed after 48 hours in any condition, nor were any cells with altered morphology i.e., pseudohyphae, were seen. This suggests that nutrient starvation is not the cause of the increase in cell size or change in morphology in the Δ PLB1 strains, but rather an influence of the macrophage itself (with the case of larger cells) or by something produced by them (in pseudohyphae-like cells).

4.4 Flow cytometry

Due to the large amount of background fluorescence, as well as co-localisation of *C. neoformans* cells with macrophage debris, flow cytometry was employed to measure amount nuclear fluorescence against the cell size measure by the forward scatter (FSC). A cut off for cells larger than a FSC of 400 units was chosen. This was due to less than 1% of cells reaching this size in all three strains, before infection. To begin with, post 18 hours infection, in all three strains the proportion of cells above the 400

FSC threshold increases. A greater proportion of cells above the 400 FSC thresholds are found in the Plb1 mutant. This suggests that there is an effect could be due to the Plb1 deficiency, causing cell size to increase during its residency in the macrophage, once phagocytosed. To determine whether this increase was due to the possible formation of titan cells, we chose to look at the nuclear content as well. This is due to previous studies showing that titan cells produced *in vivo* had increase nuclear content, with cells becoming polyploidy (Okagaki *et al.*, 2011). If this is the case for the Plb1 mutants there should be an increase in fluorescence. To determine this, populations observed through the flow cytometry were gated on the amount of fluorescence due to Hoechst staining. In pre-infection populations 98% of cells fluoresced below 10^3 , this was then used as a gate and cells, which fluoresced more than this, are assumed to have more than 'normal' nuclear content. While all populations showed an increase in cells above this threshold, with H99 and PLB1^{rec} having populations 17.7% and 16.4% of the population, the Δ PLB1 population had a dramatic increase with 50.5% of the population being above 10^3 . It would be interesting to carry this out in human PMBC to see if a similar phenomenon would be observed.

If this increase in nuclear content were due to polyploidy, there would be distinctive clustering of cells in the flow cytometry data. One reason for the increased DNA content could be increasing portions of DNA during stressful conditions. Sionov *et al.*, show that during treatment of *C. neoformans* with azoles a disomy of chromosome 1 occurs leading to resistance to the drug, due to duplication of the target of fluconazole and duplication of the exporter of fluconazole. This ability form a disomy of chromosomes may be a reaction to stressful conditions, such as those found in the

macrophage, which may also explain why you see an increase in nuclear content in the H99 and reconstituted strains. But this doesn't explain why there is a dramatic increase in Plb1 knockouts. Giant cells in other fungi, such as *Saccharomyces cerevisiae*, occur through endoreduplication. Endoreduplication is where there is an absent M phase during cell cycle and the genome is duplicated. Budding does not occur, leading to larger than normal cells that are also polyploidy. This has been suggested to involve the Pcl1 homologue in *C. neoformans*, where it interacts with cell cycle regulators like the *C. neoformans* cdc42/cdc42, as well as being involved in localization of neck bud protein Bni4 during budding (Okagaki *et al.*, 2011), where by a down regulation of Pcl103 in *C. neoformans* may lead to less budding and endoreduplication, forming titan cells. While this is a mechanism by which titan cells may form, it is still unclear where Plb1 functions in the formation. After receiving the image that showed GFP tagged Plb1 localizing near budding sites, one could ponder whether Plb1 is involved in budding and disruption of its activity may lead to disrupted cell division under stressful conditions. This may be the cause of the altered morphologies seen in the macrophage lysate, where Plb1 mutants appeared to be deficient in budding and produced ovoid cells, as well as cells which appear to have never completed budding.

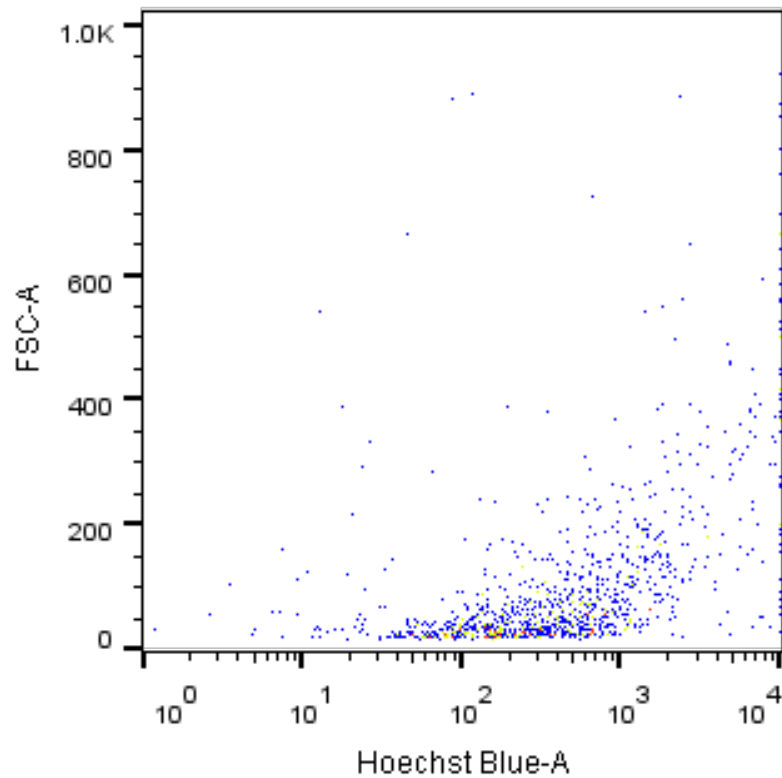
5.0 Conclusions

While these results cannot be used to definitively answer whether phospholipase B is involved in the regulation of titan cell formation. It is interesting to note that, upon deletion of Plb1, cell size of the cryptococci changes after infection, when compared to that of the H99 parental strain. To add to this, the fact that these larger cells would

appear to have an increased amount of nuclear content, as shown through flow cytometry data, teases with the possibility of these may be related to titan cells. But, this phenotype of could not be replicated in media that has been supplement with macrophage lysate which has been shown to be able to induce titan cells in other studies, suggests that this phenotype in the Plb1 mutant requires phagocytosis of the fungi. Even though the questions proposed at the beginning of the study have not been conclusively answered, this information may help in deciphering the mechanistic route required for the increase in fungal cell size.

6.0 Supplementary figures

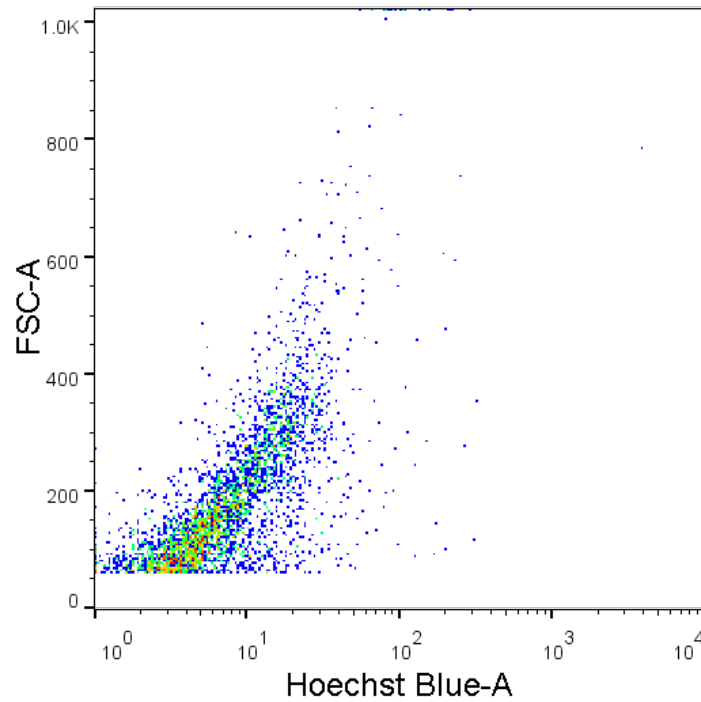
6.1 Supplementary figure 1



Supplementary figure 1: The flow cytometry plot of uninfected macrophage debris.

All post infection plots were gated on this, to remove most of the macrophage debris from the 18 hour sample. Uninfected macrophages were incubated for 18 hours, washed and lysed following the same protocol as those, which were infected with *C. neoformans*.

6.2 Supplementary figure 2



H99 cells 18 Hours Post-infection unstained_d

Supplementary figure 2: Unstained *C. neoformans* H99 18 hours after infection.

Due to the slim possibility of autofluorescence *C. neoformans* H99 were incubated and lysed in the same manner as all other post infections but were not stained with Hoechst 33342 after lysis from the macrophages.

Bibliography

Bava, J., Solari, R., Isla, G., & Troncoso, A. (2008). Atypical forms of *Cryptococcus neoformans* in CSF of an AIDS patient. **The Journal of Infection in Developing Countries**, 2 (5): 403-405

Byrnes III, E.J., Li, W., Lewit, Y., *et al.* (2010) Emergence and pathogenicity of highly virulent *Cryptococcus gattii* genotypes in the northwest United States. **PLoS Pathogens**, 6 (4): e1000850.

Casadevall, A., Cleare, W., Feldmesser, M., *et al.* (1998). Characterization of a murine monoclonal antibody to *Cryptococcus neoformans* polysaccharide that is a candidate for human therapeutic studies. **Antimicrobial Agents and Chemotherapy**, 42(6): 1437-1446.

Casadevall, A., Rosas, A.L. and Nosanchuk, J.D. (2000) Melanin and virulence in *Cryptococcus neoformans*. **Current Opinion in Microbiology**, 3 (4): 354-358.

Casadevall, A. (2010) Cryptococci at the brain gate: break and enter or use a Trojan horse? **The Journal of Clinical Investigation**, 120 (5): 1389-1392.

Chaka, W., Verheul, A.F., Vaishnav, V.V., *et al.* (1997) Induction of TNF-alpha in human peripheral blood mononuclear cells by the mannoprotein of *Cryptococcus neoformans* involves human mannose binding protein. **Journal of Immunology**, 159 (6): 2979-2985.

Chayakulkeeree, M., Johnston, S.A., Oei, J.B., *et al.* (2011) SEC14 is a specific requirement for secretion of phospholipase B1 and pathogenicity of *Cryptococcus neoformans*. **Molecular Microbiology**, 80 (4): 1088-1101.

Chen, S.C., Wright, L.C., Santangelo, R.T., *et al.* (1997) Identification of extracellular phospholipase B, lysophospholipase, and acyltransferase produced by *Cryptococcus neoformans*. **Infection and Immunity**, 65 (2): 405-411.

Chrisman, C.J., Albuquerque, P., Guimaraes, A.J., *et al.* (2011) Phospholipids trigger *Cryptococcus neoformans* capsular enlargement during interactions with amoebae and macrophages. **PLoS Pathogens**, 7 (5): e1002047.

Chrisman, C.J., Alvarez, M. and Casadevall, A. (2010) Phagocytosis of *Cryptococcus neoformans* by, and nonlytic exocytosis from, *Acanthamoeba castellanii*. **Applied and Environmental Microbiology**, 76 (18): 6056-6062.

Cogliati, M. (2013) Global molecular epidemiology of *Cryptococcus neoformans* and *Cryptococcus gattii*: an atlas of the molecular types. **Scientifica**, 2013.

Crabtree, J.N., Okagaki, L.H., Wiesner, D.L., *et al.* (2012) Titan cell production enhances the virulence of *Cryptococcus neoformans*. **Infection and Immunity**, 80 (11): 3776-3785.

Doering, T., Nosanchuk, J., Roberts, W., *et al.* (1999) Melanin as a potential cryptococcal defence against microbicidal proteins. **Medical Mycology**, 37 (3): 175-181.

Dromer, F., Gueho, E., Ronin, O., *et al.* (1993) Serotyping of *Cryptococcus neoformans* by using a monoclonal antibody specific for capsular polysaccharide. **Journal of Clinical Microbiology**, 31 (2): 359-363.

Eisenman, H.C., Casadevall, A. and McClelland, E.E. (2007) New insights on the pathogenesis of invasive *Cryptococcus neoformans* infection. **Current Infectious Disease Reports**, 9 (6): 457-464.

Emmons, C.W. (1955) Saprophytic sources of *Cryptococcus neoformans* associated with the pigeon (*Columba livia*). **American Journal of Epidemiology**, 62 (3): 227-232.

Ganendren, R., Carter, E., Sorrell, T., *et al.* (2006) Phospholipase B activity enhances adhesion of *Cryptococcus neoformans* to a human lung epithelial cell line. **Microbes and Infection**, 8 (4): 1006-1015.

Gazzoni, A. F., Oliveira, F. D. M., Salles, E. F., *et al.*, (2010). Unusual morphologies of *Cryptococcus spp.* in tissue specimens: report of 10 cases. **Revista do Instituto de Medicina Tropical de São Paulo**, 52(3), 145-149.

Ghannoum, M.A. (2000) Potential role of phospholipases in virulence and fungal pathogenesis. **Clinical Microbiology Reviews**, 13 (1): 122-43, table of contents.

Ghannoum, M.A. and Rice, L.B. (1999) Antifungal agents: mode of action, mechanisms of resistance, and correlation of these mechanisms with bacterial resistance. **Clinical Microbiology Reviews**, 12 (4): 501-517.

Goldman, D., Lee, S.C. and Casadevall, A. (1994) Pathogenesis of pulmonary *Cryptococcus neoformans* infection in the rat. **Infection and Immunity**, 62 (11): 4755-4761.

Goldman, D.L., Khine, H., Abadi, J., *et al.* (2001) Serologic evidence for *Cryptococcus neoformans* infection in early childhood. **Pediatrics**, 107 (5): E66.

Griese, M. (1999) Pulmonary surfactant in health and human lung diseases: state of the art. **European Respiratory Journal**, 13 (6): 1455-1476.

Hershkovitz, I., Donoghue, H.D., Minnikin, D.E., *et al.* (2008) Detection and molecular characterization of 9000-year-old *Mycobacterium tuberculosis* from a Neolithic settlement in the Eastern Mediterranean. **PloS One**, 3 (10): e3426.

Hill, J.O. (1992) CD4+ T cells cause multinucleated giant cells to form around *Cryptococcus neoformans* and confine the yeast within the primary site of infection in the respiratory tract. **The Journal of Experimental Medicine**, 175 (6): 1685-1695.

Ikeda, R., Sugita, T., Jacobson, E.S., *et al.* (2003) Effects of melanin upon susceptibility of *Cryptococcus* to antifungals. **Microbiology and Immunology**, 47 (4): 271-277.

Johnston, S.A. and May, R.C. (2013) *Cryptococcus* interactions with macrophages: evasion and manipulation of the phagosome by a fungal pathogen. **Cellular Microbiology**, 15 (3): 403-411.

Jones, P.M., Turner, K.M., Djordjevic, J.T., *et al.* (2007) Role of conserved active site residues in catalysis by phospholipase B1 from *Cryptococcus neoformans*. **Biochemistry**, 46 (35): 10024-10032.

Jones, P.M., Turner, K.M., Djordjevic, J.T., *et al.* (2007) Role of conserved active site residues in catalysis by phospholipase B1 from *Cryptococcus neoformans*. **Biochemistry**, 46 (35): 10024-10032.

Kechichian, T.B., Shea, J. and Del Poeta, M. (2007) Depletion of alveolar macrophages decreases the dissemination of a glucosylceramide-deficient mutant of *Cryptococcus neoformans* in immunodeficient mice. **Infection and Immunity**, 75 (10): 4792-4798.

Kozel, T.R. and Pfrommer, G.S. (1986) Activation of the complement system by *Cryptococcus neoformans* leads to binding of iC3b to the yeast. **Infection and Immunity**, 52 (1): 1-5.

Kronstad, J.W., Attarian, R., Cadieux, B., *et al.* (2011) Expanding fungal pathogenesis: *Cryptococcus* breaks out of the opportunistic box. **Nature Reviews Microbiology**, 9 (3): 193-203.

Kwon-Chung, K. (1998) Gene disruption to evaluate the role of fungal candidate virulence genes. **Current Opinion in Microbiology**, 1 (4): 381-389.

Lee, S. C., Phadke, S., Sun, S., & Heitman, J. (2012). Pseudohyphal Growth of *Cryptococcus neoformans* is a Reversible Dimorphic Transition in Response to

Ammonium That Requires Amt1 and Amt2 Ammonium Permeases. **Eukaryotic cell**, 11 (11): 1391-1398.

Lin, X. and Heitman, J. (2006) The biology of the *Cryptococcus neoformans* species complex. **Annual Review Microbiology**, 60 69-105.

Lin, X., Hull, C.M. and Heitman, J. (2005) Sexual reproduction between partners of the same mating type in *Cryptococcus neoformans*. **Nature**, 434 (7036): 1017-1021.

Ma, H., Croudace, J.E., Lammas, D.A., *et al.* (2006) Expulsion of live pathogenic yeast by macrophages. **Current Biology**, 16 (21): 2156-2160.

Maruvada, R., Zhu, L., Pearce, D., *et al.* (2012) *Cryptococcus neoformans* phospholipase B1 activates host cell Rac1 for traversal across the blood–brain barrier. **Cellular Microbiology**, 14 (10): 1544-1553.

Matsui, H., Ito, T., and Ohnishi, S. (1983). Phagocytosis by macrophages. III. Effects of heat-labile opsonin and poly (L-lysine). **Journal of Cell Science**, 59 (1): 133-143

Metin, B., Findley, K. and Heitman, J. (2010) The mating type locus (MAT) and sexual reproduction of *Cryptococcus heveanensis*: insights into the evolution of sex and sex-determining chromosomal regions in fungi. **PLoS Genetics**, 6 (5): e1000961.

Nielsen, K., Cox, G.M., Wang, P., *et al.* (2003) Sexual cycle of *Cryptococcus neoformans* var. *grubii* and virulence of congenic α and α isolates. **Infection and Immunity**, 71 (9): 4831-4841.

Okagaki, L.H., Strain, A.K., Nielsen, J.N., *et al.* (2010) Cryptococcal cell morphology affects host cell interactions and pathogenicity. **PLoS Pathogens**, 6 (6): e1000953.

Okagaki, L.H. and Nielsen, K. (2012) Titan cells confer protection from phagocytosis in *Cryptococcus neoformans* infections. **Eukaryotic Cell**, 11 (6): 820-826.

Okagaki, L.H., Wang, Y., Ballou, E.R., *et al.* (2011) Cryptococcal titan cell formation is regulated by G-protein signaling in response to multiple stimuli. **Eukaryotic Cell**, 10 (10): 1306-1316.

Oliveira, D.L., Freire-de-Lima, C.G., Nosanchuk, J.D., *et al.* (2010) Extracellular vesicles from *Cryptococcus neoformans* modulate macrophage functions. **Infection and Immunity**, 78 (4): 1601-1609.

O'Meara, T.R. and Alspaugh, J.A. (2012) The *Cryptococcus neoformans* capsule: a sword and a shield. **Clinical Microbiology Reviews**, 25 (3): 387-408.

Park, B.J., Wannemuehler, K.A., Marston, B.J., *et al.* (2009) Estimation of the current global burden of cryptococcal meningitis among persons living with HIV/AIDS. **AIDS**, 23 (4): 525-530.

Perfect, J.R., Dismukes, W.E., Dromer, F., *et al.* (2010) Clinical practice guidelines for the management of cryptococcal disease: 2010 update by the infectious diseases society of America. **Clinical Infectious Diseases**, 50 (3): 291-322.

Ryoyama, K., Nomura, T. and Nakamura, S. (1993) Inhibition of macrophage nitric oxide production by arachidonate-cascade inhibitors. **Cancer Immunology, Immunotherapy**, 37 (6): 385-391.

Santangelo, R., Zoellner, H., Sorrell, T., *et al.* (2004) Role of extracellular phospholipases and mononuclear phagocytes in dissemination of cryptococcosis in a murine model. **Infection and Immunity**, 72 (4): 2229-2239.

Shibuya, K., Hirata, A., Omuta, J., *et al.* (2005) Granuloma and cryptococcosis. **Journal of Infection and Chemotherapy**, 11 (3): 115-122.

Siafakas, A.R., Sorrell, T.C., Wright, L.C., *et al.* (2007) Cell wall-linked cryptococcal phospholipase B1 is a source of secreted enzyme and a determinant of cell wall integrity. **The Journal of Biological Chemistry**, 282 (52): 37508-37514.

Siafakas, A.R., Wright, L.C., Sorrell, T.C., *et al.* (2006) Lipid rafts in *Cryptococcus neoformans* concentrate the virulence determinants phospholipase B1 and Cu/Zn superoxide dismutase. **Eukaryotic Cell**, 5 (3): 488-498.

Simmer M. (2003) A Peach of a pathogen: *Cryptococcus neoformans*. **The Science of Creative Quarterly**, (8).

Sionov, E., Lee, H., Chang, Y.C., *et al.* (2010) *Cryptococcus neoformans* overcomes stress of azole drugs by formation of disomy in specific multiple chromosomes. **PLoS Pathogens**, 6 (4): e1000848.

Smith, L.M. and May, R.C. (2013) Mechanisms of microbial escape from phagocyte killing. **Biochemical Society Transactions**, 41 (2): 475-490.

Stano, P., Williams, V., Villani, M., *et al.* (2009) App1: an antiphagocytic protein that binds to complement receptors 3 and 2. **Journal of immunology**, 182 (1): 84-91.

Steenbergen, J.N., Nosanchuk, J.D., Malliaris, S.D., *et al.* (2003) *Cryptococcus neoformans* virulence is enhanced after growth in the genetically malleable host *Dictyostelium discoideum*. **Infection and Immunity**, 71 (9): 4862-4872.

Steenbergen, J.N., Shuman, H.A. and Casadevall, A. (2001) *Cryptococcus neoformans* interactions with amoebae suggest an explanation for its virulence and intracellular pathogenic strategy in macrophages. **Proceedings of the National Academy of Sciences of the United States of America**, 98 (26): 15245-15250.

Tucker, S.C. and Casadevall, A. (2002) Replication of *Cryptococcus neoformans* in macrophages is accompanied by phagosomal permeabilization and accumulation of vesicles containing polysaccharide in the cytoplasm. **Proceedings of the National Academy of Sciences of the United States of America**, 99 (5): 3165-3170.

Vermes, A., Guchelaar, H.J. and Dankert, J. (2000) Flucytosine: a review of its pharmacology, clinical indications, pharmacokinetics, toxicity and drug interactions. **The Journal of Antimicrobial Chemotherapy**, 46 (2): 171-179.

Voelz, K. and May, R.C. (2010) Cryptococcal interactions with the host immune system. **Eukaryotic Cell**, 9 (6): 835-846.

Wang, Y. and Casadevall, A. (1994) Growth of *Cryptococcus neoformans* in presence of L-dopa decreases its susceptibility to amphotericin B. **Antimicrobial Agents and Chemotherapy**, 38 (11): 2648-2650.

Wright, L.C., Santangelo, R.M., Ganendren, R., *et al.* (2007) Cryptococcal lipid metabolism: phospholipase B1 is implicated in transcellular metabolism of macrophage-derived lipids. **Eukaryotic Cell**, 6 (1): 37-47.

Zaragoza, O., García-Rodas, R., Nosanchuk, J.D., *et al.* (2010) Fungal cell gigantism during mammalian infection. **PLoS Pathogens**, 6 (6): e1000945.

Project 2

A study into proteins proposed to be involved
in C-di-GMP signalling and predation from
Bdellovibrio bacteriovorus – Bd1483, Bd1996,
Bd2538 and Bd3100

7.0 Introduction

Bdellovibrio bacteriovorus is a Gram negative bacterium of the δ -proteobacterium class (Sockett 2009). Most notable about the species is its predatory lifestyle, whereby it preys upon other Gram-negative bacterium, notably pathogenic species like *Escherichia coli* and *Salmonella enterica* (Sockett 2009, Atterbury *et al.*, 2011 Dwidar *et al.*, 2012). *B. bacteriovorus* is found ubiquitously throughout the environment from soil to sea to the mammalian intestine (Schwudke *et al.*, 2011, Hopley 2005, Sockett 2009, Iebba *et al.*, 2013). Its highly motile nature allows it to move through these environments in search for prey, other Gram negative bacterium (Lambert *et al.*, 2006, Lambert *et al.*, 2011). It goes about this by the use of both gliding and flagella motility on/through solid and liquid environments, respectively (Lambert *et al.*, 2006, Lambert *et al.*, 2011). Gliding motility, in particular, has been implicated in the predation and escape from prey on solid surfaces (Lambert *et al.*, 2011, Hopley *et al.*, 2012). This predation, in turn, has been shown to be dependent on cyclic-di-guanosine monophosphate (C-di-GMP) signalling (Hopley *et al.*, 2012). C-di-GMP signalling has known roles in decision making in bacterial lifestyles, the mechanisms of how this decision making occurs or how predation of the prey is initiated remains to be understood (Krasteva *et al.*, 2012). In view of this, this study will attempt to shine some light on the mediators of C-di-GMP signalling in *B. bacteriovorus*, through the techniques of protein biochemistry and crystallography. Hopefully deciphering the roles of the lipid binding protein (Bd2538), von Willebrand domain protein (Bd1483) and suspected GYF-PilZ domain proteins (Bd1996 and Bd3100) in *Bdellovibrio* prey recognition and C-di-GMP signalling that lead to prey

invasion. This information will then be useful in producing a hypothesis for this important part of the *Bdellovibrio* lifecycle.

7.1 Possible uses of *Bdellovibrio* spp.

The discovery of *Bdellovibrio* in the early sixties led to a great interest in this interesting predatory bacterium, leading to the coined 'golden age', which has since led to a slowing down of research, albeit a few dedicated individuals. (Stolp and Petzold, 1962, Stolp and Starr, 1963, Sockett *et al.*, 2004, Sockett 2009) Recently, there has been a great resurgence in interest with the bacterium with the emergence of multidrug resistant bacteria, leading to the discussion as to whether *Bdellovibrio* could be the first 'living antibiotic'. Due to resistance to predation being rarely seen in *E. coli* prey, and then only transient (Sockett 2009, Dwidar *et al.*, 2011, Lerner *et al.*, 2012 Kadouri *et al.*, 2013).

Although there have been a few limitations noted; these include an optimal temperature for growth of 29°C, and its apparent aerobic way of life (Varon and Shilo, 1968, Sockett 2009, Atterbury *et al.*, 2011). Both of these have shown not to be a great hurdle, as *Bdellovibrio* have been isolated from the faeces of humans overcoming the high temperatures and anaerobic environment found in the gut (although *Bdellovibrio* have developed ways to respire anaerobically, such is the environment inside the bdelloplast) (Sockett *et al.*, 2004, Atterbury *et al.*, 2011 Iebba *et al.*, 2013). As well as this, its safety has been brought into question due to similar predatory α -proteobacterium that have been shown to invade mitochondria of parasitic ticks, and if the presence of *Bdellovibrio* will have negative effects on the microbiota of the gut or induce an inflammatory response in humans (Rendulic *et al.*, 2004, Sacchi *et al.*, 2004). While experiments on the effects of *Bdellovibrio* treatment

directly on mammalian hosts have not been undertaken, Atterbury *et al.*, 2011 undertook a study using chickens as a surrogate. *Salmonella* fed chickens showed reduced levels of *Salmonella* in the gut and faeces after *Bdellovibrio* introduction. Chickens that were not fed *Salmonella* were also treated with *Bdellovibrio*, while the overall gut microbiota changed after 2 days there were no adverse health effects (Atterbury *et al.*, 2011). To add to the evidence that *Bdellovibrio* do not harm hosts, by changing the overall gut microbiota, a study by Iebba *et al.*, 2013, showed a relationship between the absence of *Bdellovibrio* in the intestine of patients with inflammatory bowel disease and celiac disease. While this is not conclusive these studies provide tantalizing prospects that the use of *Bdellovibrio* as a therapeutic probiotic may treat a variety of digestive diseases.

7.2 The lifecycle of host dependent *B. bacteriovorus*

B. bacteriovorus tracks down its prey through chemotactic responses to amino acids and biofilms (with *B. bacteriovorus* HD100 containing 20 genes required for chemotaxis) (LaMarre *et al.*, 1977, Sockett 2009). It was previously believed that *Bdellovibrio* entered prey by 'punching' themselves into prey via their fast flagella motility, this has been disproven with flagella motility mutants still being able to predate, if placed upon their prey (Sockett, 2009). *Bdellovibrio* attachment, to prey, occurs from the non-flagella pole of the bacterium (figure 1), with this attachment being shown to be transient and reversible (Rendulic *et al.*, 2004, Sockett, 2009).

While it is unknown what mediates attachment, but through fluorescently tagged microscopy proteins have been shown to localize at the non-flagella pole. These include proteins involved in C-di-GMP signalling that are known to be up regulated

and secreted during attachment (figure 1) (Hobley *et al.*, 2012, Capeness *et al.*, 2013, Milner *et al.*, 2014).

Once attached to the prey cell, *Bdellovibrio* must enter and pass through the outer membrane (figure 2). It has now been discovered that a cocktail of degradative enzymes are required (Milner *et al.*, 2014). Although the mechanism of attachment has not been fully discovered, it has been shown that type IV pili play a major role in this attachment. Similar to some pathogenic bacteria, that use type IV pili to attach to the host structures. Type IV pili retractable fibre knockouts were shown to be unable to predate upon fluorescently tagged prey, even when placed a top of them (Craig *et al.*, 2004, Evans *et al.*, 2007, Hobley, *et al.*, 2012, Milner *et al.*, 2014).

Invasion across the outer membrane takes 2 minutes to complete, and occurs through a pore that is smaller to the diameter of invading *Bdellovibrio* (Sockett 2009). The formation of the initial localised pore still remains uncharacterised, as does how *Bdellovibrio* reseals the hole once it has entered the periplasmic space. Entry has been suggested to occur through secreted twitching pili that attach to the peptidoglycan of the prey cell and provide an anchorage point to drag the *Bdellovibrio* into the prey, and then the flagellum is shed (figure 2) (Rendulic *et al.*, 2004, Evans *et al.*, 2007, Lerner *et al.*, 2012). As *Bdellovibrio* begins to break down the host macromolecules it begins expression of membrane transporters that are believed to be involved in the import of prey nutrients into the predatory cell (Beck *et al.*, 2004, Rendulic *et al.*, 2004). While inside the bdelloplast, *Bdellovibrio* begin secretion of a multitude of hydrolytic enzymes required for prey degradation (Lerner *et al.*, 2012). Of these, certain transpeptidases have been shown to be involved in prey rounding. Bd3459 and Bd0816 are 'penicillin binding protein 4' (PBP4) like DD-

endo/carboxytranspeptidase, which are often used in maintenance of cell shape and division. Upon invasion, both of these proteins are up regulated and are involved in prey rounding, by breaking the peptide bridges that link the strands of peptidoglycan (PG) together, loosening the PG (Lerner *et al.*, 2012). These proteins have also been implicated in the preventing 'tailgating' *Bdellovibrio* from entering the invaded cell. This was suggested to be due to the softening of the PG, removing a sturdy anchorage point for other *Bdellovibrio* to invade cell (Lerner *et al.*, 2012).

As the *Bdellovibrio* resides in the bdelloplast it begins to replicate its DNA using host components (Sockett, 2009). But, the genome of prey is, more often than not, insufficient to provide the amount of nucleotides required for the progeny (Sockett, 2009). This means that nitrogen-containing macromolecules must be catabolised for the production of nucleotides (Rosson and Rittenburg 1981, Sockett 2009). Replication occurs without septation, initially, forming a long filamentous cell in the bdelloplast. Once resources have been exhausted in the predated cell the long filamentous cell undergoes septation, which leads to odd and even numbers of *Bdellovibrio* progeny (figure 2). When the progeny have septated, flagella motility is induced and a burst of hydrolytic enzymes degrade the rest of the PG shell and the progeny swim away in attack phase looking for their next prey (Rendulic *et al.*, 2004). This whole process from invasion to escape takes around 4 hours (Sockett, 2009) (figure 2).

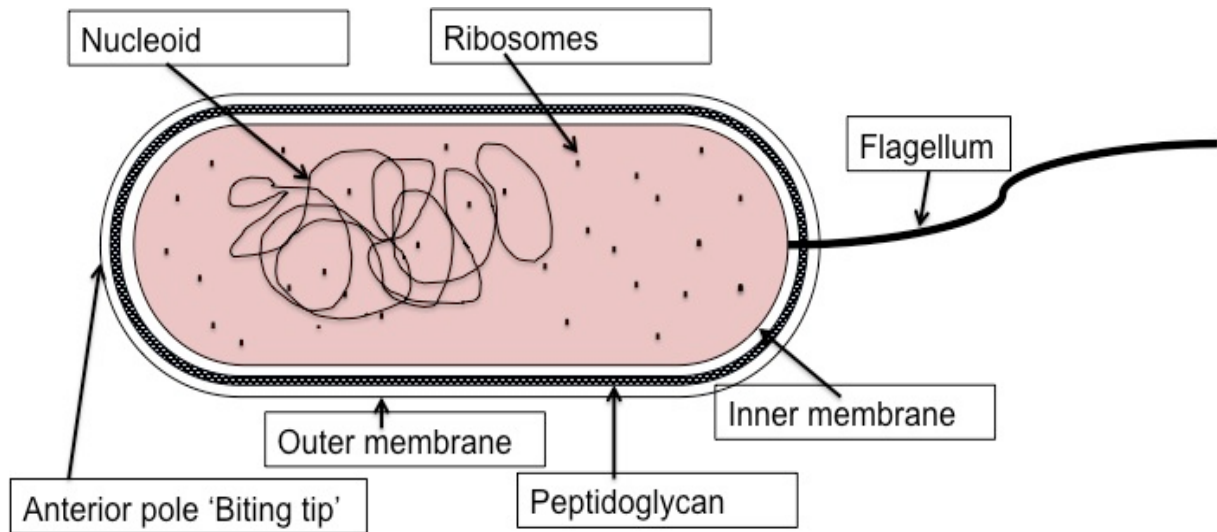


Figure 1. Cartoon structure of a *Bdellovibrio bacteriovorus* cell.
 A cartoon structure of a *Bdellovibrio bacteriovorus* cell, noting the anterior biting tip where recognition and penetration of prey occurs and secretion of and localisation C-di-GMP signalling proteins localise. At the posterior end the single flagellum required for locomotion, is depicted

7.2.1 Host independent strains

Gene deletions within certain amino acid synthesis pathways have been discovered lending more credence to *Bdellovibrio*'s obligate predatory lifestyle (Rendulic *et al.*, 2004, Sockett 2009). But host independent strains (HI) have been cultured on extremely nutrient rich peptone-yeast (PY) media, which provide the bacterium with the nutrients it cannot synthesise itself (Rendulic *et al.*, 2004, Sockett 2009). One strain has been shown to live both predatory and anexically (host independent). Termed Tiberius, due to its discovery from the River Tiber, Italy, this strain has acquired host independency that is distinct from the more common mutations in proteins from the *hit* locus, namely bd0108 (bdt0101 in Tiberius), which are observed

in a laboratory setting (Cotter and Thomashow, 1992, Rendulic *et al.*, 2004, Hobbey *et al.*, 2012a, Capeness *et al.*, 2013). Proteins in the *hit* locus have been shown to be involved in pilus regulation, with knockouts of bd0108 lacking pili (Rendulic *et al.*, 2004, Capeness *et al.*, 2013). Mutations in this locus occur in 89% of lab HI strains (Capeness *et al.*, 2013). This ability to live predatory and anexically has been attributed to the high levels of organic pollutants, faecal waste, and rich variety of prey bacteria in the river (Hobbey *et al.*, 2012a). As well as the rich environment from which it came from, this host independent phenotype has been linked to lateral gene transfer from 'sub-optimal' prey, such as marine bacterium, which are found in the river Tiber, along with its standard laboratory prey *E. coli* and *S. enterica* (Hobbey *et al.*, 2012a).

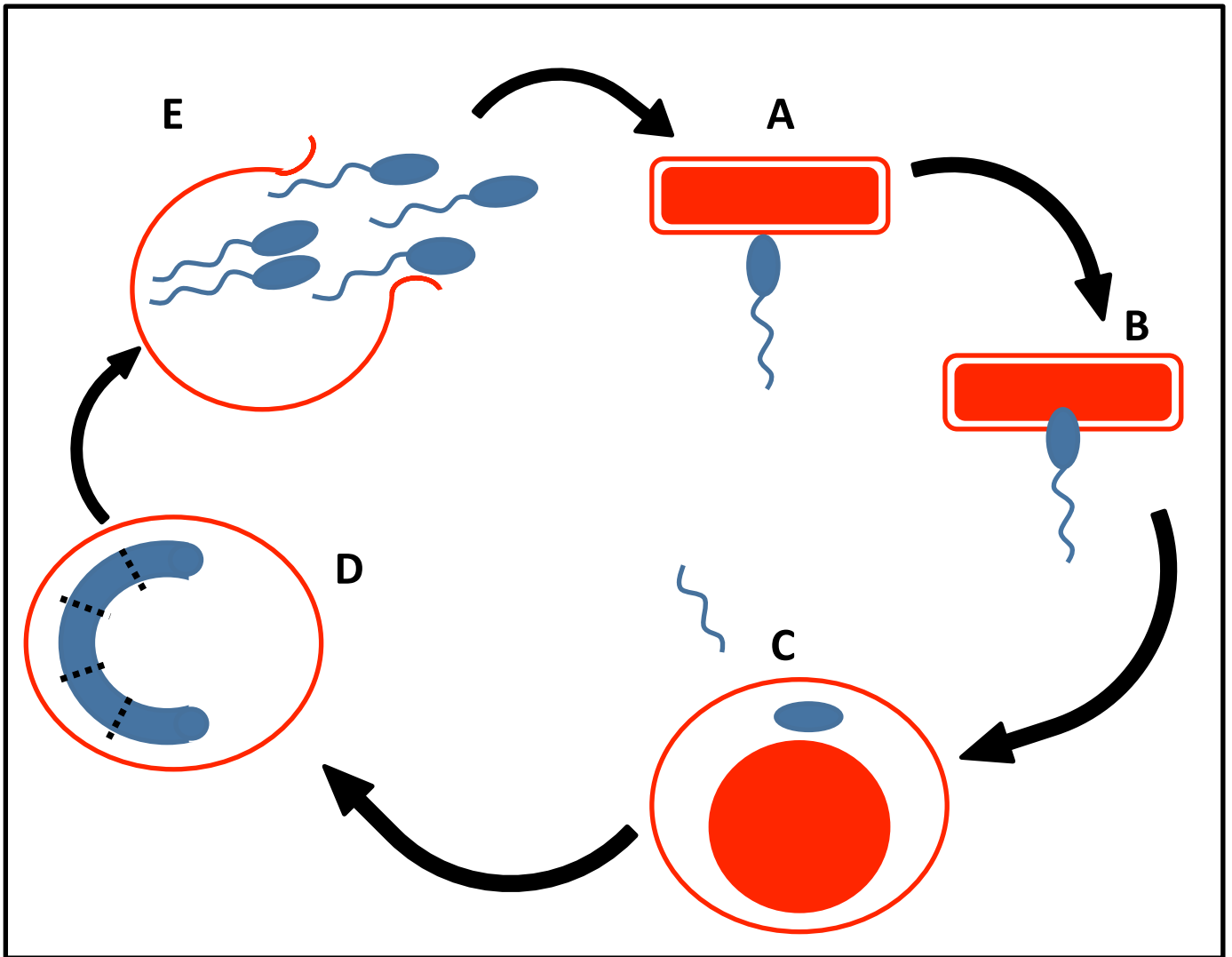


Figure 2. The lifecycle of host dependent *Bdellovibrio bacteriovorus*.

A) Attachment to the prey cell (Red) by attack phase *B. bacteriovorus* (Blue). B) Invasion into the periplasmic space due to pilus retraction. C) The release of hydrolytic enzymes modifies the host cell forming the bdelloplast. D) Replication occurs, forming a long filamentous *Bdellovibrio* that divides by septation. E) Flagella motility is induced and the progeny lyse the bdelloplast in attack phase searching for Gram negative prey.

7.3 Cyclic di-GMP signalling

7.3.1 A brief introduction

First discovered as a regulator of cellulose synthase in *Gluconacetobacter xylinus*, cyclic di-guanosine monophosphate (C-di-GMP) has been shown to be an important signalling molecule for many bacterial species across many different bacterial lineages (Ross *et al.*, 1987, Weinhouse *et al.*, 1995, Romling *et al.*, 2005, Amikan *et al.*, 2006, Jenal and Malone, 2006). Production of C-di-GMP in bacteria is catalysed by a group of proteins known as diguanylate cyclases. Proteins of this class contain a GGDEF motif and, as with adenylate cyclases, dimerisation is required for fully functional activity (Romling *et al.*, 2005, Romling and Amikan 2006). These GGDEF-containing proteins are also under feedback inhibition with a conserved RxxD motif, termed 'I sites'; these bind C-di-GMP and inhibit the formation of c-di-GMP (Jenal and Malone, 2005, Schirmer and Jenal, 2009, Krasteva *et al.*, 2012, Hogley *et al.*, 2012). While no GGDEF containing proteins have been found in eukaryotic genomes, showing the lack of this signalling pathway, there remains receptors of this molecule, presumably used by the innate immune system as recognition of bacterial infection (Romling *et al.*, 2005 Krasteva *et al.*, 2012). Break down of C-di-GMP is carried out by phosphodiesterases containing EAL and HD-GYP domains. EAL domains are highly specific phosphodiesterases that require either Mg²⁺ or Mn²⁺ as cofactors (Schirmer and Jenal, 2009, Krasteva *et al.*, 2012). These domains are understood to be regulated through accessory domains that catalyse the degradation of C-di-GMP to pGpG that can then be further degraded to GMP (Romling *et al.*, 2005, Schirmer and Jenal, 2009). The other motif involved in the degradation of C-di-GMP is HD-GYP. Only recently a few HD-GYP domains have been structurally

deciphered, including an unconventional HD-GYP domain containing protein from *B. bacteriovorus* (Lovering *et al.*, 2011, Bellini *et al.*, 2014). These studies have shown that this HD-GYP is an iron binding protein as well as showing that bacterial HD-GYFs can be grouped into two families of proteins with bi- or tri- nuclear metal binding centres (Lovering *et al.*, 2011, Bellini *et al.*, 2014).

PilZ domain proteins were first observed in cellulose synthase from *G. xylinus*. PilZ domains follow a phylogenetically similar distribution to C-di-GMP metabolising enzymes (Weinhouse *et al.*, 1995, Amikan and Galperin, 2006). PilZ binding domains are characterised by 6-antiparallel β barrel strands which contain conserved C-di-GMP binding sequences, RxxxR and D/NxSxxG, located on the N termini of β 2 and β 3 respectively (Krasteva *et al.*, 2012). While PilZ domains recognise C-di-GMP they have many different conformational reorganization upon binding of the nucleotide, as well as changing dimeric states (Krasteva *et al.*, 2012). PilZ domain proteins have been shown to be required for type 4 pili (T4P) formation in *P. aeruginosa*, upon transition to a biofilm forming state. Also, they have been involved in changing motility states, C-di-GMP has been shown to influence gene regulation, often switching on/off genes required for lifestyle choices in bacteria such as *V. cholera* and *P. aeruginosa* (Schirmer and Jenal, 2009, Krasteva *et al.*, 2012). They have also been observed in *M. xanthus* and are required for normal spore formation (Amikan and Galperin, 2006). Along with PilZ domains, degenerate GGDEF domain containing proteins have been implicated as receptors for C-di-GMP (Schirmer and Jenal, 2009, Hogley *et al.*, 2012, Krasteva *et al.*, 2012). Binding is due to the preservation of the C-di-GMP binding I site. These proteins have been implicated in signalling, biofilm formation and motility, of which their role in *B. bacteriovorus* will be

discussed later (Schirmer and Jenal, 2009, Hogley *et al.*, 2012, Krasteva *et al.*, 2012).

7.3.2 What is known of C-di-GMP signalling in *B. bacteriovorus*?

As described previously, C-di-GMP signalling has been shown to be involved in changes of lifestyle for many bacteria and it is becoming apparent that this is the case for *B. bacteriovorus* as well. This can be inferred from a genomic context, as from its 3.8Mbp genome it has been shown to have a high C-di-GMP 'intelligence' (Hogley *et al.*, 2012). Sequencing and bioinformatics data show 15 predicted PilZ domain containing proteins, including Bd3100 and Bd1996, are associated with C-di-GMP signalling (Amikan and Galperin, 2006). *B. bacteriovorus* HD100 also contains 5 GGDEF containing proteins, 4 of which are functional C-di-GMP producing enzymes and one with a degenerate GGDEF motif that has been shown to be a receptor for C-di-GMP signalling (Hogley *et al.*, 2012). As far as ceasing the signal induced by C-di-GMP, *B. bacteriovorus* HD100 contains 7 phosphodiesterases, 1 EAL and 6 HD-GYP proteins. An overall diagram for C-di-GMP signalling in *B. bacteriovorus* has been summarised in figure 3.

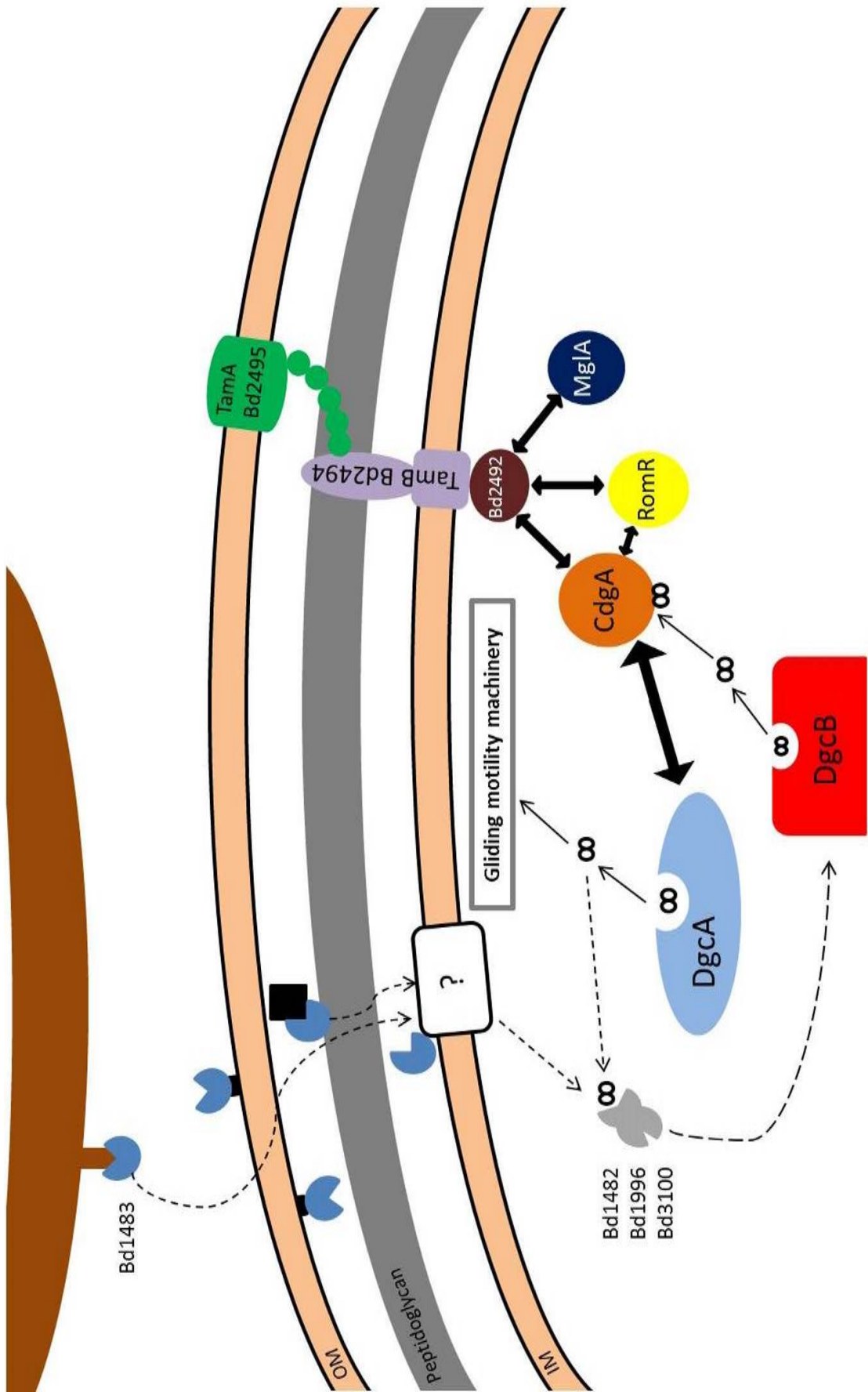
Studies undertaken by Hogley *et al.*, 2012 have shown that knocking out 4 of the five GGDEF domain proteins, termed DgcA-C (**d**iguanylyl **c**yclase) and CdgA (the degenerate GGDEF domain with predicted receptor activity), produce visible phenotypes in *B. bacteriovorus*. They also show interesting phenotypes when over expressed in the highly motile *E. coli* strain, MG1655. The fifth GGDEF, DgcD, showed no phenotype when knocked out in *B. bacteriovorus*, nor when over expressed in *E. coli* (Hogley *et al.*, 2012). This is interesting as this protein is not conserved in the Tiberius strain of *B. bacteriovorus* (Hogley *et al.*, 2012). When over

expressed in *E. coli* MG1655, DgcA-C causes this highly motile strain to become sessile, presumably due to their production of C-di-GMP. This has been shown previously, with pathogenic strains of *E. coli*, to signal a transition to a sessile, biofilm-forming state, which is related to virulence. (Ryan *et al.*, 2006, Hobley *et al.*, 2012, Hu *et al.* 2013). When the degenerate GGDEF, CdgA, is over expressed a motile phenotype in *E. coli* is observed. Presumptively, this due to CdgA binding host C-di-GMP therefore acting as a sink for the signalling molecule (Hobley *et al.*, 2012). In *B. bacteriovorus* the knockout of DgcA produces a phenotype that was immobile, similar to the $\Delta fliC$ mutant, and could predate prey bacteria if placed directly upon them but are unable to induce motility once the prey has become exhausted and end up stuck in the dead prey's shell, even though the exit pore has been formed (Lambert *et al.*, 2006, Hobley *et al.*, 2012). This shows that DgcA is required for gliding motility in *Bdellovibrio* and has been suspected to interact with a PilZ domain containing protein, Bd1482, which is found in a gliding motility operon (figure 3) (Lambert 2011, Luciano *et al.*, 2011, Hobley *et al.*, 2012). DgcB, when knocked out in *B. bacteriovorus*, was shown to produce a phenotype that was non-predatory and could only be grown anexically. Although rare cases have been observed where a suppressed predatory phenotype is observed, which will be important for research use (Hobley *et al.*, 2012). This GGDEF domain is linked to a forkhead domain that is believed to be involved in the signalling and gets activated when DgcB begins to synthesis C-di-GMP, due to active site mutants not rescuing the mutant phenotype (figure 3) (Hobley *et al.*, 2012). Forkhead domains are abundant in eukaryotes and have been associated with regulation of many bacterial processes from cell shape to signal transduction to host-bacterium interactions (Pallen *et al.*, 2002). Due to this it

has been suggested that DgcB signals the cell to start production of hydrolytic enzymes, upon prey biting (Hobley *et al.*, 2012). DgcB has also been implicated in the downstream signalling to CdgA (figure 3). Δ CdgA mutants were grown anexically but later shown to predate, albeit slowly, especially during prey entry (Hobley, *et al.*, 2012). CdgA was also shown to locate at the 'biting' anterior tip of the bacterium (figure 1). This, along with results from Milner *et al.*, 2014 show that CdgA also associates gliding motility machinery proteins, RomR and MglA (figure 3). Both of which associate at the biting tip and are involved in gliding motility in *M. xanthus*, also MglA is required for prey invasion through type 4 pili (T4P) extrusion (Milner *et al.*, 2014).

MglA and RomR, in *M. xanthus*, have been shown to regulate the leading tip for gliding motility via the Frz chemotactic response, but this Frz pathway is missing in *Bdellovibrio* (Milner *et al.*, 2014). So, it is suggested that CdgA is the signal required for RomR and MglA to begin extrusion of the T4P required for prey invasion, this links C-di-GMP with prey invasion through T4P upon stimulation of prey biting as well as C-di-GMP involvement in prey escape, via gliding motility (Hobley, *et al.*, 2012, Milner *et al.*, 2014). MglA has also been associated with invasion through an interaction with a tetratricopeptide repeat (TPR) motif protein, Bd2492, as both knockouts prevent invasion but not attachment (Milner *et al.*, 2014). Adding weight to there proposed roles in T4P extrusion (Milner *et al.*, 2014). The TPR repeat protein interacts with the TamAB transporter system, suggested to secrete proteases and other hydrolytic enzymes for prey invasion/digestion, as well as secretion of extracellular polysaccharides and polyelectrolytes both required for pilus retraction in *M. xanthus* (figure 3) (Milner *et al.*, 2014). TamA is an Omp85 membrane pore that

has been associated with secretion of proteases, auto-transporters and adhesins in *E. coli*. TamB associates with the inner membrane and is co-purified with TamA in *E. coli* (Selkrig *et al.*, 2012). This shows a specific interconnectivity between C-di-GMP and its involvement in gliding motility (DgcA), secretion of hydrolytic (DgcB regulating expression of and its signalling to CdgA) and pilus retraction (CdgA/MglA/RomR/TamAB) (figure3).



∞ – C-di-GMP

Figure 3. A diagram of C-di-GMP signalling in *Bdellovibrio bacteriovorus* at the anterior pole.

Bd1483 (Blue pie), a protein with a vWA domain, is suggested to be involved in prey recognition either by interacting directly with the prey cell or involved in a mediator (black square) responding to the prey cell (brown circle). While it is known that Bd1483 is secreted it is unknown where it localises. So here it has been placed in the periplasm, extracellular milieu and associated with the inner and outer membrane. Signalling due to Bd1483 is predicted to be transmitted by an unknown membrane associated partner (white box), which transmit the signal to the cytoplasmic PilZ/DUF4339 domain proteins (Grey) (Bd1482, Bd1996 and Bd3100). These PilZ/DUF4339 proteins are, in turn, influenced by the cyclic-di-GMP producing protein DgcA (light blue oval), with the DUF4339 domains interacting with downstream signalling proteins, possibly including the GGDEF proteins. C-di-GMP from DgcA is believed to regulate the gliding motility machinery. DgcA has also been shown to directly interact with CdgA (orange circle), which is involved in gliding motility and T4P extrusion, which in turn was shown to be influenced by C-di-GMP synthesised by DgcB (red square). CdgA interacts with RomR (yellow circle), TPR Bd2492 (burgundy circle), and along with MglA (dark blue circle) are believed to regulate the TamAB transporter proteins (purple and green) at the anterior biting pole of the *Bdellovibrio*.

[Figure modified from Hogley *et al.*, 2012 and Milner *et al.*, 2014]

7.4 Proteins of interest for the project

Bd1483, a protein implicated in prey recognition

The interconnectivity of gliding motility, T4P and enzyme secretion still requires the discovery of a stimulus, from prey 'biting' or attachment. This is where Bd1483 has been implicated. Bd1483 is a secreted von Willebrand type a (vWA) domain containing protein (Dori-Bachash *et al.*, 2008, Medina *et al.*, 2008). The signal peptide, required for secretion is found at the N-terminal end, and the vWA domain is found between residues Iso42 and Thr92 (figure 4a). Von WA domains were discovered in eukaryotes and have been implicated in adhesion and complement activation, while in bacteria they have been implicated in platelet aggregation in *Streptococcus* spp (Fitzgerald *et al.*, 2006, Springer, 2006). Von WA domains often have a conserved motif that mediates binding of a divalent cation (Springer 2006). This motif, known as a **Metal-Ion Dependent Adhesion Site (MIDAS)**, is required for ligand binding, and is found in integrins (Springer 2006). Along with their role in cell-cell adhesion, vWA domains have been implicated in the gliding motility and invasive capabilities of the human pathogen *Toxoplasma gondii* (Song *et al.*, 2012, Song and Springer, 2014). In *Bdellovibrio* there is no known external stimuli known to induce invasion through C-di-GMP signalling. Therefore, with Bd1483 being a secreted protein associated with adhesion and gliding motility in other invasive organisms it could be a mediator in the recognition of prey. It may bind directly to components of the prey's outer membrane, or could be involved in the signalling transduction from the 'biting' protein internal signalling, through an, as yet unknown, membrane bound partner. This is suggested because *bd1483* knockout mutants have been shown to be unable to predate upon biofilms (Medina *et al.*, 2008). This signal could be

transmitted to cytoplasmic PilZ-(DUF4339) GYF domain proteins, specifically Bd1482 (expressed within the same operon). This localisation of vWA, PilZ/GYF proteins on the same operon have been replicated elsewhere in the genome, Bd3099 (vWA) Bd3100 (PilZ/GYF). To add to this it has been shown through bacterial two hybrid experiments that Bd3100 interacts with DgcA, the GGDEF domain protein that has been implicated in gliding motility out of the prey (Pers. Comms. Lovering 2014).

Bd1996 and Bd3100, predicted C-di-GMP and polyproline binding proteins

Both Bd3100 and Bd1996 are PilZ domain containing proteins with DUF4339 (domain of unknown function) accessory domains (2 in Bd3100 and 1 in Bd1996) (Figure 4b and 4c). Through protein threading these DUF4339 domains have been shown, to harbour putative glycine-tyrosine-phenylalanine (GYF) domains, which are known to bind polyproline rich sequences (PRS) (Kofler *et al.*, 2005; Ash *et al.*, 2010). They have also been found in *M. xanthus* genes involved in adventurous gliding motility regulation. GYF domains have been attributed to regulating riboswitches and splicing machinery in eukaryotes, specifically in binding of the U5 ribonucleoprotein (Balaji and Aravind, 2007). They contain a conserved W-X-Y-X₆₋₁₁-GPF-X₄-M-X₂-W-X₃-GYF, found in the RAGNYA fold of which other RNA associated binding motifs are found. A minimal consensus sequence of proline-proline-glycine and been shown to be required for GYF binding (Balaji and Aravind, 2007). While many bacterial GYF domains have flanking polyproline residues there are none of these obviously in Bd3100 or Bd1996. GYF domains have been found in numbers across all bacterial lineages, especially α -proteobacteria, but are absent in Archaea (Balaji and Aravind, 2007). Along with this, it is suggested that eukaryotic GYF

domains may have originated from the α -proteobacteria that are the ancestors of modern day mitochondrion (Balaji and Aravind, 2007).

Bd3100 is 275 amino acids long and has a molecular weight of 31.1 kDa. It contains two PilZ, C-di-GMP recognition, domains, spanning Gln16 to Leu60 and Glu95 to Arg138, as well as a DUF4339 (GYF) domain spanning from Arg167 to Thr271 (figure 4B). Bd3100 has been shown to interact with Bd0367 along with being shown to localise to the anterior pole of the cell, through fluorescent tagging (Pers Comms Lovering 2014). Previous attempt to express and purify this protein have led to the formation of inclusion bodies, which solubilisation in chaotropic agent and subsequent refolding have not yielded any soluble product (unpublished data).

Bd1996 is another PilZ domain containing protein, which is 227 amino acids in length with a molecular weight of 25.2 KDa. It contains one N-terminal DUF4339 domain from residue Asp5 to Try43 and the PilZ spanning Arg127 to Arg222 (figure 4C). This has also been shown by fluorescent tagging to localise at the anterior tip of *Bdellovibrio*, along with the homologues Bd3100 and Bd1482 (Pers comm Lovering 2014). This protein has not, to current knowledge, been previously overexpressed in *E. coli*. So, this protein's expression and solubility are unknown.

Bd2538, a predicted lipid binding protein possibly involved with membrane degradation

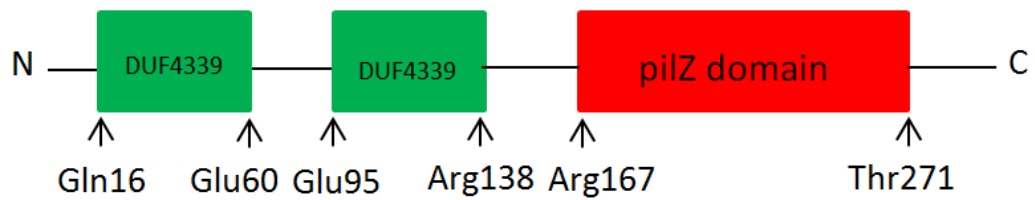
A fourth protein, Bd2538, is a 63 KDa protein that has been shown to contain a DUF2785 domain. Through protein threading this is believed to be a putative TULIP domain protein (figure 4D). TULIP (tubular lipid binding) domain proteins are commonplace in the innate immune systems of humans, being involved in

recognition and scavenging of bacterial lipids, predominantly lipopolysaccharides, as well as being involved in cholesterol metabolism in the blood (Kopec *et al.*, 2011). Recently, TULIP-domain proteins have been implicated in catalysing the movement of lipids from the mitochondria to the endoplasmic reticulum and back (Kopec *et al.*, 2010; Schauder *et al.*, 2014). This possibly implicates Bd2538 in pore formation, with the removal of lipids from the prey outer membrane. As with Bd1483 and Bd1996 there has been no previous work on cloning, overexpression, or purification of this protein.

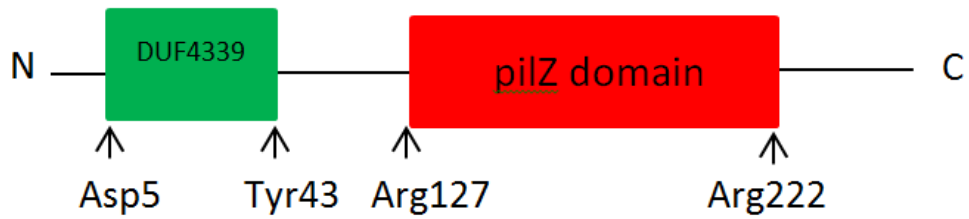
A) Bd1483



B) Bd3100



C) Bd1996



D) Bd2538

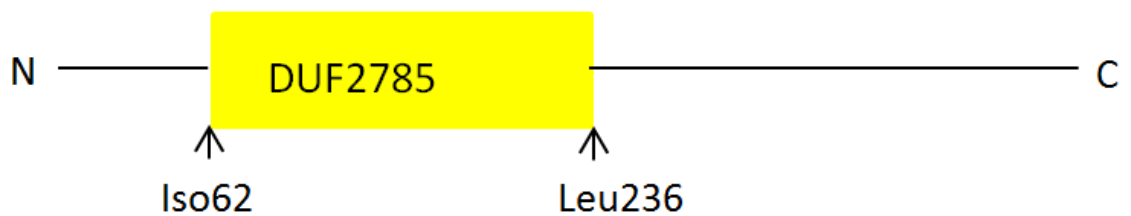


Figure 4. Domain diagrams of the projects investigated: Bd1483, Bd3100, Bd1996 and Bd2538.

A) The domain diagram of Bd1483. The orange domain is predicted to be a von Willebrand domain that has been suggested to be involved recognition and gliding motility in Plasmodium spp.

B) The domain diagram of Bd3100. The 2 N terminal DUF4339 domains (green) have been shown, through protein threading, to be predicted GYF domains, which are known to bind proline rich sequences. The 3rd domain, located towards the C terminus is a predicted PilZ domain (red). These domains have roles in C-di-GMP signalling and are often found in proteins with secondary domains that have a function.

C) The domain diagram of Bd1996. Like Bd3100 it contains an N terminal DUF4339 domain along with a C terminal PilZ domain.

D) The domain diagram of Bd2538. The DUF2785 domain (yellow) has been predicted, through protein threading, to a putative TULIP domain, which are known to bind lipids and could have implications for prey recognition.

7.5 Project aims

The overall aim of this project is to clone, overexpress and purify Bd1483, Bd3100, Bd1996 and Bd2538. With the hope of using these purified recombinant proteins in crystal trials and other biochemical assays. This will hopefully provide us with information on the structure and function of these proteins, which can lead to information on the polyproline binding specificity of Bd3100 and Bd1996 and whether this binding is dependent on C-di-GMP binding. As well as the first possible structures of DUF4339 domains. For Bd1483, a structure will help predict its possible *in vivo* binding partner(s) and whether they are exogenous or endogenous. With this information these proteins could be fitted into the current model for C-di-GMP signalling involvement in prey biting to invasion (figure 3).

8.0 Methods

8.1 Constructs used in the study

bd1996 – pET41c expression vector C-terminal hexa-histag (His₆).

pET41c is modified from the pET41 plasmid (NOVAGEN) with the glutathione-S-transferase tag removed.

bd1483 – pET26B expression vector with a periplasmic leader sequence and N-terminal His₆ tag.

M13*bd3100* – pET41c expression vector with a C-terminal His₆ tag.

bd2538 – pET41c expression vector C-terminal His₆ tag.

8.2 Preparation and storage of cell lines.

8.2.1 The making of competent cells

Buffers used were filter sterilised through a 0.2 µm filter:-

TBF1- pH 5.8

TFB2- pH 6.8

100mM RbCl₂

100mM CaCl₂

50mM MnCl₂

15% Glycerol

30mM Potassium Acetate

10mM CaCl₂

15% Glycerol

BL21* and DH5α stocks (Invitrogen) were streaked out for single colonies on antibiotic free LB agar and incubated overnight at 37°C. Single colonies of BL21* and DH5α were picked and used to inoculate 25 mL of sterile antibiotic free LB broth and grown overnight at 37°C. 1 mL of the overnight cultures were used to inoculate 100 mL of LB broth, and grown at 37°C in an orbital shaker until OD₆₀₀ reached 0.6. Cells were spun at 4000xg for 5 minutes and the supernatants were discarded. From then on cells were kept on ice at all times. Cells from the 100 mL of LB broth were re-suspended in 30mL cold TFB1 and incubated on ice for 90 minutes and then pelleted again at 4000xg for 5 minutes. The supernatants were discarded and re-suspended in 4 mL of TFB2. Aliquots of this were snap frozen in liquid nitrogen and stored at -80°C.

8.3 Cloning of genes of interest

8.3.1 Primers and restriction free cloning

Primers for *bd1996*

Forwards primer

5'-GTTTAACTTTAAGAAGGAGATATACATATGAATCCAAAAACTGGTCCGTGCTTAC-3'

Reverse primer

5'-GCTGCACTACCGCGTGGCACAAGCTTAACCATGGCAAACCTTGCGCACGTATT C-3'

Primers for the 1st and 2nd attempts of restriction free cloning of *bd2538*

Forwards primer

1: 5'-GTTTAACTTTAAGAAGATATACATATGACGGATGCCAATCCGCAGATTGC-3'

2: 5'-TTAACTTTAAGAAGGAGATATACATATGACGATGCCTTTCCGCAGATTGAAACAAG-3'

Reverse primer

1: 5'-GCTGCACTACCGCGTGGCACAAGCTTGTTTGCTCCTGTTTTCGCGTAATC-3'

2: 5'-GCTGCACTACCGCGTGGCACAAGCTTGTTTGCTCCTGTTTTC GCGTAATCCAGAAT AC-3'

Prior to the study the initial cloning and transformation of the pET26b-*bd1483* construct had been undertaken and colonies of transformed DH5 α were stored at 4°C ready for colony PCR and sequencing. Again, prior to the start of the study stocks of BL21* transformed with pET41c-M13*bd3100*, that were known to express

Bd3100, were prepared by Dr. Andrew Lovering. These cells were stored at -80°C and were used for all Bd3100 expression.

Cloning was undertaken using restriction free methods previously described by van den Ent and Lowe, 2006, using primers, which have homologous sequences for both the gene of interest and destination vector. The product of the primary PCR was then used in the secondary PCR, which would incorporate the gene of interest into the destination plasmid, using the destination plasmid as a template for replication. This second round of amplification was then purified using Qaigen PCR clean up kit and eluted with 40µL of dH₂O. Purified plasmids were concentrated from 40 µL to around 15 µL using the Hetovac (Heto lab) VR-1 vacuum centrifuge.

8.3.2 Transformation of competent bacterial strains

120 µL of thawed competent *E. coli* DH5α cells (Invitrogen) were placed upon the concentrated plasmid and then incubated at 4°C for 30 minutes. Cells were then subjected to heat shock for 1 minute, at 42°C, then incubated for 1 hour at 4°C. 1 mL of antibiotic free LB broth was placed on top of the cells and the incubated for 1 hour at 37°C for recovery. The cultures were then spun at 4500xg for 1 minute and 100 µL of pelleted cells were plated out on kanamycin (50µg/mL) selective LB agar plates.

Transformation of competent *E. coli* BL21* (DE3) cells (Invitrogen) were carried out in the same manner with the exception that 100 µL of BL21 * cells were transformed with 1.5 µL of sequenced plasmid containing the gene of interest.

8.3.3 Colony PCR and sequencing

To check whether transformed *E. coli* DH5α had up taken the plasmid of interest, PCR was undertaken on colonies that had grown overnight. Each reaction consisted

of 15 μL MyTaq Red mix 2X (Bioline), 2 μL of pET21 forward and reverse primer mix and made up to a 30 μL total reaction volume, with sterilised dH_2O . Colonies were picked with a sterile loop and spread across a kanamycin selective LB agar plate prior to the colony being placed in the reaction mixture. After PCR amplification, 6 μL of the product was run on a 1% agarose gel. Gels were imaged on an uvitec Alliance 4.7 imager and analysed with UVIsoft.

Colonies that contained an insert of correct size were picked for sequencing. Colonies were grown overnight in LB broth at 37 °C in an orbital shaker. Overnight cultures were minipreped as instructed by the Qaigen miniprep kit and plasmid eluted off the spin column with 50 μL dH_2O . Plasmids were sequenced at the functional genomics facility housed in the University of Birmingham. Plasmids that sequenced with the desired insert were stored at -20 °C.

8.4 Expression of the genes of interest

8.4.1 Small scale expression test

Prior to full scale expression of recombinant protein, small scale trials were carried out to observe whether the recombinant proteins were soluble, and if not, whether changing the temperature during expression aided solubility. As well as this, both the media used was varied between 1x LB broth and 2X LB broth and the amount of inducing agent, isopropyl β -D-1-thiogalactopyranoside (IPTG), was varied to see whether this impacted expression of soluble/insoluble protein. 0.5 mL of overnight cultures with cells picked from colonies containing plasmid with sequenced gene of interest were used to inoculate 50 mL of test expression media (1x LB and 2X LB) and grown at 37°C in an orbital shaker, rotating at 200rpm until an optical density 0.6

at 600 nm was reached. Then, cultures were induced with varying amounts of isopropyl β -D-1-thiogalactopyranoside (IPTG), ranging from 25mM to 1000mM and cultures were grown at 18°C overnight for 18 hours in an orbital shaker at 200rpm. 3mL samples of the cultures were taken at 5 hours and 24 hours post induction. Samples were spun at 6000xg for one minute to sediment the cells. Samples were lysed at room temperature in BugBuster for 1 hour and a 4 μ L sample was taken for SDS-PAGE analysis of the 'whole cell' (WC) fraction. The lysates were spun at 17000xg and the supernatant containing the soluble components were sampled with 4 μ L and ran on a SDS-PAGE. To the samples, 16 μ L of 2x SDS loading dye was added. Samples were boiled for 10 minutes at 100 °C and 10 μ L of each sample was ran on SDS-PAGE at 150V for 30 minutes and stained with coomassie stain overnight at room temperature.

8.4.2 Scale up expression of recombinant protein

Initial overnight cultures, for expression tests, consisted of 5 mL sterile 1x LB broth, containing 50 μ g/mL kanamycin. Cultures were inoculated with a single picked colony of *E. coli* BL21* containing the desired plasmid insert and grown overnight in a shaker at 37°C.

For all expressions 500 mL of 2x LB (50 μ g/mL kanamycin) were inoculated with 5 mL (1% inoculum) of the grown overnight culture and grown at 37°C in an orbital shaker at 200 rpm. Cultures were grown until they reached an OD₆₀₀ of 0.5 and the induced with IPTG and grown overnight at 18°C. For expression of Bd1996 BL21 cells were grown in 1xLB and induced with 50 μ M IPTG, cultures expressing Bd1483 were induced with 50 μ M IPTG in 2xLB broth, while cultures expressing Bd3100 were

induced with 500 μ M IPTG in 2xLB broth. After 18 hours of expression cells were spun successively at 4500xg for 6 minutes (4°C) to pellet the cells. Cell pellets were stored at -20°C until required.

8.4.3 Purification of over expressed protein

8.4.3.1 Buffers for purification

Buffer A – 20 mM Imidazole, 300 mM NaCl, 0.05% Tween 20 – pH 7.0

Low imidazole buffer A – 5 mM Imidazole, 300 mM NaCl, 0.05% Tween 20 – pH 7.0

Buffer B – 400 mM Imidazole, 300 mM NaCl, 0.05% Tween 20 – pH 7.0

Buffer C – 20mM Imidazole, 300 mM NaCl, 0.05% Tween, 50mM EDTA – pH 7.0

8.4.3.2 Purification

Cell pellets were defrosted at room temperature in 30 mL of buffer A (Bd1996 and Bd3100) or low imidazole buffer A (Bd1483). Pellets were re-suspended at room temperature by rotating at 200 rpm in the presence of hen egg white lysozyme. Once re-suspended cells were lysed via sonication. With an output of 60% cells were sonicated for 20 seconds bursts and allowed to rest on ice for 2 minutes between bursts. This was repeated for 6 cycles. Once lysed the lysates were spun at 40,000xg for 1 hour (4°C) (soft spin). The supernatant was decanted and, if needed, spun at 170,000xg for 1 hour (4°C) (hard spin) to pellet lipids. The clarified supernatants were passed over an equilibrated 1 mL HisTrap FF IMAC column loaded with 100mM NiSO₄ at a flow rate of 1mL/minute with a peristaltic pump. The flow through was collected for sampling on SDS-PAGE.

The loaded column was then attached to the AKTA prime fast protein liquid chromatography protein purification system to elute off the target protein. The column

was washed with 20 mL of buffer A (or low imidazole Buffer A for Bd1483) to wash off non-specifically bound protein. To elute non-specifically bound the column was washed with 10% buffer B. To fully elute Bd1483, the column was washed with 20 mL of 100% buffer B. To elute Bd1996, 15 mL of Buffer C was passed over the column due to high concentrations of imidazole causing Bd1996 to precipitate after elution. Throughout the duration of purification the eluent was analysed for protein content by measuring absorbance at 280nm. At all points of purification on the FPLC the eluents were retained in 5 mL fractions, fractions containing target protein were immediately placed on ice.

8.4.4 Buffer exchange and concentrating of target protein

FPLC fractions containing target protein were placed in dialysis tubing (MWCO 10,000 Daltons) and dialysed overnight in 20mM HEPES (pH 7.0) and 200mM NaCl, or 20mM BIS-TRIS (pH 6.5) and 200mM NaCl. To concentrate the target protein after dialysis, the proteins were spun in Vivaspin-20 centrifugal concentrators at 2900xg (4°C) until protein reached a concentration between 20-35mg/mL. Once concentrated, the proteins were snap frozen in liquid nitrogen and stored at -80°C until use.

8.4.5 Initial screening of target protein for crystallization

Concentrated target proteins were initially screened for crystallisation using screens obtained from Molecular Dimensions via sitting drop method at 18°C. Drops consisted of 2 µL of protein solution mixed thoroughly with 2 µL of reservoir solution. Trays were checked at regular intervals for crystal growth.

Screens used for crystallization were all obtained from Molecular Dimensions: JCSG+, MIDAS, Proplex and Pact premier.

8.4.6 Custom screening of initial hits

To hits found in the initial trials factorial screens varying; the buffer pH, concentration of salt and precipitant, were undertaken. Throughout the optimization, variations in drop size as well as the addition of additives (10 mM Xylitol, 10% ethanol and 10mM IPTG) were investigated. Generally custom tray drops were trialed with the hanging drop method with 2 μ L of protein solution mixed with 2 μ L of the reservoir.

8.4.6.1 Glycerol custom screen of Bd1483

Glycerol was added to concentrate Bd1483 (34 mg/mL) to bring glycerol to a total weight per volume of 10% glycerol (protein at a concentration of 30.6 mg/mL). This was then screened against the JCSG+ sparse matrix. 120 μ L reservoirs, sitting drop consisted of 2 μ L reservoir and 2 μ L protein, bringing the total w/v of glycerol to 5%. These were maintained at 18 °C.

8.4.6.2 Sodium malonate/JCSG+ custom screen

Reservoir solutions consisted of 108 μ L 0.88 M sodium malonate, 0.11 M HEPES-NaOH pH 7.0 and 0.55% Jeffamine M2005 (molecular dimensions) mixed with 12 μ L of JCSG+ screen. This brought the overall reservoir concentration to 0.8 M sodium malonate, 0.1 M HEPES-NaOH pH 7.0 and 0.5% jeffamine M2005 with the JSCG+ as a 10% additive. Crystallization was trailed by sitting drop method with 2 μ L protein solution mixed thoroughly with 2 μ L reservoir solution.

All images of crystals were taken on a high-definition colour camera head DS-Fi2 with a Nikon DS L3 microscope control unit.

8.4.6 Cryoprotection of Bd1483 crystals

Cryoprotection was achieved by supplementing the mother liquor with 20% ethylene glycol in 0.2M magnesium formate and 20% PEG 3350, from which Bd1483 crystals were seen in. When crystals were extracted they were flash cooled in liquid nitrogen, prior to being sent to the Diamond light source for data collection.

9.0 Results

9.1 Expression and refolding of the suspected C-di-GMP binding protein, Bd3100

9.1.1 Test expression of Bd3100 showed it to be insoluble across all tested conditions

To hopefully optimise the overexpression of Bd3100 before scaling up to 3 litres of culture, small-scale expressions were carried out in 15mL of LB. These conditions varied the concentration of IPTG used to induce expression. As figure 5 shows, in all whole cell fractions, both at 5 hours (figure 5A) after induction and 24 hours (figure 5B) after induction, Bd3100 remains insoluble, forming inclusion bodies. This is true for all conditions tested.

When Bd3100 was expressed the presence of varying amounts of glycylglycine, no improvement of soluble Bd3100 after 18 hour induction was observed (Figure 6). This was the case for all concentrations of glycylglycine tested. As shown in figure 6a the soluble fractions showed no major band at 31 kDa, while this band was found in all whole cell fractions (figure 6b). This shows that glycylglycine does not affect the solubility of this protein, as it has done for others (Ghosh *et al.*, 2004). These results led to changing the focus of Bd3100 expression from improve the solubility of the protein, to denaturing and refolding inclusion bodies of Bd3100

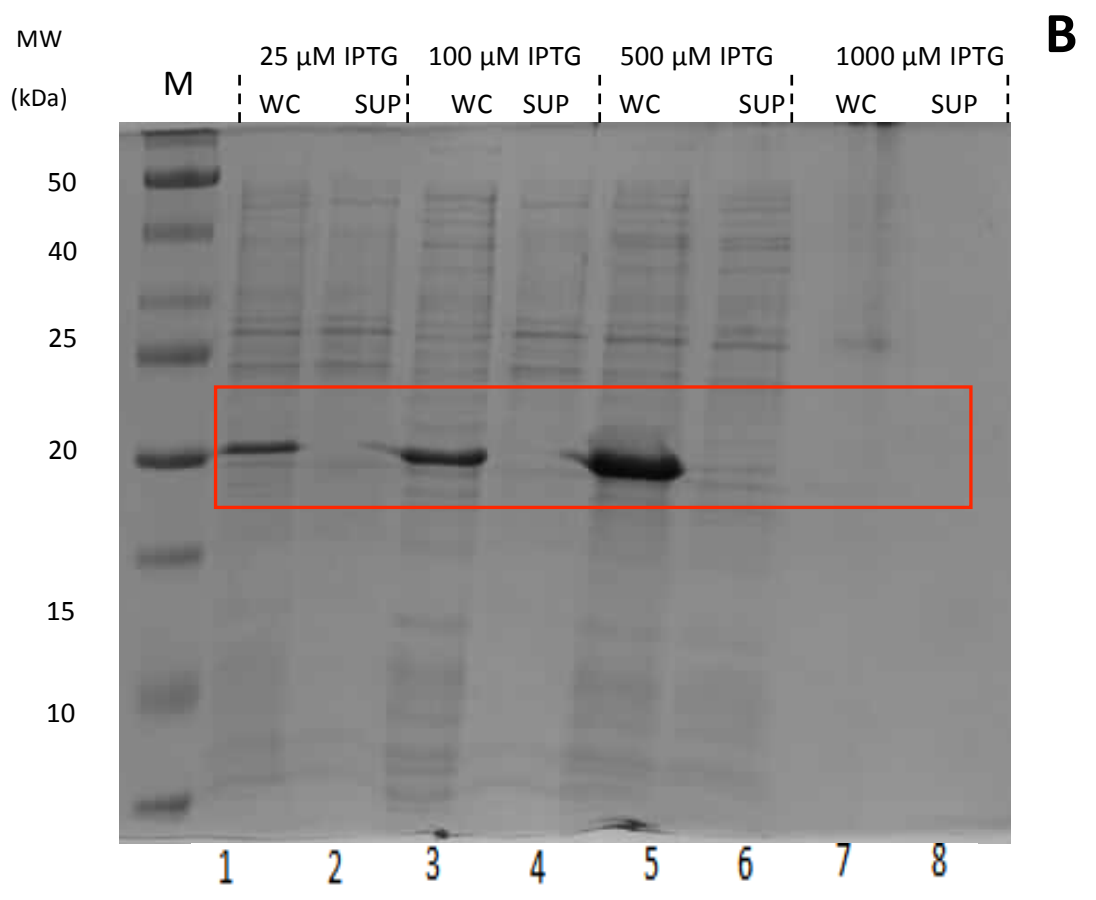
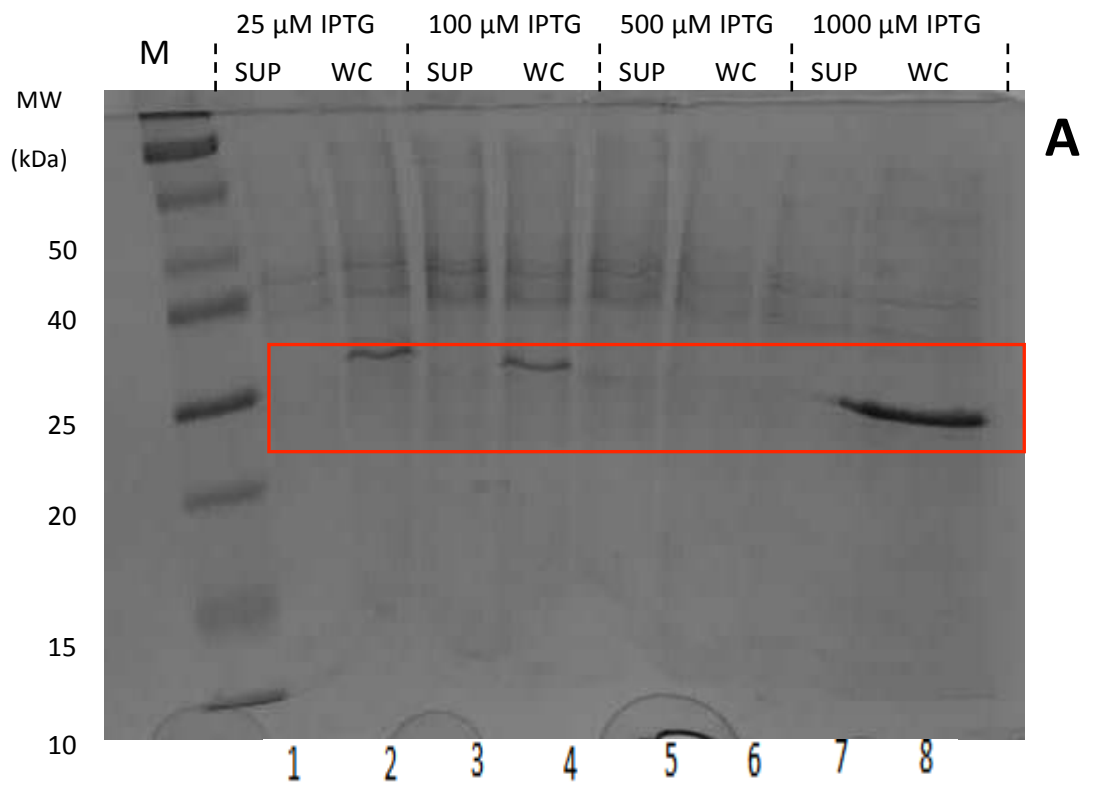


Figure 5. Test expression of Bd3100 in varying conditions 5 and 24 hours after induction with IPTG at 18°C.

A) A SDS-PAGE of whole cell vs. soluble supernatant of samples *E. coli* cultures expressing Bd3100, 5 hours post induction with IPTG. Lanes 2, 4, 6 and 8 show samples of the whole cell fractions (WC) when cells have been lysed in BugBuster™. Lanes 1, 3, 5 and 7 show the soluble supernatant fractions (SUP) once the whole has been spun at 13,000 rpm to remove insoluble debris. A band above the 25 kDa marker, representing Bd3100 (31kDa), can only be seen in the whole cell sample (Lanes 1, 3, and 5) while it is absent from the soluble supernatant fractions (Lanes 2, 4 and 6). This shows that at 5 hours post induction at 18°C Bd3100 expresses in an insoluble form at all concentrations of IPTG.

B) An SDS-PAGE of whole cell vs. soluble supernatant of samples *E. coli* cultures expressing Bd3100, 24 hours post induction with IPTG. Lanes 1, 3, 5 and 7 show samples of the whole cell fractions (EC) when cells have been lysed in BugBuster™. Lanes 2, 4, 6 and 8 show the soluble supernatant fractions (SUP) once the whole has been spun at 13,000 rpm to remove insoluble debris. A band above the 25 kDa marker, representing Bd3100 (31kDa), can only be seen in the whole cell sample (Lanes 1, 3, and 5) while it is absent from the soluble supernatant fractions (Lanes 2, 4 and 6). This shows that at 24 hours post induction at 18°C Bd3100 expresses in an insoluble form at all concentrations of

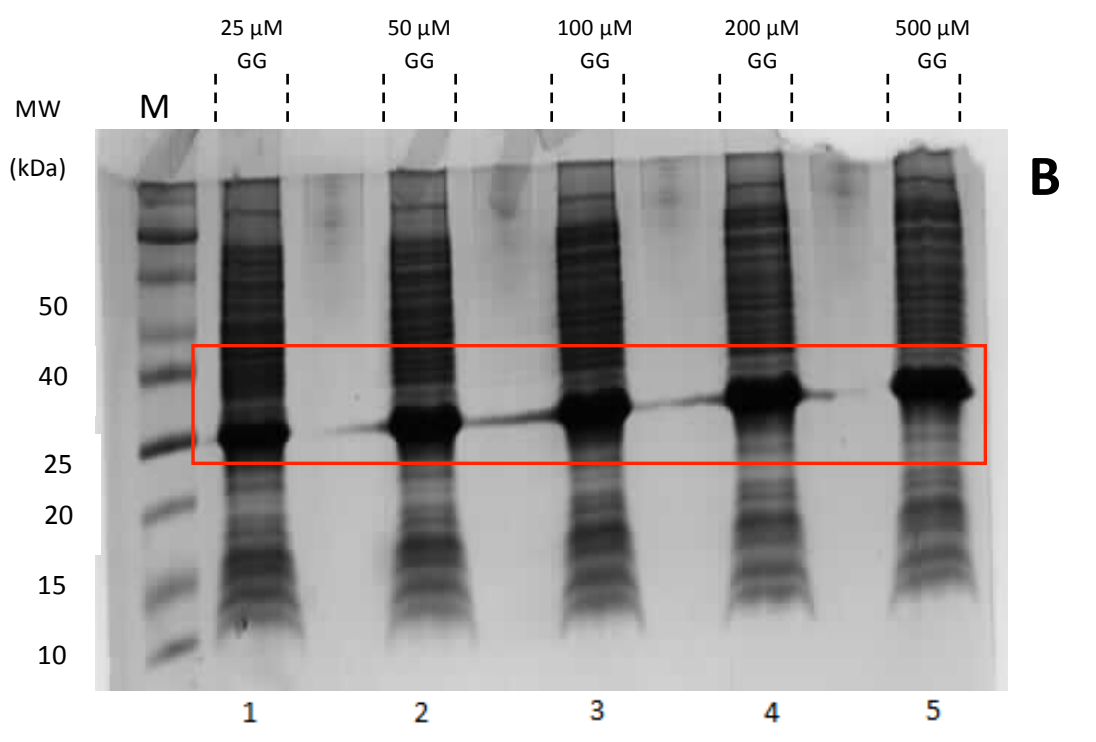
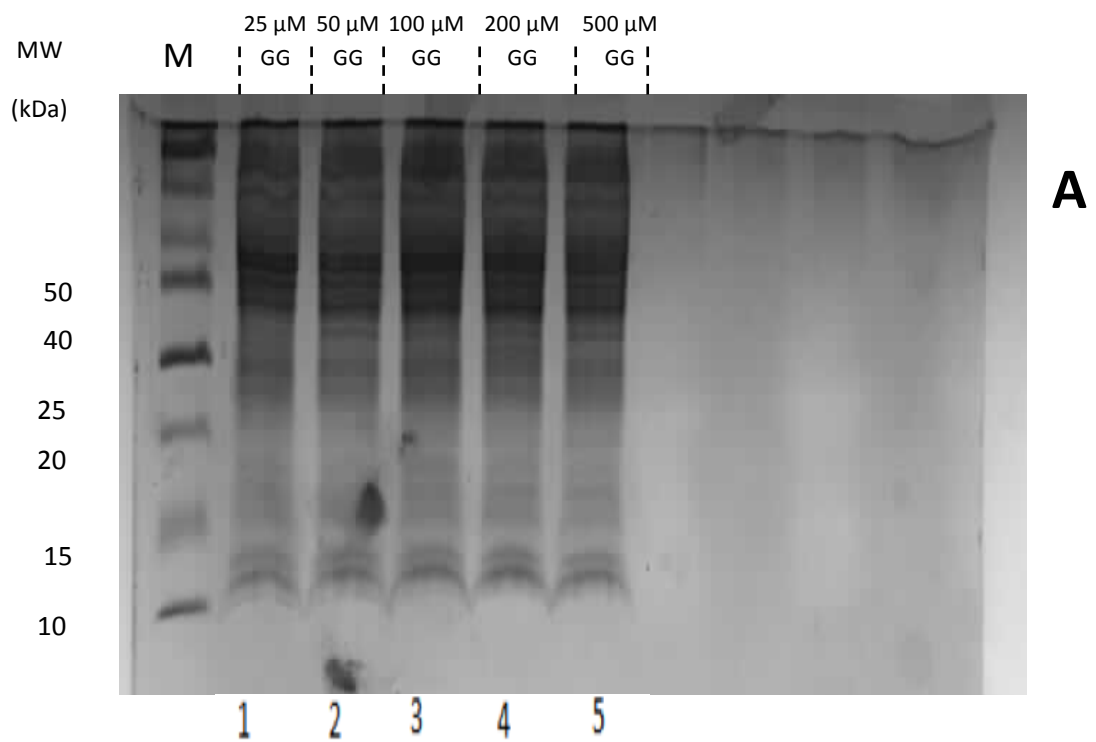


Figure 6. Test expression of Bd3100 in media supplemented with sterile glycyglycine.

A) An SDS-PAGE of the soluble supernatant of samples of *E. coli* cultures expressing Bd3100 in the presence of glycyglycine, 18 hours post induction with IPTG. Cells were lysed in BugBuster™ and spun at 13,000 rpm to remove insoluble debris. A band above the 25 kDa marker, representing Bd3100 (31kDa), cannot be seen any on the supernatant fraction which would indicate Bd3100 being soluble at all concentrations of glycyglycine.

B) An SDS-PAGE of whole cell samples of *E. coli* cultures expressing Bd3100 in the presence of glycyglycine, 18 hours with IPTG. Whole cell fractions when cells have been lysed in BugBuster™. A band above the 25 kDa marker, representing Bd3100 (31kDa), can be seen in the whole cell sample at every concentration of glycyglycine. This shows that at 18 hours post induction at Bd3100 expression is not hampered by the addition of glycyglycine.

9.1.2 On-column refolding of Bd3100 was unsuccessful

Due to Bd3100 forming inclusion bodies, insoluble aggregations of overexpressed protein, we attempted to denature these inclusion bodies, solubilising the aggregated protein and purifying from that point. Once denatured, the protein would then be refolded in the correct conformation by removing the denaturing agent. In an attempt to refold the denatured target protein the supernatant was passed over the nickel charged column in denaturing conditions, 8M urea. While bound to the column, a buffer of a slowly decreasing denaturant gradient was passed over the column in an attempt to refold Bd3100. Once the buffer was at 0M urea the bound protein was eluted using 400mM imidazole (pH 7.0) and 200mM NaCl. When ran on an SDS-PAGE (not shown) it appeared that the protein was not eluted off of the column. Due to this it can be assumed that the protein misfolded and remained on the column.

9.1.3 Shock refolding of Bd3100 proved more successful but the protein was not pure

Because the initial attempt at full scale refolding was not successful, a small scale approach was taken to discover what buffer, if any, would allow for the refolding of Bd3100 from a soluble denatured state to a folded soluble state. Following the refolding protocol set out by Vincentelli *et al.* 2004, a refolding screen was set up using a range of buffer (50 mM Sodium acetate pH 4.6, 50 mM MES pH 5.8, 50 mM CHES pH 9.0 and 50 mM TRIS-HCl pH 7.2) and a range of additives (100 mM KCl, 200 mM NaCl, 100 mM non-detergents sulfobetaines, 1mM EDTA, 10 mM β -mercaptoethanol and 20% glycerol). 100 μ L of Bd3100 was added to each condition and fluorescence was measured at 340nm, to measure precipitation. Sodium acetate with NDSB, EDTA, β -ME and 20% glycerol proved best for soluble refolded protein

(table 1). Due to sodium acetate proving to be the best across all additives the 1 mL samples containing sodium acetate were kept at 4°C for 30 minutes and measured for optical density at 340 nm again, to see if precipitation had occurred (Table 1). After this incubation, the conditions, which proved to be most suitable for stable refolding, included those with the NDSB, EDTA, β -ME and 20% glycerol additives. Due to glycerol's inhibitory effect on nucleation during crystallization we chose to not carry on with this condition. We chose to use the condition containing β -ME for large scale shock refolding. 20 mL of protein solution was shock refolded into 600 mL of 50mM sodium acetate pH 4.6 and 10mM β -ME. This was left overnight at 4°C to equilibrate. One caveat to the use of sodium acetate is that you cannot purify with IMAC columns due to the pH of the buffer being too low, which would strip the column of nickel ions. As well as this, previous attempts at purification of Bd3100 by a fellow researcher in the group failed when inclusion bodies of Bd3100 were solubilised in 6 M GndHCl or 8 M urea. After overnight incubation, at 4°C, there was no visible precipitation, so concentration of the suspected Bd3100 began. Unfortunately, during concentration, the protein solution began to precipitate even when kept at 4°C and did not resolubilise when brought up to room temperature, like other proteins (Pers comms Dr. Ian Cadby). A 1 mL sample of the precipitated solution was run on a SDS-PAGE to check the purity of the sample (figure 7). As figure 7 shows Bd3100 was not completely pure, as shown by the two faint bands found in the sample.

OD measured at 340nm	KCl 100 mM	NaCl 200 mM	NDSB 100 mM	EDTA 1 mM	β -ME 10 mM	Glycerol 20%
Na Acetate pH 4.6	0.081 0.180	0.166 0.430	0.041 0.076	0.054 0.070	0.043 0.070	0.038 0.063
MES pH 5.5	0.51	0.93	0.17	1.31	0.163	0.14
TRIS-HCl pH 7.0	1.22	1.12	1.34	0.891	1.076	1.284
CHES pH 9.1	0.841	0.88	1.34	1.41	0.755	1.27

Table 1. The absorbance of protein precipitant at 340 nm when Bd3100 was refolded in 1 mL of buffer.

Bd3100 was measured immediately at 340 nm after addition of 100 μ L of Bd3100 solution to the buffer screen (black). 30 minutes after refolding, fluorescence was measured again at 340 nm, to observe whether solubility was maintained (red).₁

The conditions that proved best for refolding, both immediately and 30 minutes after refolding, were: 50 mM Na acetate pH 4.6, with the 1 mM EDTA, 10 mM β -ME and 20% glycerol as additives.

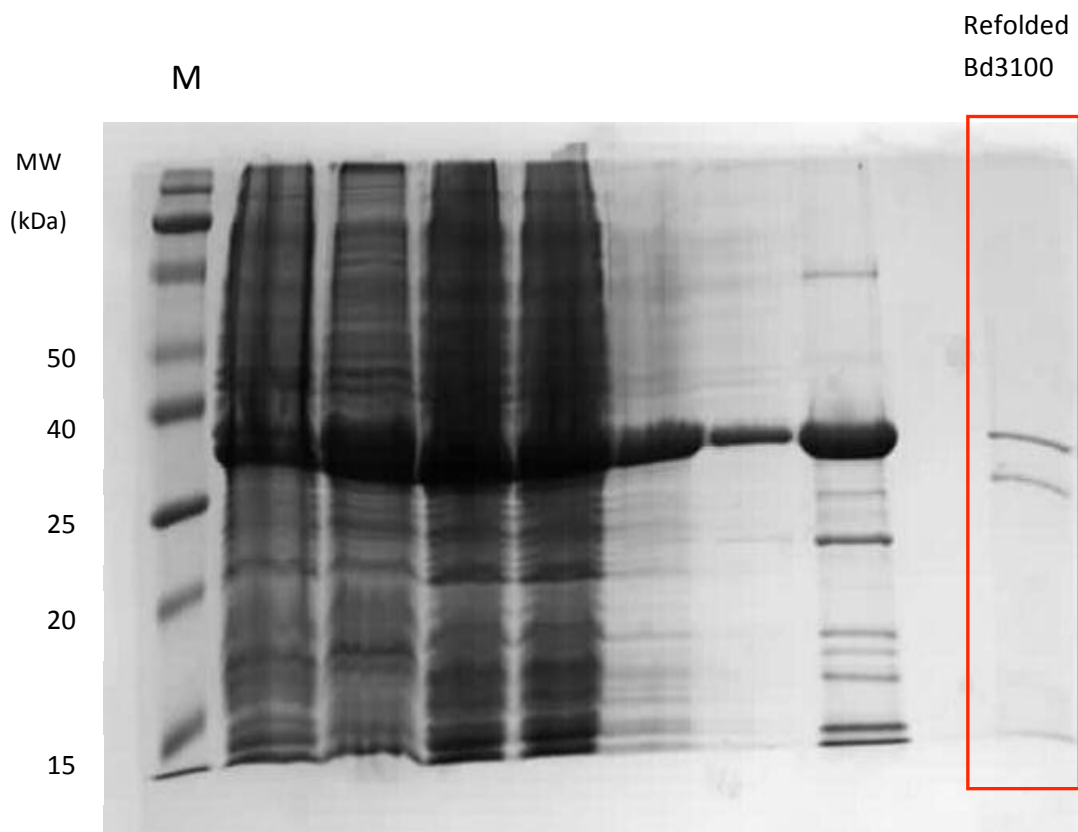


Figure 7. The purity of Bd3100 post refolding from inclusion bodies without IMAC purification.

A SDS-PAGE of refolded Bd3100. Bd3100, from inclusion material, was solubilised in 20 mM Tris-HCl, 500 mM NaCl, 2% triton™ X-100 and 6M guanidine hydrochloride and shock refolded in 600 mL 50 mM sodium acetate pH 4.6 and 10 mM β -ME. The lane labelled 'Refolded Bd3100' shows a sample of Bd3100 after concentration. Bd3100 is not pure as there is a band found above 25 kDa that represents Bd3100 (31kDa) there is also a band above it at a higher molecular weight.

9.2 Expression, purification and crystallization of the predicted binding protein, Bd1483

9.2.1 Cloning of bd1483 was successful

Initial cloning procedures, as well as initial transformations of *E. coli* DH5a with suspected pET26b-*bd1483* constructs, had been previously carried out. Colony PCR was undertaken on DH5a colonies that were believed to contain the pET26b-*bd1483* plasmid. Of these, 4 colonies showed that insert DNA was present (figure 8 lanes 3, 10, 11 and 12). These colonies were then grown overnight and samples sent off to the functional genomics facility in the University of Birmingham for sequencing. One of these plasmids was shown to have the correct sequence for *bd1483* and this plasmid was then used for the transformation of BL21*.

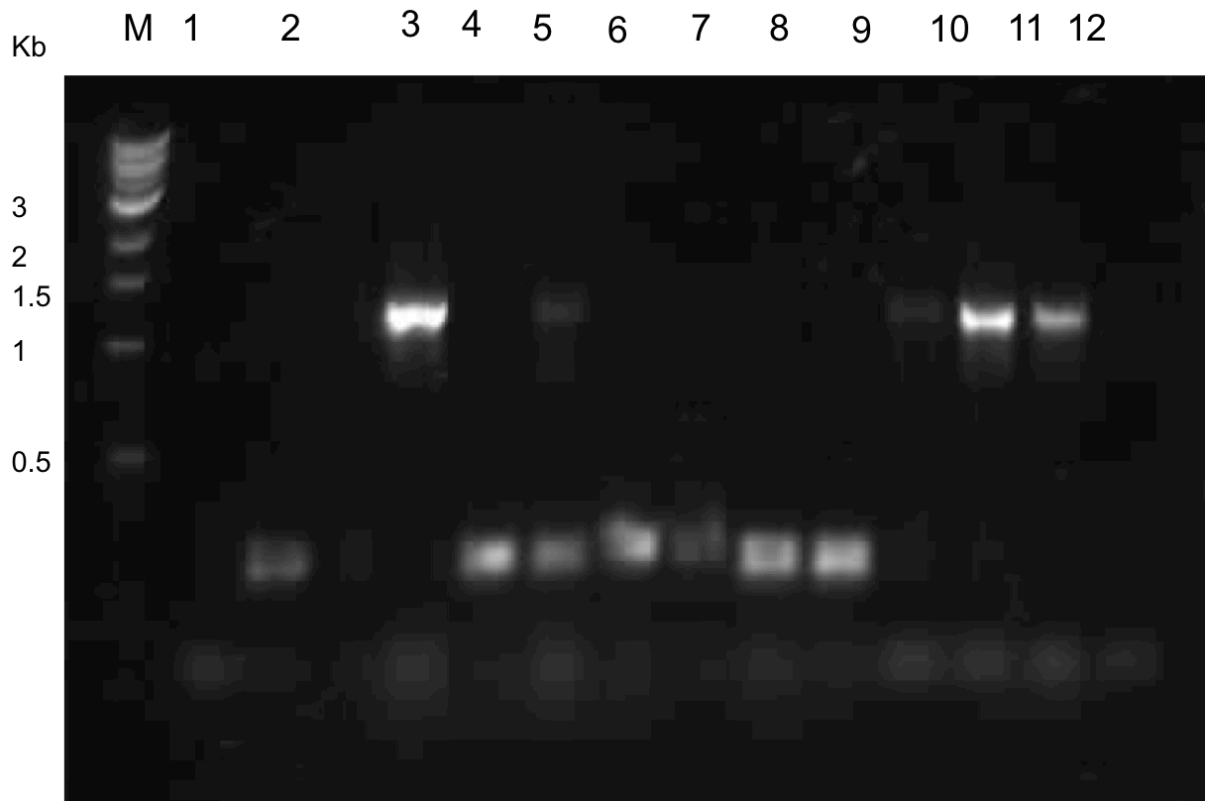


Figure 8. An agarose gel of the colony PCR of suspected pET26b-bd1483 transformants.

A 1% agarose gel of the PCR conducted on suspected transformed *E. coli* DH5 α transformed with pET26b-Bd1483. Lanes 3, 10, 11 and 12 show colonies that are resistant to the kanamycin LB agar plates that have taken up the pET26b-*bd1483* plasmid, with a band slightly above the 1 Kb marker. All other lanes have become kanamycin resistant through other mechanisms.

9.2.2 Bd1483 was shown expresses and remain soluble in all expression conditions tested

To determine what growth conditions, if any, best allowed for the expression of soluble Bd1483, prior to full scale expression, test expressions were carried out on colonies that had been transformed with sequenced pET41c-*bd1483* in 50mL of LB broth. Figure 9 shows that Bd1483 is soluble when expressed at 1x LB 50µM IPTG, 2x LB 25µM IPTG, 2x LB 50µM IPTG and 2x LB 500µM IPTG. Expression was seen in all conditions tested with the greatest amount of soluble protein being observed in 2x LB 25µM IPTG. So, this condition was used to scale up for full-scale expression of Bd1483 in 3 litres of culture.

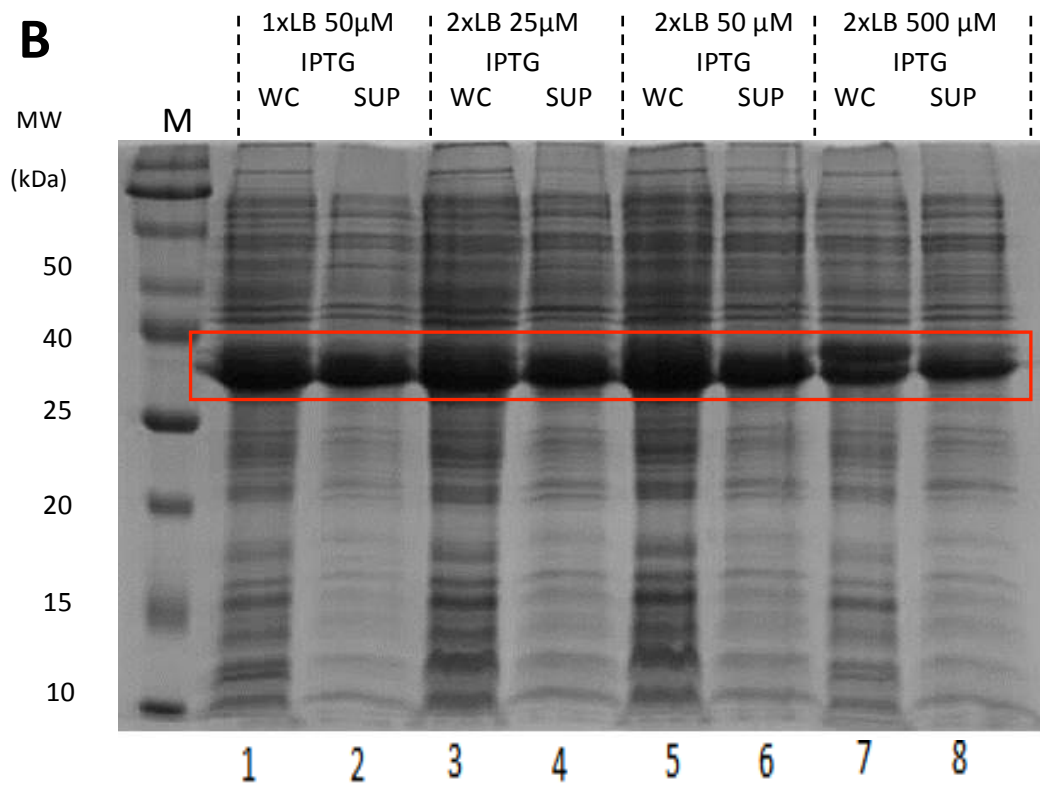
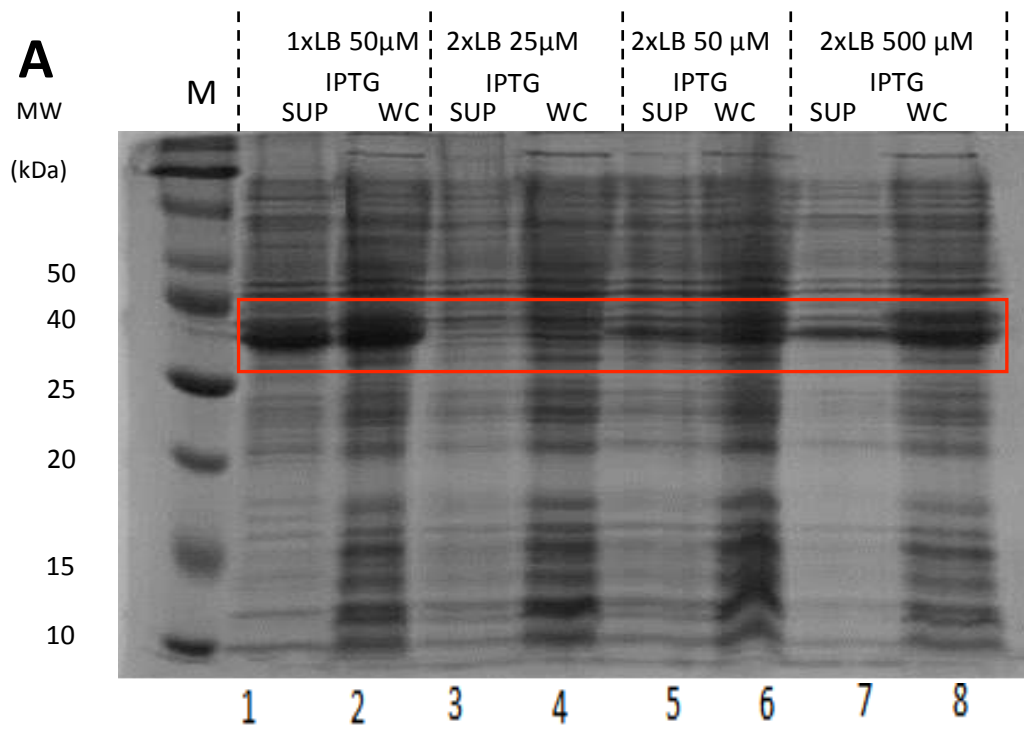


Figure 9. Test expression of Bd1483 in *E. coli* BL21*

A) A SDS-PAGE of whole cell versus soluble supernatant of samples *E. coli* BL21* cultures expressing Bd1483, 5 hours post induction with IPTG. Lanes 2, 4, 6 and 8 show samples of the whole cell fractions (WC) when cells have been lysed in BugBuster™. Lanes 1, 3, 5 and 7 show the soluble supernatant (SUP) fractions once the whole has been spun at 17,000xg to remove insoluble debris. A band below the 40 kDa marker, representing Bd1483 (39kDa), can be seen in lanes 1 and 2 (25 μM IPTG, 2x LB broth), 5 and 6 (500 μM IPTG, 2x LB broth) and 7 and 8 (1000μM IPTG, 2x LB broth) showing that after 5 hours post induction Bd1483 expression is soluble.

B) A SDS-PAGE of whole cell vs. soluble supernatant of samples *E. coli* BL21* cultures expressing Bd1483, 18 hours post induction with IPTG. Lanes 1, 3, 5 and 7 show samples of the whole cell fractions (WC) when cells have been lysed in BugBuster™. Lanes 2, 4, 6 and 8 show the soluble supernatant (SUP) fractions once the whole has been spun at 17,000xg to remove insoluble debris. A band below the 40 kDa marker, representing Bd1483 (39kDa), can be seen all lanes. This shows that, 18 hours after induction at 18°C, Bd1483 expression is soluble in all conditions tested.

9.2.3 Scale up expression of Bd1483 was successful but purification was found to be difficult due to the protein binding weakly to the nickel loaded column

Upon the scale up of overexpression, Bd1483 expressed well and was found to be soluble, as it was in small-scale trials. Initially it was found to bind weakly to a nickel loaded IMAC column, with the majority of the target protein coming out in the flow through rather than binding to the column. This was seen when cells expressing Bd1483 were lysed in buffer A. To remedy this the flow through was diluted into 150 mL of low imidazole buffer A (5mM imidazole) to bring total imidazole concentrations to below 10mM. The diluted flow though was passed over the column once again, and it was found to bind to the column. Due to this, all subsequent preparations of Bd1483 were lysed in low imidazole buffer A. When in a low imidazole buffer A, Bd1483 bound to the column and then eluted using a buffer consisting of low imidazole buffer A and 10% buffer B. Bd1483 eluted off the column at around <50mM imidazole. To remove any remaining bound Bd1483 the column was washed with 100% buffer B. Figure 10b shows that there remains some strongly bound Bd1483, even after the majority has been eluted off at <50mM imidazole.

After purification, it was found that in the presence of the high imidazole buffer B (400mM) Bd1483 crashed out of solution, if not quickly diluted with 50% low imidazole buffer A. This, along with a quick dialysis, helped lower the amount of Bd1483 that precipitated. During concentration of the protein it was found that Bd1483 could be concentrated between 30 to 34mg/mL, during the study.

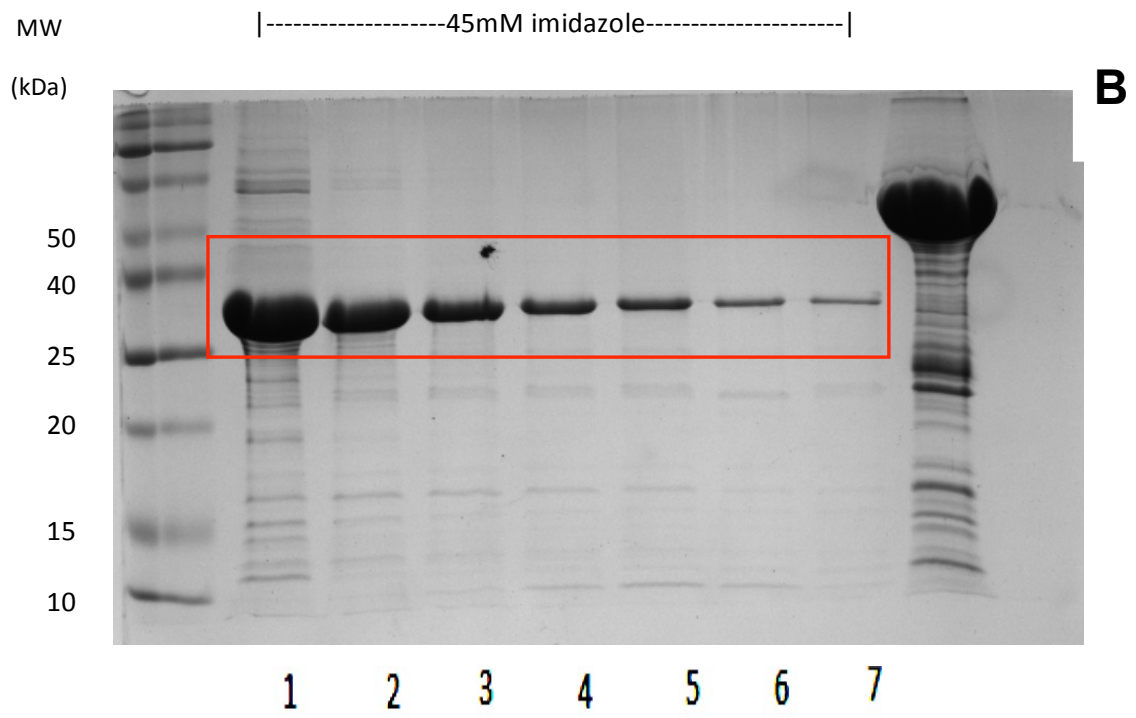
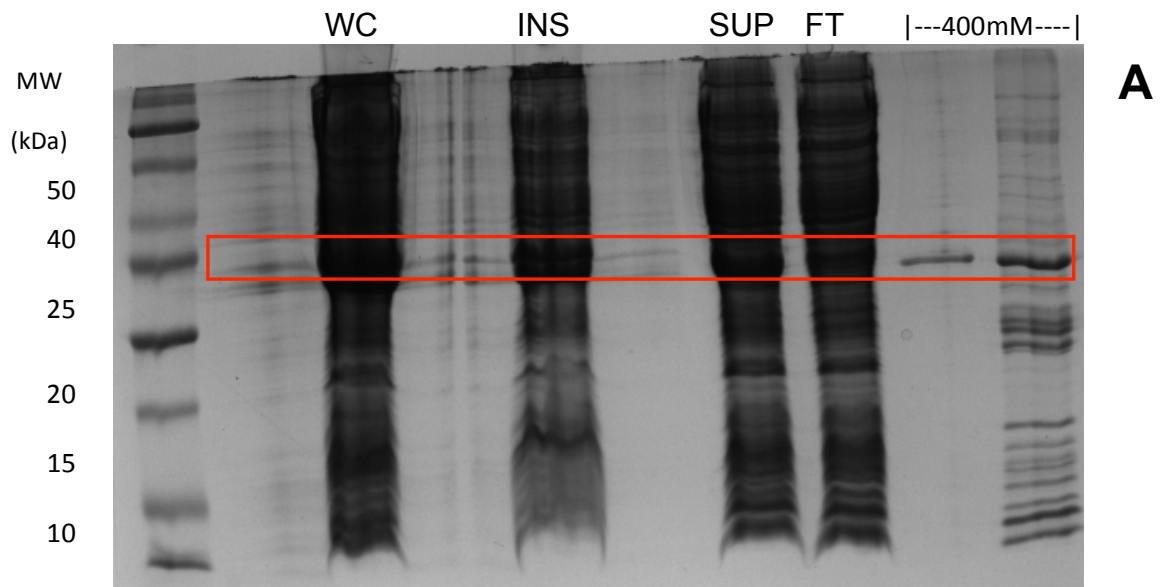


Figure 10. Full scale expression of Bd1483 in *E. coli* BL21*

A) A SDS-PAGE showing the purification and expression of Bd1483. Lane 2 is the whole cell fractions taken after sonication. Lane 4 is the insoluble debris after centrifugation at 17,000xg. Lane 6 shows the soluble supernatant after centrifugation at 17,000xg. Lane 7 shows the flow through of the supernatant after it has been passed over a nickel loaded HisTrap column. Lanes 8 and 9 show the elution of Bd1483 at 400 mM imidazole. The large band below 40 kDa represents Bd1483.

B) A SDS-PAGE showing the purification of Bd1483. Lanes 1-7 show the elution of Bd1483 at 45mM imidazole in the elution buffer. The large band below 40 kDa represents Bd1483. While this scale up expression showed that Bd1483 remains soluble during scale-up the protein is relatively contaminated with other proteins.

9.2.4 Screening of conditions for Bd1483 crystallisation

9.2.4.1 Initial screens proved promising, with many conditions yielding crystal formation

To determine the structure of recombinant protein, via X-ray diffraction, the next requisite was to obtain protein crystals of Bd1483, which would be of high enough quality. Initial screening of Bd1483 was carried out with the JCSG+ buffer screen. This yielded promising results as after one week, of incubation at 18°C, with a number of hits being observed in various conditions. These have been summarised in figure 11. Hits B, I, J, K and M were followed up with custom screens but crystals that would diffract were not observed during the duration of the study

After 2 months of incubation at 18°C 3D crystals were found in a condition of 0.2 M magnesium formate and 20% w/v PEG 3350 (pH was not identified) (figure 10 condition b). This condition was then subjected to a factorial custom screen varying the pH of magnesium formate as well as the concentration of PEG 3350. This yielded no crystals of equal morphology as those found in the original hit, but these had not been incubating for a similar amount of time, as the original condition, by the end of the study.

When Bd1483 was trialled in the MIDAS alternative precipitant screen 3 hits were observed:

Figure 12a: 30% w/v Polyacrylate 5100 sodium salt, 10% ethanol and 1 M MES-NaOH pH 6

Figure 12b: 10% w/v poly(vinyl pyrrolidone) K15, 0.2 M ammonium formate and 20% w/v PEG4000

Figure 12c: 15% w/v poly(vinyl pyrrolidone) K15, 0.1M TRIS-HCl pH 8.0 and 25% w/v PEG5000 MME

As is shown in figure 12a, needles appear to begin forming barrels. Due to this we undertook custom screening of this condition but could not replicate the crystal morphologies again (data not shown).

When Bd1483 was trialled in proplex no hits were observed over the course of the study. This was the case for Bd1483 when the protein was dialysed into a buffer of 0.1 M TRIS-HCl pH 8.0 and 200mM NaCl, as well. In this buffer, Bd1483 precipitated quickly when trialled in JCSG+ and no hits were seen throughout the study.

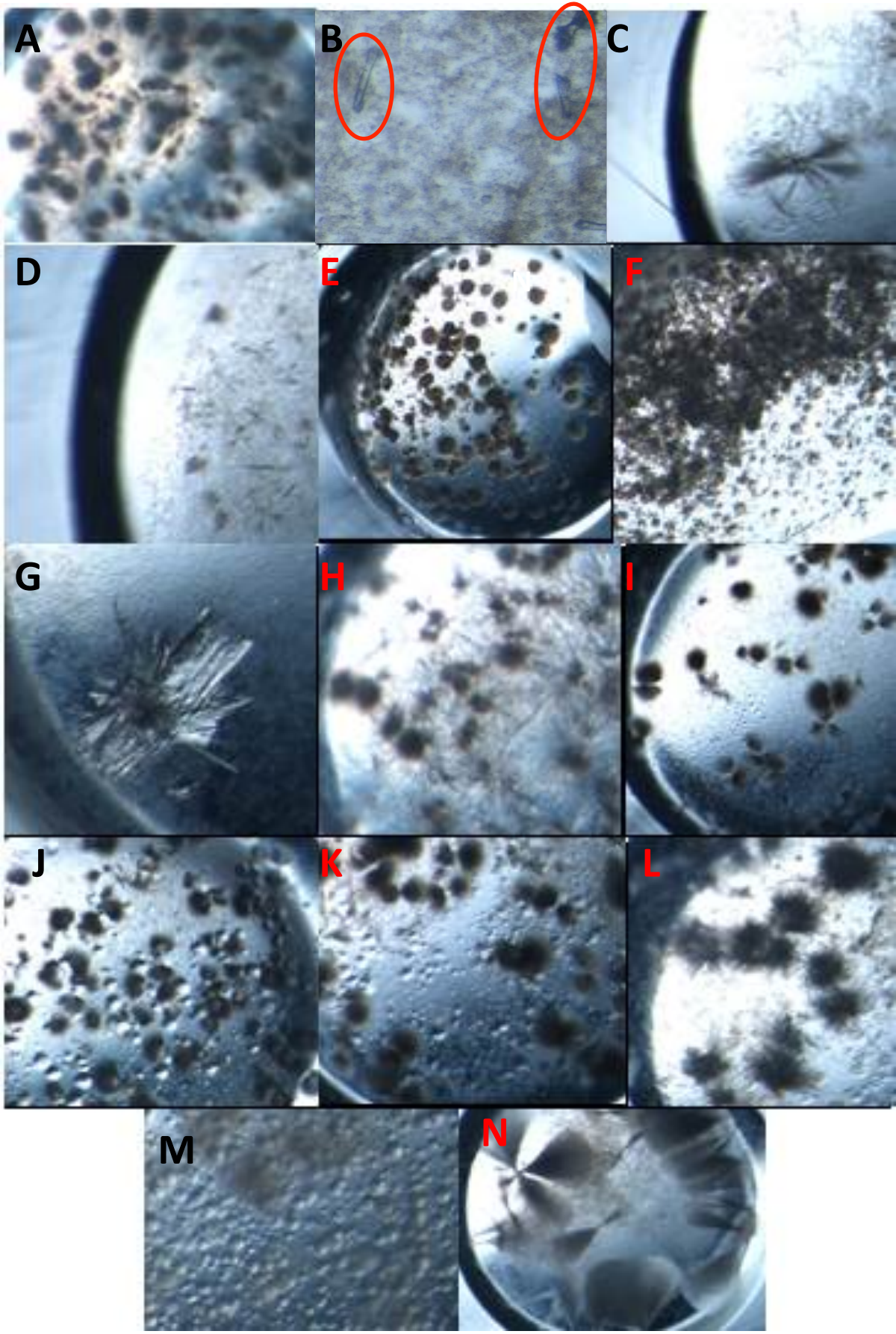


Figure 11. Hits for Bd1483 observed from the JSCG+ screen.

- A) 0.1 M sodium acetate pH 5.5 and 20 % w/v PEG3000
- B) 0.2 M magnesium formate and 20 % w/v PEG 3350
- C) 0.2 M ammonium chloride and 20% w/v PEG 3350
- D) 0.1 M Bicine pH 9.0 and 20 % w/v PEG 6000
- E) 0.2 M NaCl, 0.1M phosphate/citrate 4.2 and 20 % w/v PEG 6000
- F) 0.2 M ammonium nitrate and 20% w/v 3350
- G) 10 % w/v PEG 1000 and 10 % w/v PEF 8000
- H) 0.1 M imidazole pH 8.0 and 10 % w/v PEG 8000
- I) 0.1 M MES pH 6.5 and 1.6 M magnesium sulphate
- J) 1.1 M Sodium maonate, 0.1 M HEPES 7.0 and 0.5 % w/v Jeffamine ED-2001
- K) 0.02 M MgCl₂, 0.1 M HEPES 7.5 and 22% w/v polyacrylic acid 5100 sodium salt
- L) 0.1 M BIS-TRIS pH 5.5 and 25 % w/v PEG 3350
- M) 0.2 M lithium sulphate, 0.1 M BIS-TRIS pH 5.5 and 25 % w/v PEG 3350
- N) 0.2 M magnesium chloride, 0.1 M BIS-TRIS pH 5.5 and 25 % w/v PEG 3350

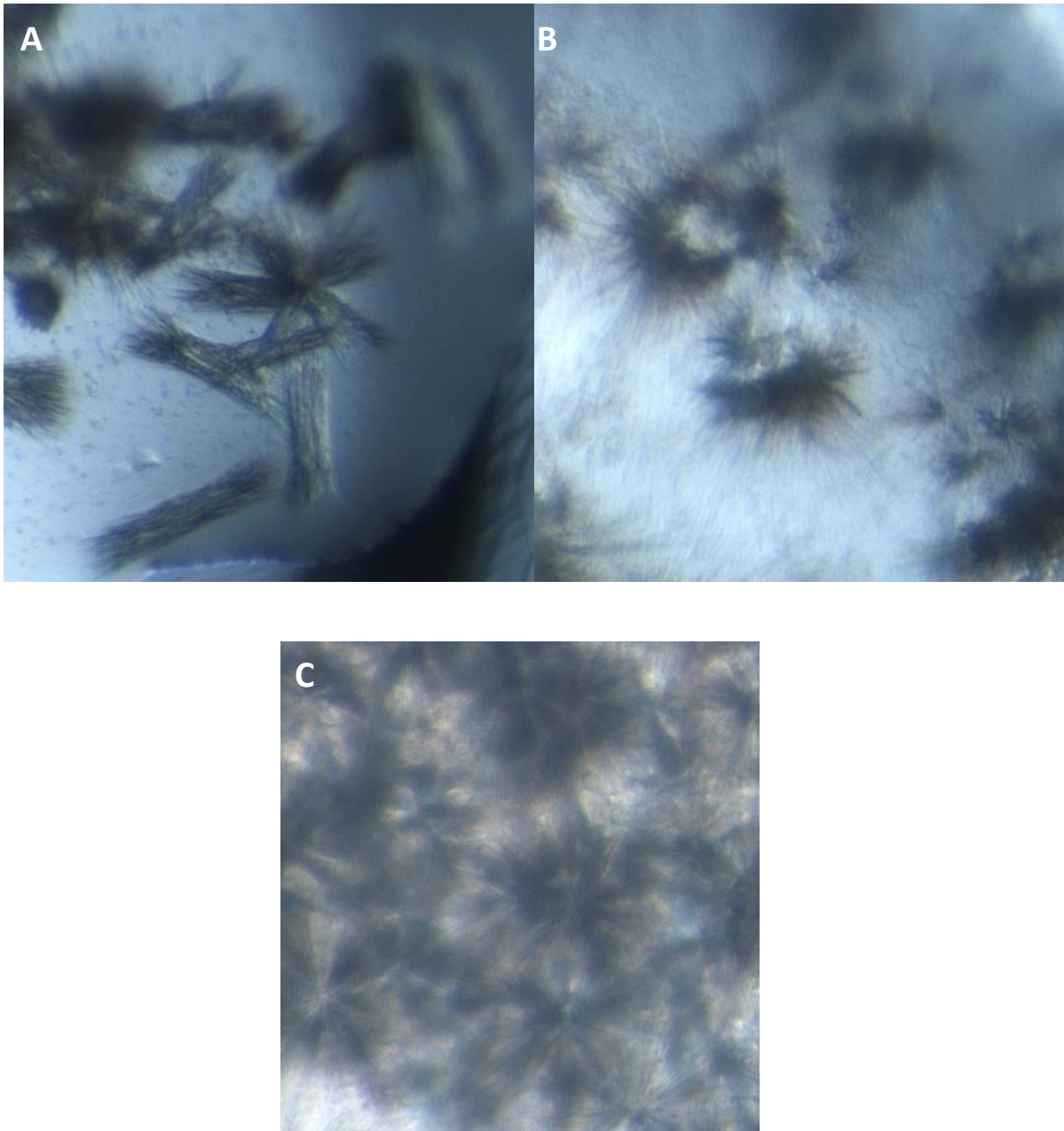


Figure 12. **Crystal hits for Bd1483 in the MIDAS screen.**

A) 30% w/v Polyacrylate 5100 sodium salt, 10% ethanol and 1 M MES-NaOH pH 6

B) 10% w/v poly(vinyl pyrrolidone) K15, 0.2 M ammonium formate and 20% w/v PEG4000

C) 15% w/v poly(vinyl pyrrolidone) K15, 0.1M TRIS-HCl pH 8.0 and 25% w/v PEG5000 MME

9.2.4.2 When 20% glycerol was added to JCSG+ screen no hits were seen

Due to crystals of Bd1483 forming spherulites and needle clusters, 20% glycerol was added to each condition of the JCSG+ screen. The addition of glycerol to the screen was an attempt to slow down the rate of nucleation events occurring during incubation. Thus, improving the quality of single crystals in the drop. Unfortunately, with the addition of glycerol to the conditions, no hits were seen in the screen.

9.2.4.3 Sodium malonate JCSG+ screen yield no crystals that were of better quality than those found in the initial screens

Due to the crystals observed in conditions containing 0.8 M sodium malonate, 0.1 M HEPES pH 7.0 and 0.5 % v/v Jeffamine ED-2001/ M2005, Bd1483 was trialled in a 96 well custom screen involving the addition of 10% JCSG+ screens to a 90% 0.8 M sodium malonate, 0.1 M HEPES pH 7.0 and 0.5 % v/v Jeffamine M2005 condition. This trial yielded hits, but none of these hits were better than that found in the original JCSG+ screen.

9.2.4.4 EDTA treated Bd1483 was found to crystallise, but true crystals could not be obtained

During the purification of Bd1483, the nickel loaded columns appeared to lose the nickel upon elution of the protein. With the possibility that Bd1483 was chelating Ni²⁺, and introducing heterogeneity into the purified protein, we attempted to introduce homogeneity to the protein by treating the sample with one divalent cation. To do this the purified protein was treated with 2 times the protein concentration of EDTA to remove any bound divalent cations. Before incubation with a single divalent cation species by dialysis, the EDTA-treated protein was trialled in JCSG+ to examine if crystals could be obtained in a cofactor free state. These yielded results after 48

hours in the condition containing 0.15 M potassium bromide 30 % w/v PEG 2000 MME (figure 13a and b).

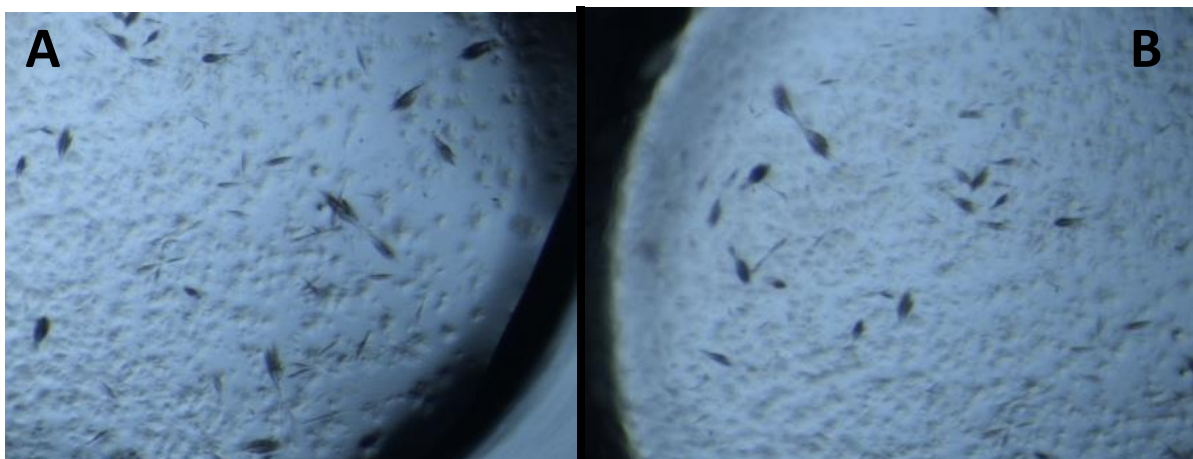


Figure 13. **Crystal hits of EDTA treated Bd1483 in JCSG+**

Both images are of Crystals of suspected Bd1483 in a condition of 0.15 M potassium bromide 30 % w/v PEG 2000 MME.

9.2.4.5 Conditions containing Bd1483 treated with 10mM manganese chloride yielded suspected salt crystals.

After treating Bd1483 with EDTA, the protein was dialysed for 3 hours in the presence of 10mM $MnCl_2$. This was chosen as other vWA domain containing proteins have been shown to bind this divalent cation, and its limited availability in the growth media may have introduced heterogeneity into the original protein sample. Screening of this protein was undertaken in JCSG+ and after 2 days incubation 1 hit was observed (figure 14). This hit was found in a condition of 0.1M sodium acetate pH 4.5 and 1.0M di-ammonium hydrogen phosphate.

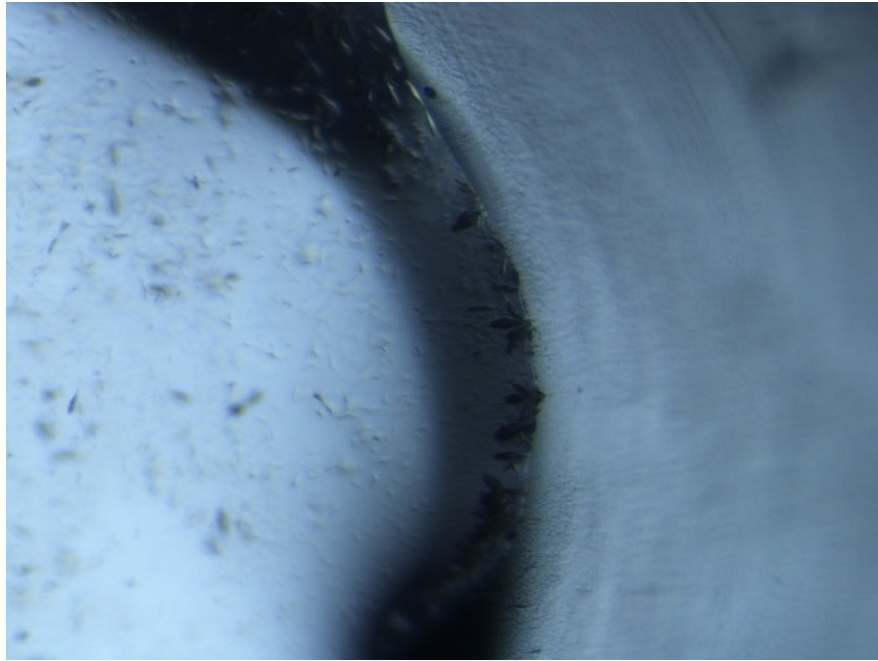


Figure 14. **Crystal hits of 10 mM MnCl₂ treated Bd1483 in JCSG+ screen**

One hit was obtained in this screen. But his may be due to salt formation rather than proteinaceous crystals.

9.2.4.6 Conditions containing Bd1483 treated with 10mM magnesium chloride yielded suspected salt crystals

As with the manganese treated Bd1483, protein was dialysed for 3 hours into 10mM MgCl₂. This was also trialled in the JCSG+ screen and 2 hits were seen after 48 hours. These hits were found in 0.2M sodium chloride/0.1M Na/K phosphate pH 6.2 with 50% PEG 200 (figure 15a) and 0.1M sodium acetate pH 4.5 with 1.0M di-ammonium hydrogen phosphate (figure 15b). As with the manganese treated Bd1483, these were also likely to be salt crystals and no further investigation was undertaken.

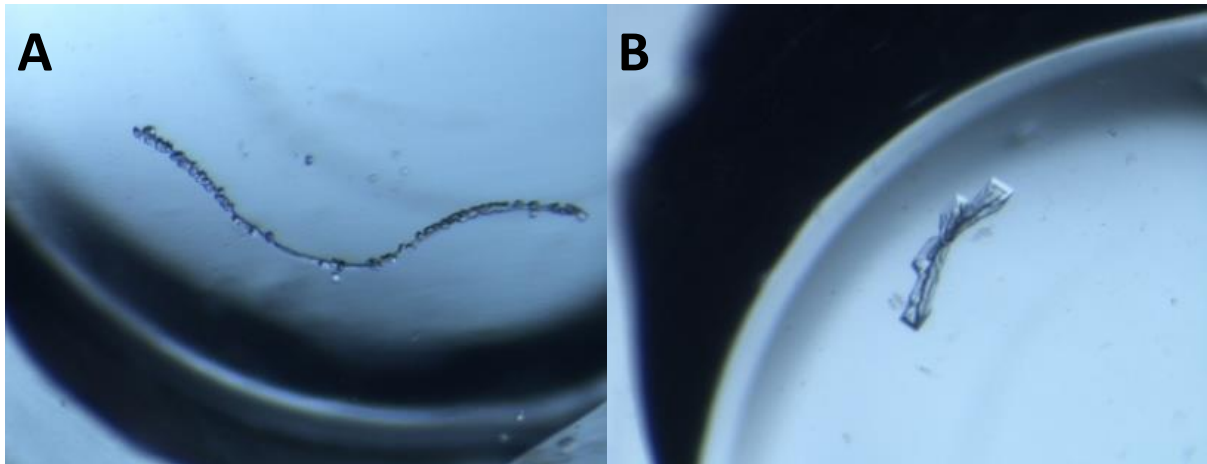


Figure 15. **Crystal hits found in JCSG+ when trailing 10mM MgCl₂ treated Bd1483**

A) 0.2M sodium chloride/0.1M Na/K phosphate pH 6.2 with 50% PEG 200

B) 0.1M sodium acetate at pH 4.5 and 1.0M di-ammonium hydrogen phosphate

Unfortunately both of these hits can be attributed to phosphate crystals.

9.2.4.7 Suspected Bd1483 crystals showed no diffraction

With the crystals of suspected Bd1483 found in 0.2M magnesium formate and 20% PEG 3350 showing promise for proteinaceous crystals that may diffract (figure 11B), these crystals were cryoprotected, looped from the drop, flash frozen and sent to Diamond light source for data collection. Unfortunately, no diffraction spots were detected for any of the crystals that were sent (data not shown).

9.3 Cloning, expression, expression and crystallization studies of the suspected C-di-GMP binding protein, Bd1996

9.3.1 Cloning of bd1996 proved successful

To clone our gene of interest, *bd1996*, from the genomic DNA of *Bdellovibrio bacteriovorus* HD100, PCR amplification was undertaken using primers specific for the *bd1996* gene. This product was then used for further cloning. Primary PCR amplification was undertaken using the velocity enzyme. This proved successful (lane 7, 9 and 10 of figure 16A). This primary product was then purified and used in a secondary PCR to clone the *bd1996* gene into the pET41c plasmid. After Dpn1 treatment and purification, *E. coli* DH5 α cells were transformed with the purified plasmid. Colonies were picked and subjected to colony PCR amplification to see if the up taken plasmid had the insert of the gene of interest, which would show as a band above the 0.5 kb marker. Of the 6 transformed colonies 2 showed that insert DNA was present (Lane 7 and 9 of figure 16B). These colonies were then grown overnight and samples of purified plasmids sent off to the functional genomics facility in the University of Birmingham for sequencing. One of these plasmids were shown to have the correct sequence for *bd1996* and this plasmid was used to transform *E. coli* BL21*.

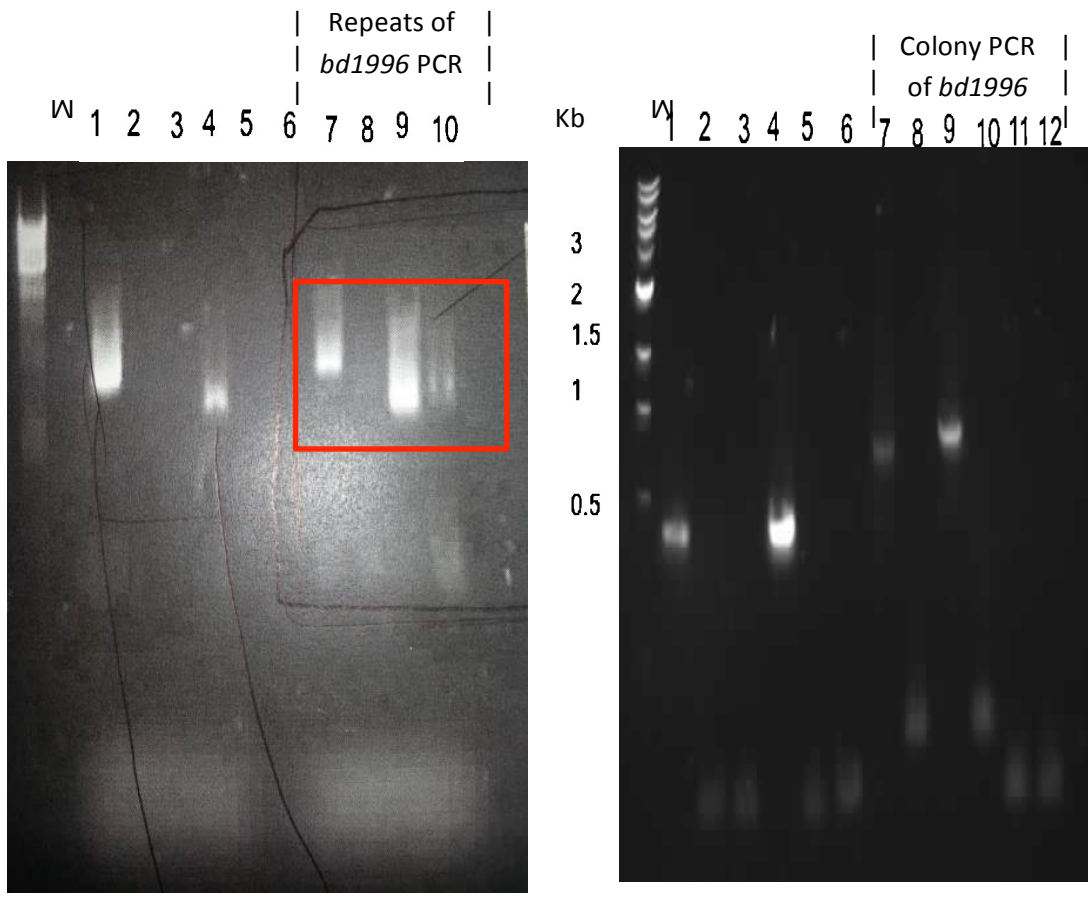


Figure 16. Agarose gels of PCR products during the cloning of *bd1996*.

A) A 1% agarose gel showing the primary PCR product of *bd1996* amplification in lanes 7, 9 and 10. Lanes 1-4 shows non-related results while lanes 7-10 show 4 PCR reactions attempting to clone *bd1996*. These products were then used for secondary PCR in the presence of the pET41c plasmid. Unfortunately, the marker and samples as a whole had not run correctly so the marker cannot be used to label the gel accurately.

B) A 1% agarose gel of the PCR conducted on suspected transformed *E. coli* DH5 α transformed with pET41c-*bd1996* on lanes 7-12. Lanes 7 and 9 show colonies that are resistant to the kanamycin LB agar plates that have taken up the pET41c plasmid, with a band near the 1 Kb marker. All other lanes have become kanamycin resistant through some other mechanism.

9.3.2 Test expression of Bd1996 showed that Bd1996 was possibly insoluble upon overexpression

Test expressions were carried out to check the solubility of Bd1996. This was undertaken to hopefully optimise expression before scaling to litres of culture. Figure 17 shows the SDS PAGE analysis out of the test expressions in different conditions. As figure 17 shows that in all conditions tested, Bd1996, was expressed with a band seen at roughly 27 kDa in the whole cell fraction, with an induction of 1000 μ M IPTG showing greatest amount of expression after 5 hours of expression (figure 17A). Expression was low in the soluble fractions (lanes 2, 4, 6, 8) indicating that this protein, as with other previously studied PilZ/DUF4339 domain proteins (Bd3100), had a low solubility when over expressed in *E. coli* BL21*. This was also seen after overnight incubation at 18°C. Figure 17b shows the expression of Bd1996 after 18 hours of incubation at 18°C, in the lanes containing whole cell samples (1, 3, 5 and 7) there is overexpression of Bd1996 at 27kDa. Oddly, overexpression with 1000 μ M IPTG yielded less protein when analysed by SDS-PAGE. As with the time point taken at 5 hours post induction, there appears to be little Bd1996 found in the soluble fraction, with most soluble protein being seen in the condition where cells were grown in 2x strength LB broth and induced with 25 μ M IPTG. Even though expression of soluble protein seemed low we decided to carry on with full scale expression, growing cultures in 2x strength LB broth, inducing with 25 μ M IPTG and incubating overnight at 18°C.

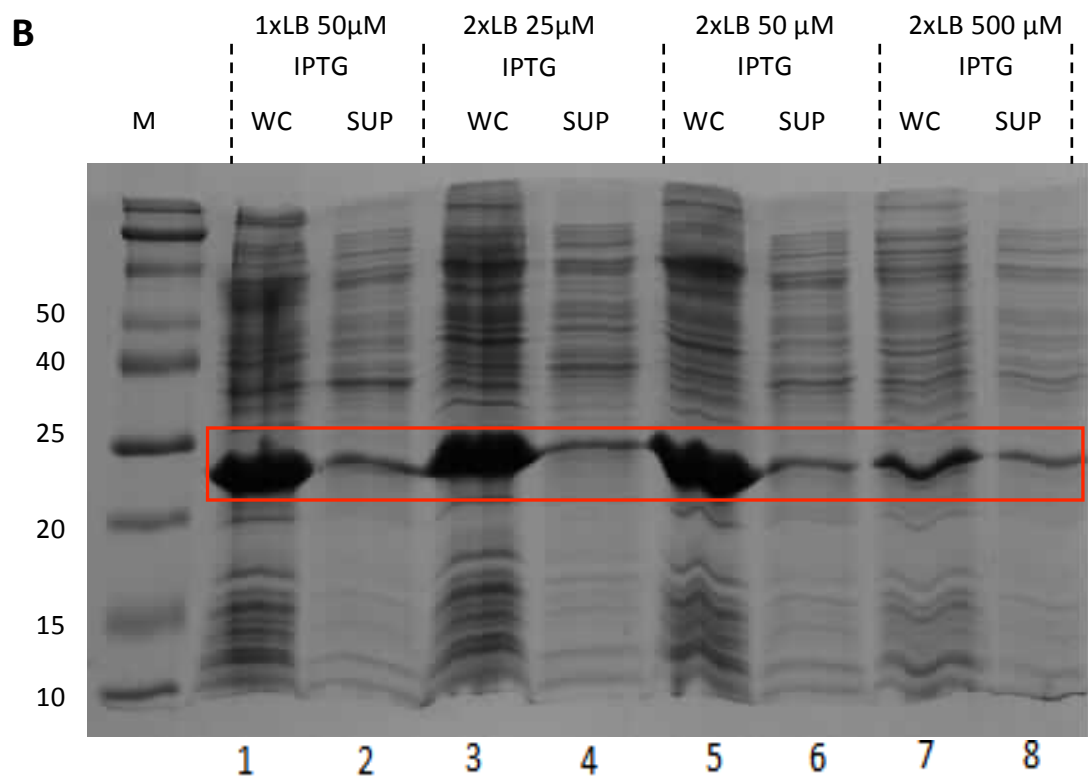
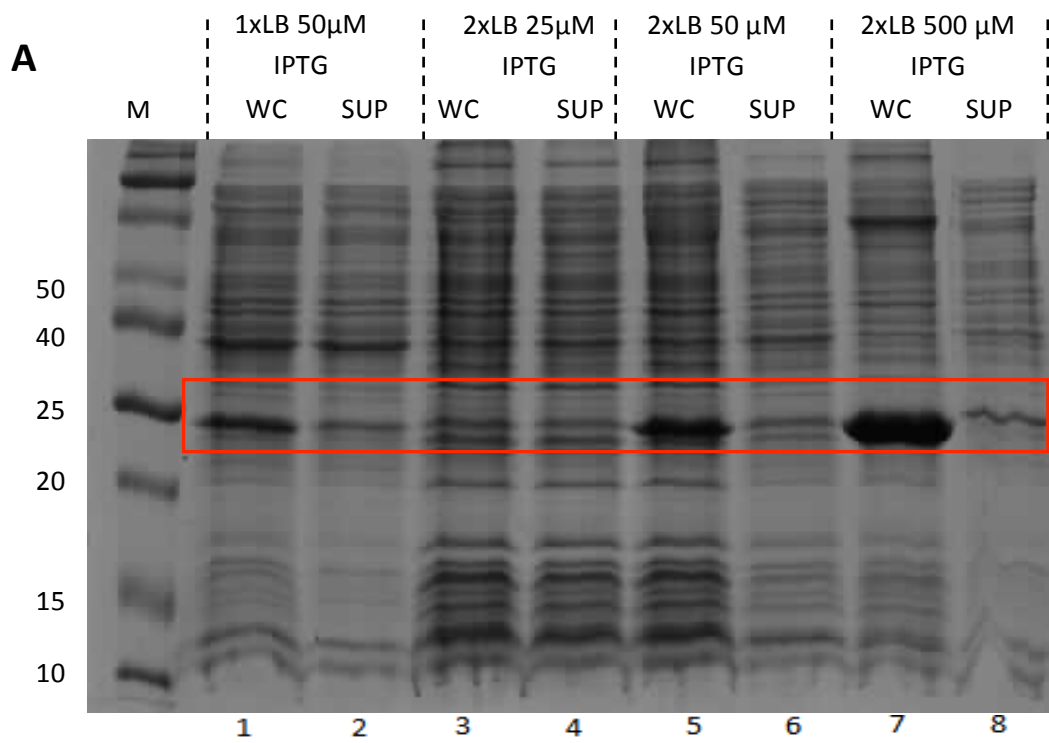


Figure 17. Test expressions of Bd1996 in *E. coli* BL21*.

A) A SDS-PAGE of whole cell vs. soluble supernatant of samples *E. coli* BL21* cultures expressing Bd1996, 5 hours post induction with IPTG. Lanes 1, 3, 5 and 7 show samples of the whole cell fractions when cells have been lysed in BugBuster™. Lanes 2, 4, 6 and 8 show the soluble supernatant fractions once the whole has been spun at 17,000xg to remove insoluble debris. A band below the 25 kDa marker, representing Bd1996 (27kDa), can be seen in lanes 1 (50 μM IPTG, 1x LB broth), 3 (25μM IPTG, 2xLB broth), 5 (50 μM IPTG, 2x LB broth) and 7 (500μM IPTG, 2x LB broth). Due to the absence of a band at 25 kDa in the soluble supernatants these SDS-PAGEs suggest that after 5 hours post induction Bd1996 expression is insoluble.

B) A SDS-PAGE of whole cell vs. soluble supernatant of samples *E. coli* BL21* cultures expressing Bd1996, 24 hours post induction with IPTG. Lanes 1, 3, 5 and 7 show samples of the whole cell fractions (WC) when cells have been lysed in BugBuster™. Lanes 2, 4, 6 and 8 show the soluble supernatant (SUP) fractions once the whole has been spun at 17,000xg to remove insoluble debris. A band below the 25 kDa marker, representing Bd1996 (27kDa), can be seen in lanes 1, 3, 5 and 7, the whole cell fractions. This suggests that 24 hours after induction at 18°C Bd1996 expresses insoluble in all conditions tested.

9.3.3 Bd1996 expresses as a soluble protein upon scale up, but the stability of Bd1996 is dependant upon the buffer

When expression was scaled up, cells were lysed, spun down and supernatants passed over a HisTrap FF IMAC. Initial purification was undertaken using buffer B to elute Bd1996 off of the column. Bd1996 eluted off the column at 10% buffer B (~80 mM imidazole) and 100% buffer B (400mM imidazole). It was noted that if fractions containing Bd1996 were left in the high imidazole buffer B these fraction would precipitate shortly after elution, even at 4°C. When the precipitant was pelleted and soluble fraction dialysed into a low imidazole buffer the protein remained unstable, and once concentrated to 22mg/mL it continued to precipitate out of solution. SDS-PAGE analysis of the purification, shown in figure 18b, shows that the 100% imidazole elution was not pure. Although a large band at around 27 kDa can be seen, which is found in the other elution fractions, and is at the correct size for Bd1996, contaminants can also be seen in the sample. Even though this purification provided unstable protein that crashed when screened in crystallization trials, it shows that Bd1996 is indeed soluble, contrary to what the expression tests suggested.

To avoid the precipitative effects that imidazole exerts on proteins when in high concentrations, further purifications of Bd1996 were carried out in the same manner with the elution of protein at 10% buffer B. The final elution, to remove all bound protein, was carried out using buffer C (containing 50mM EDTA) to strip the column of nickel ions, therefore, eluting the rest of the bound protein. When the final elution was carried out in buffer C the eluted protein was more stable and did not precipitate upon elution. As shown by figure 19 this final elution step (buffer C) proves to be

more pure than the previous purification. With concentrated Bd1996, that was stable, crystal trials were undertaken.

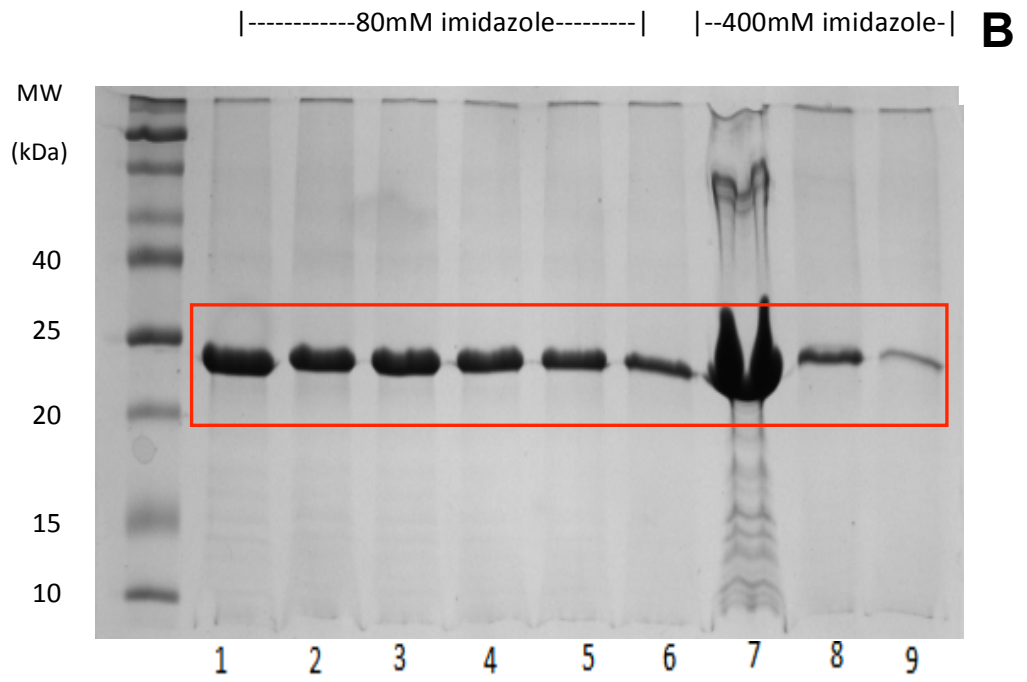
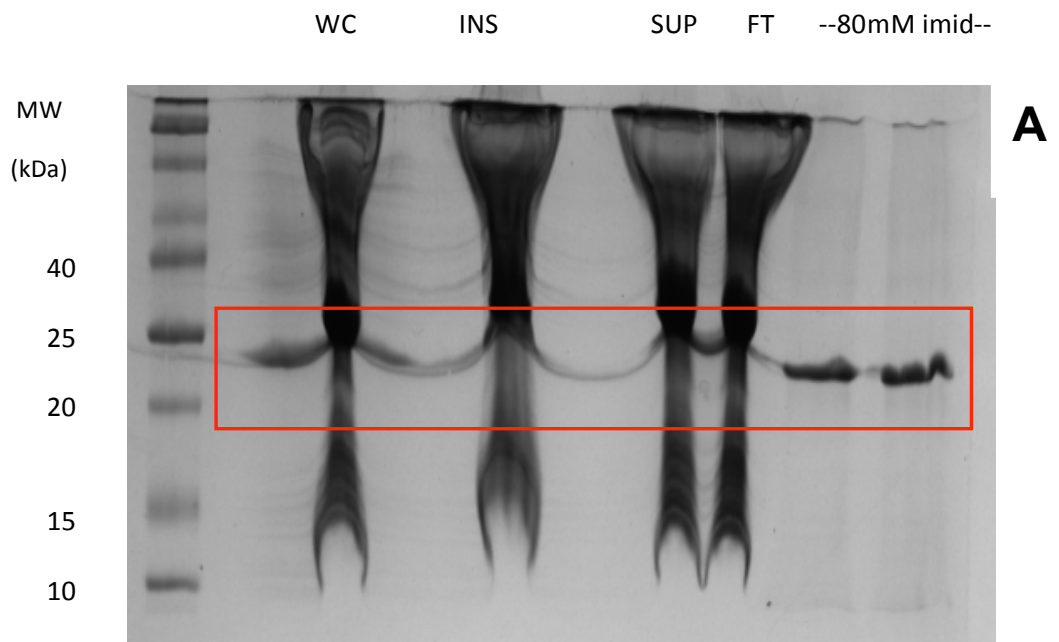


Figure 18. Scale-up expression of Bd1996

A) An SDS-PAGE showing the purification and expression of Bd1996. Lane 2 is the whole cell fractions taken after sonication. Lane 4 is the insoluble debris after centrifugation at 17,000xg. Lane 6 shows the soluble supernatant after centrifugation at 17,000xg. Lane 7 shows the flow through of the supernatant after it has been passed over a nickel loaded HisTrap column. Lanes 8 and 9 show the elution of Bd1483 at \approx 80 mM imidazole. The large band below 25 kDa represents Bd1996.

B) An SDS-PAGE showing the purification of Bd1996. Lanes 1-6 show the elution of Bd1996 at 80 mM imidazole. The large band below 25 kDa represents Bd1996. Lanes 7-9 show the elution at 400mM imidazole. This scale up expression shows that Bd1996 is soluble and bind relatively tightly to the HisTrap column, but when eluted with 400mM imidazole contaminants are eluted with it.

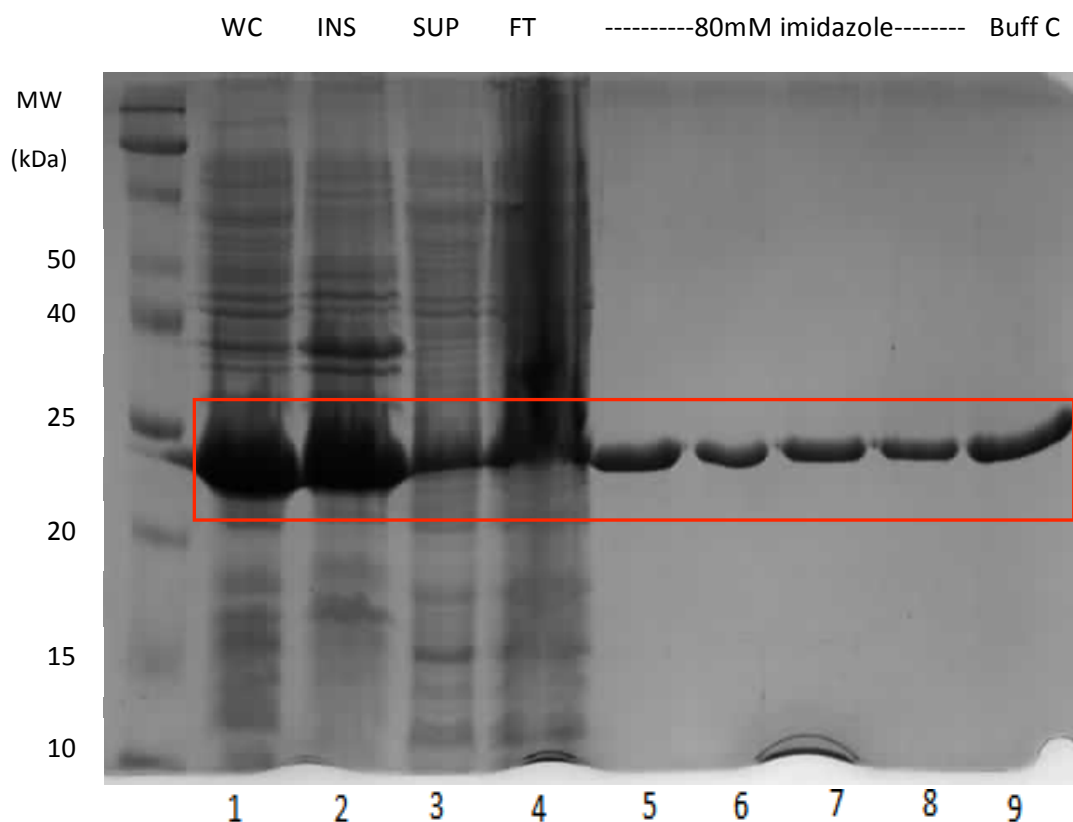


Figure 19. Elution of Bd1996 with buffer C.

An SDS-PAGE of the expression and purification of Bd1996, when eluted with buffer C. Lanes 1, 2, 3 and 4 represent the whole cell fraction, insoluble material, supernatant (after centrifugation at 17,000xg) and flow through of the supernatant (after being passed over a nickel loaded IMAC column), respectively. Lanes 5-8 show the fractions of elution with 80 mM imidazole. Lane 9 shows the elution of Bd1996 with buffer C.

9.3.4 Crystallisation screens of Bd1996 yielded conditions that showed the beginnings of crystal formation, but these conditions could not be optimised

As with Bd1483, we required crystals of Bd1996 for x-ray diffraction, to decipher the structure this protein's structure. So, to discover what conditions yielded the best quality of crystal, trialling of buffer conditions was undertaken. When screening Bd1996, the initial protein stock was unstable and trials in JCSG+ proved unfruitful with the majority of the conditions precipitating instantly or overnight. Due to this, a trial in the proplex buffer screen was undertaken. Unfortunately, this led to precipitation in the drop immediately or overnight.

With stable protein stocks (22 mg/mL), trials in JCSG+ yielded better results. Even though a lot of conditions precipitated immediately those that did not precipitate, generally, remained stable overnight and further. This was also seen when Bd1996 was trailed in the MIDAS screen. After 1 month of incubation at 18°C crystal shards were observed in 0.1M BIS-TRIS, pH 5.5 and 0.3M magnesium formate (figure 20). This condition was then optimised by undertaking a factorial screen by ranging the pH of the BIS-TRIS buffer from 5.5 to 7.2, and varying the amount of magnesium formate from 0 M to 0.5M. At the time of writing there has been no replication of crystal shards in the custom tray.

When Bd1996 was dialysed into the BIS-TRIS pH 6.5 and 200mM magnesium formate buffer, as suggested by the thermal shift buffer screen, trials in JCSG+ and MIDAS were undertaken. These conditions remained more stable than previous, with less causing precipitation of Bd1996, but at the time of writing there have been no observed crystals in these conditions.

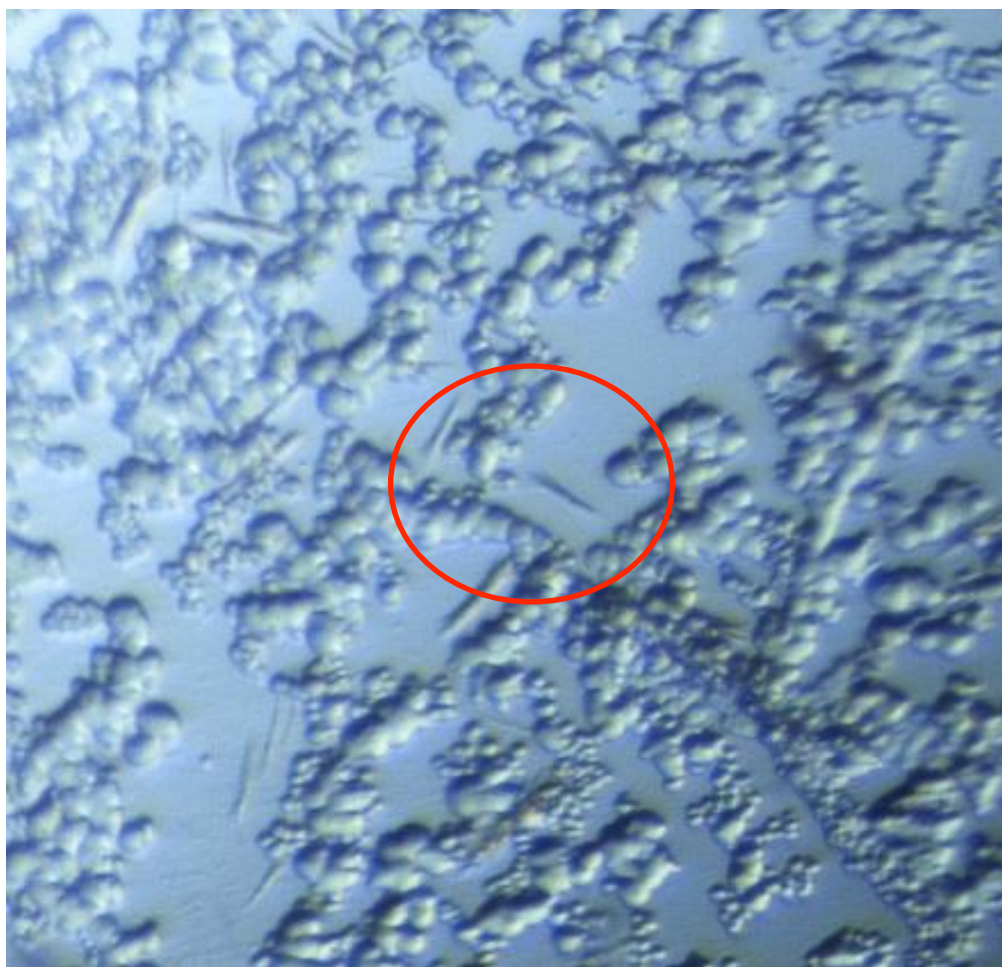


Figure 20. **Crystal hits of Bd1996 when trialled in JCSG+ screen.**

Shard like crystals found in condition 0.1M BIS-TRIS pH 5.5 and 0.3 M magnesium formate.

9.4 Cloning of the suspected lipid binding protein, Bd2538

9.4.1 Cloning and transformation of *bd2538* plasmids proved difficult with no plasmid constructs being produced

Initial cloning of *bd2538* was undertaken, first-of-all, using the velocity enzyme with the PCR protocol that worked previously for *bd1996*. This proved unsuccessful, as there was no PCR product of the required length, ≈ 1.6 Kb, found on the gel (figure 21A). This was repeated with and without the addition of DMSO to see if the DNA interfering nature of DMSO improves amplification with a touchdown PCR protocol, to find an annealing temperature that may produce product (figure 21B). Due to the relatively high GC content of primers (67% forwards and 58% reverse) PCR amplification was attempted using the Phusion™ enzyme, with GC buffer that has been optimised for high GC content PCR and higher temperatures (figure 21C). Again, this proved unsuccessful as no product was produced. Due to this the primers were analysed using IDT oligo analyser web tool (<http://www.idtdna.com/analyzer/Applications/OligoAnalyzer/>), which showed that the forwards primer had a high melting temperature of 63.6-72°C, and also produced 2° structures with itself, including hairpins, GC clamps and primer dimers. Due to this, one last attempt at producing PCR product with these was attempted using PFU polymerase before designing another *bd2538* forwards primer. This polymerase has a greater thermo-stability, so, it could hopefully be used at higher temperature during extension. Reactions were carried out, with eight conditions at four temperatures, 65°C, 60°C, 55°C, 50°C, with and without the addition of DMSO. No conditions attempted yielded PCR product (figure 21D).

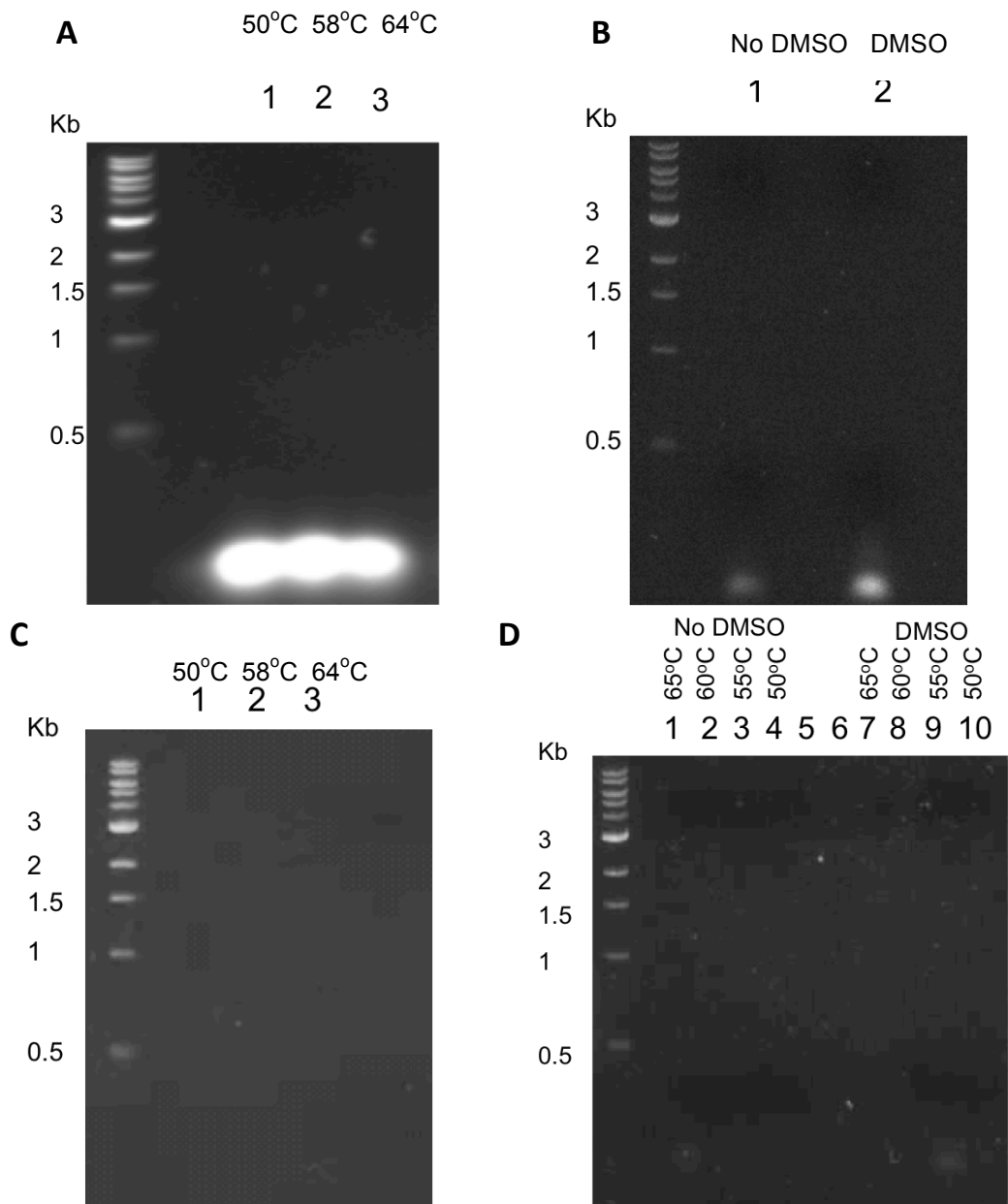


Figure 21. The four attempts at the initial PCR amplification of the *bd2538* gene.

A) A 1% agarose gel of the first attempt at PCR amplification of *bd2538*. Lanes 1-3 were run with the velocity enzyme with an annealing step at 50°C, 58°C and 64°C, respectively. No PCR product was found.

B) A 1% agarose gel of the PCR amplification of *bd2538* using the Velocity™ enzyme in a touchdown protocol in the presence and absence of DMSO. Lanes 1 (No DMSO) showed no product, neither did lane 2 (containing DMSO).

C) A 1% agarose gel of the PCR amplification of *bd2538* using the Phusion™ enzymes. Lanes 1-3 were run with an annealing step at 50°C, 58°C and 64°C, respectively. No PCR product was found.

D) A 1% agarose gel of the PCR amplification of *bd2538* using the PFU™ enzyme in the presence and absence of DMSO and in a touchdown protocol. Lanes 1-4 have no DMSO and show no product; neither did the conditions containing DMSO (6-10). 4 PCR amplifications each were carried at different temperatures annealing going: 65°C, 60°C, 55°C and 50°C, from left to right for both the no DMSO conditions and DMSO conditions

PCR was attempted with new a new forwards primer and was carried out by another researcher in the lab, this yielded PCR product. This product was then purified to remove the enzyme. Figure 22 A shows the gel of the PCR product after purification. This primary product was the used in secondary PCR to produce plasmid with the required insert. This secondary PCR product was then Dpn1 treated, purified and used to transform competent *E. coli* DH5 α cells. Transformed cells were plated on kanamycin selective LB agar and incubated at room temperature for 60 hours. Colonies were spotted onto agar and used in colony PCR to look for the plasmid in these cells. Unfortunately, of the 3 colonies that were picked, none were shown to have taken up plasmid with the required insert (figure 22 B).

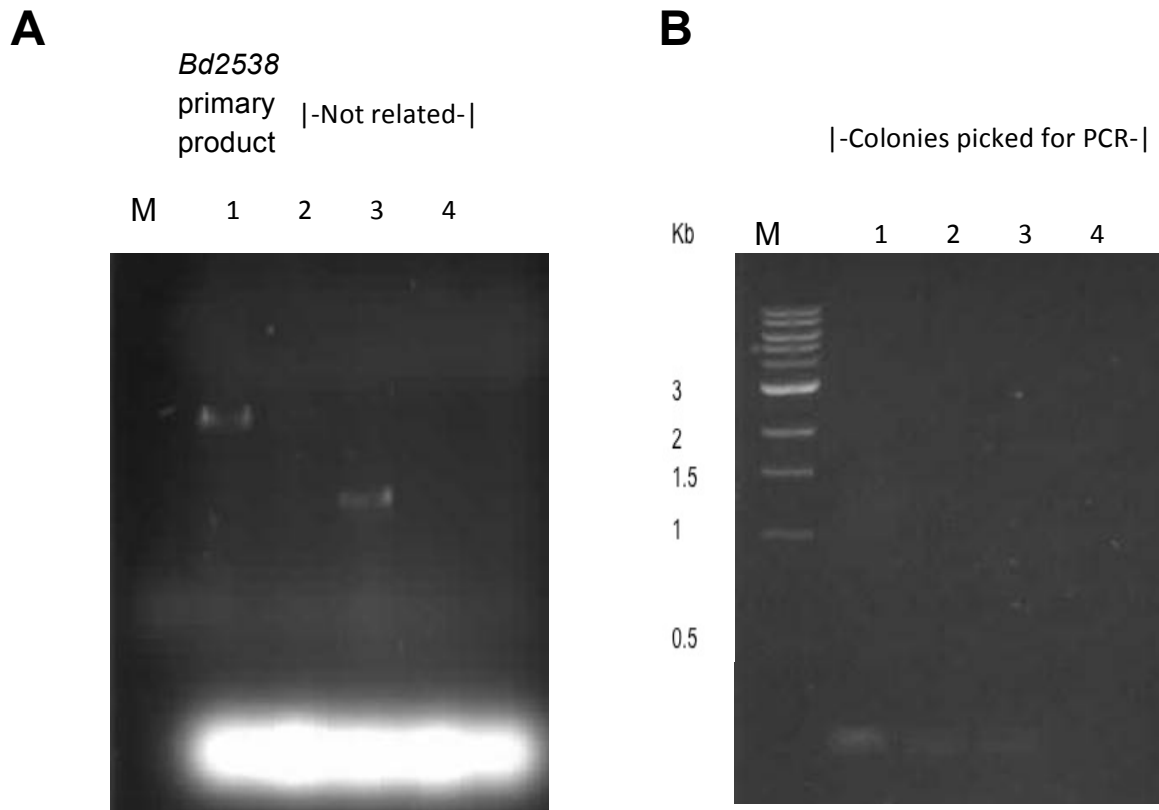


Figure 21 **Agarose gels of PCR products during the cloning of *bd2538* with new primers.**

A) A 1% agarose gel showing the purified primary PCR product of *bd2538* in lane 1. These products were then used for secondary PCR in the presence of the pET41c plasmid. Unfortunately due to an unfortunate omission of the ladder from the gel the size of the size of the primary product could not be determined.

B) A 1% agarose gel of the PCR conducted on suspected transformed *E. coli* DH5 α transformed with pET41c-*bd2538*. No lanes showed plasmid insert present.

10.0 Discussion

Although no structures were determined by x-ray crystallography, or by other means, during the study, initial expression and purification of 2 previously unexpressed *Bdellovibrio* proteins, Bd1483 and Bd1996, had been undertaken in *E. coli*. Expression and crystallization conditions for the vWA domain containing protein, Bd1483, have been uncovered, along with a single crystal that proved to be non-diffracting. Bd1996, a putative C-di-GMP binding protein, has also been cloned, expressed and crystal trials were undertaken, with mixed results. Although Bd3100, another putative PilZ/GYF domain protein, remained insoluble when overexpressed we have described the initial attempts to refold Bd3100, with promising results that may lead to avenues of study.

10.1 Bd3100

10.1.1 Bd3100 expression is insoluble even when expression is optimised

Even though previous studies (unpublished) showed that over expression of Bd3100 aggregates into insoluble inclusion bodies, test expression were carried out to confirm this. Even with expression in low IPTG/temperature conditions inclusion bodies of insoluble Bd3100 were produced. Inclusion bodies can form when recombinant protein expression out speeds the rate at which native chaperones can accommodate and assist in the correct folding of nascent polypeptides being transcribed across the polyribosomal mRNA (Baneyx and Mujacic, 2004). If chaperones are limited, nascent polypeptide strands begin to interact with each other leading to misfolded polypeptides and aggregation as misfolded insoluble inclusion bodies. Other studies have shown how the co-expression of molecular chaperones allows for the expression of previously insoluble proteins (Nishihara *et al.*, 1998;

Alderwick *et al.*, 2008; Yan *et al.*, 2012, Xu *et al.*, 2014). While this may seem a good route of investigation the amount of time required to achieve this meant this avenue of investigation was out of the scope of this project. So, instead of co-expressing recombinant chaperones, we attempted to increase the expression of native chaperones by addition of glycyglycine to the growth media (Ghosh *et al.*, 2004). Ghosh *et al.*, have shown that the addition of glycyglycine to the growth media increases the solubility of previously insoluble proteins of mycobacterial origin, which are notorious for expressing as insoluble aggregates in *E. coli*. The authors attributed this to glycyglycine inducing an osmotic stress upon *E. coli*, as well as slowing down metabolism. Thusly, slowing down the translation of the over expressing protein. Due to this, we chose test whether the addition of glycyglycine, to the media, enhanced the solubility of Bd3100. Unfortunately this did not improve the solubility of Bd3100 at any of the concentrations tested, so focus was moved onto solubilising and refolding the inclusion material containing Bd3100.

10.1.2 Shock refolding of Bd3100 yields soluble, but unstable, protein

Seeing as all initial growth conditions tested produced inclusion bodies of Bd3100, which were not improved with the addition of glycyglycine, full-scale expression of Bd3100 went ahead in the condition that produced the greatest amount of inclusion material. The inclusion bodies were solubilised in 6M guanidine hydrochloride, a chaotropic agent that destabilises hydrophobic effects that cause proteins to fold by interrupting hydrogen bonding in water (Rashid *et al.*, 2005). The buffer used for this contained 2% Triton X-100™ to hopefully free protein from membranes that are associated with inclusion body material. β -mercaptoethanol was added to the buffers to prevent the possible formation of disulphide bonds that would not be found in the

native protein, as this may lead to misfolded protein leading to precipitation (Monera *et al*, 1994). Initial refolding on the column did not yield soluble protein, in fact it was found to have precipitated on the column. So, a buffer screen of shock refolding conditions was undertaken. This proved initially successful with the sodium acetate buffers providing stable soluble protein upon shock refolding. Upon scale up of the shock refolding in a 50 mM sodium acetate pH 4.6 and 1 mM β -ME, Bd3100 remained soluble, but spin concentrating proved difficult and was lengthy. To the point where suspected Bd3100 was beginning to precipitate out of solution, even when stored at 4°C. In light of this we decided to check the purity of the suspected refolded Bd3100 and found that while there was Bd3100 present in the solution, it was not pure. This can be attributed to forgoing IMAC purification that had proven to be difficult with the unfolded Bd3100 when attempted by another researcher in the group. We decided to forgo this due to inclusion bodies generally being highly pure for the over expressed protein. Others have used this solubilisation of inclusion material without purification before, namely with overexpressed *E. coli* RNA polymerase (Burgess 1996). If time was not a limiting factor it would be interesting continue with the shock refolding method and begin optimisation. With soluble and presumably refolded Bd3100, it would be interesting to carry out ion exchange chromatography to remove the contaminating protein found in the inclusion bodies.

10.1.3 Further work with Bd3100

To check if the protein was refolded correctly, we could undertake circular dichroism on to study whether the composition of secondary structures in the refolded sample is similar to that of the predicted protein. This would be able to be undertaken even with a small yield of protein. If yield was large enough, crystallization screening could

be undertaken, along with biochemical characterisation such as size exclusion chromatography and analytical ultracentrifugation, to study whether this protein forms homodimers in the presence, or absence, of C-di-GMP. Along with this it may be possible to undertake pull-down experiments with *Bdellovibrio* lysate. This could be undertaken in the presence and absence of C-di-GMP, to see whether binding to native proteins is induced by conformational changes brought on by C-di-GMP binding, then mass spectrometry could be applied to the pulled down proteins to identify what Bd3100 binds *in vivo*. This could hopefully place Bd3100 in the C-di-GMP signalling network.

10.2 Bd1996

10.2.1 Bd1996 expression is soluble but relatively unstable in the presence of imidazole

Bd1996 was soluble upon over expression and signifies the first time that a protein containing a PilZ domain and DUF4339 domain has been soluble when overexpressed in *E. coli*. Although, it precipitated overnight and remained unstable to begin with, this can be attributed to the high imidazole used to elute off the IMAC column. This was remedied by eluting the protein off the column with EDTA. Imidazole can act as a chaotropic agent at high concentrations, which can lead to protein precipitation, as in this case. Because of this, a buffer containing EDTA was used to chelate the nickel ions bound to the column. Therefore, eluting the bound protein off the column. This avoids the use of high concentrations of imidazole.

10.2.2 Crystallization of Bd1996 gave hits but could not be optimised to give diffractable crystals and further study.

During the crystallization trials, conditions that showed crystal shard formation were optimised for crystal growth. These trials undertaken did not produce diffractable crystals. It is noted though; Bd1996 did not behave well in any the screens used, with a lot of the conditions leading to precipitation. This may need further study to try and improve stability, which may help in obtaining diffractable crystals. If crystallization is not possible, it may be possible to determine protein structure through other methods, such as nuclear magnetic resonance. Along with this it would be good to undertake similar biochemical characterisation as was suggested with Bd3100. Histag pull-downs with this protein and *B. bacteriovorus* lysates were planned, but due to time constraints they could not be completed during this study. This would be used to decipher the binding partners of Bd1996 and would help place Bd1996 into a model for C-di-GMP signalling. This would also give insight into how the DUF4339 domains function in prokaryotes. As with Bd3100, analytical ultracentrifugation in the presence and absence of C-di-GMP could also be undertaken to investigate whether this protein forms homodimers, as many PilZ domain proteins do (Krasteva *et al.*, 2012).

10.3 Bd2538

10.3.1 Initial primers for *bd2538* hampered initial efforts at cloning but altered primers remedied this

As stated in the results, cloning of the suspected lipid binding protein proved difficult and unsuccessful. Initial cloning was halted due to the forwards primer forming secondary structures, such as GC clamps, hairpin loops and others, which prevented

amplification. Also, the forward primer melting temperature was excessively high. To remedy this, different DNA polymerases were investigated, to see if any of these were suitable. Different PCR reactions were attempted, such as touchdown, to no avail. After these showed no PCR product DMSO was added to the PCR. DMSO binds to cytosine nucleotides, decreasing the melting temperature of the primer, which is specifically useful in GC rich primers (Chester and Marshek, 1993, Jensen *et al.*, 2010). DMSO also aids in preventing secondary primer structures such as, primer dimers and hairpin loops, but can lead to an increased mutational rate during PCR, although this is controversial (Hardjasa *et al.*, 2010, Jensen *et al.*, 2010). Even with the addition of DMSO primary PCR could not be obtained. So, an altered forwards primer was designed and used. This proved successful and produced primary product, which was then used to produce recombinant plasmid.

10.3.2 Cloning of *bd2538* could not be carried on past the initial plasmid

Plasmid, suspected to have the *bd2538* gene, was then used to transform competent DH5 α . Three transformant colonies were obtained, but when these colonies were PCR amplified to check for an insert no insert was observed. This could be due to *E. coli* gaining a random mutation leading to kanamycin resistance or these colonies may have been transformed with pET41c that did not have the insert cloned into the plasmid.

10.4 Bd1483

10.4.1 Bd1483 expression is soluble and it crystalizes readily with non-diffracting crystals.

Bd1483 was soluble upon over expression and remained stable upon purification in a HEPES buffer, which allowed for crystal trials. These trials led to many hits. Most of

these hits were needle cluster, similar to sea urchin crystal morphologies, which were not useable for x-ray diffraction. Many of these conditions were then taken forward and optimised for crystal growth. These were all undertaken using a factorial screen altering the pH of the condition and the molarity of salt or additives. Unfortunately none of these optimisation trials yielded crystals that were better than that found in the original drops. Due to this we attempted to alter the original crystallization conditions in the Bd1483 screens.

10.4.2 Altering the initial screening conditions of Bd1483 in JCSG+ led to interesting results

10.4.2.1 The addition of glycerol to the screen inhibited crystallization

Due to the large amounts of needle clusters forming it was assumed that many nucleation events were taking place. So, to combat this we added 10% glycerol to each drop of a JCSG+ screen. Similar studies have shown that the addition of glycerol decreases the amount of nucleation allowing for true crystal formation (Vera *et al.*, 2011). Unfortunately, this proved unsuccessful with no hits being seen over the study. This is probably due to glycerol's property of stabilising proteins in solution therefore inhibiting nucleation (Vegende *et al.*, 2009, Vera *et al.*, 2011).

10.4.2.2 The sodium malonate/JCSG+ screen did not improve hits that were previously seen

Because the condition of 0.8 M sodium malonate, 0.1 M HEPES pH 7.0 and 0.5 % v/v Jeffamine ED-2001 yielded crystals in every JCSG+ screen undertaken, and showed hits in custom screens (although not as well formed as the original hit), it was decided that using this condition with a 10% supplementation of the other JSCG+ conditions may yield diffractable crystals. Although hits were seen in this screen,

none of these hits were usable for structure determination, nor did they surpass the original hits in the JCSG+ screen.

10.4.2.3 Treating Bd1483 with EDTA and divalent cations did not improve crystallization

Next, the effect of Bd1483 bound cofactors on crystallisation was examined. Other vWA containing proteins have been shown to bind divalent cations, notably Mg^{2+} and Mn^{2+} (Whittaker *et al.*, 2002). Due to the T7 polymerase's requirement for Mg^{2+} this cation may be limited during overexpression leading Bd1483 to bind divalent cations that it would not normally bind with, for example Ni^{2+} from the IMAC column. This may be one possible reason for the failure in producing diffracting Bd1483 crystals. To try and combat this Bd1483 was treated with EDTA to remove the bound divalent cofactor and then dialysed in a buffer supplemented with 10mM of a divalent cation, to hopefully obtain a solution of Bd1483 with homogenously bound cations. This was tested with both magnesium and manganese. When these dialysed proteins were trialled across JCSG+ screen crystals were seen after 2 days, but due to the conditions they were found in, along with crystal morphology, it was assumed that these crystals were salt and not proteinaceous. Crystal shards were seen in EDTA treated Bd1483, but these crystals could not be optimised further.

10.4.3 0.2M magnesium formate with 20% PEG 3350 gave geometric crystals but these could not be repeated, nor did they diffract

After 2 months of incubation at 18°C, suspected Bd1483 crystals were observed in 0.2M magnesium formate with 20% PEG 3350. To try and replicate this two custom screens were carried out, one using a factorial screen varying the pH of the solution (molecular dimension state that magnesium formate has a pH of 7.6) and varying the

percentage of PEG 3350. One trial to decrease the amount of time for crystal formation, which from the original condition was 2.5 months, was attempted. The screen varying pH of the condition and percentage of PEG-3350 did not prove to yield crystals at the time of writing, but may yield crystals in the future. The second screen contained an increasing concentration of ammonium sulphate in the reservoir. This increasing concentration ammonium sulphate speeds up the rate of diffusion of water from the hanging drop, equilibrating the drop quicker. This proved unsuccessful with higher concentration of ammonium sulphate, in the reservoir, causing precipitation of Bd1483 in the drop. Crystals that were obtained in 0.2M magnesium formate with 20% PEG 3350 taken to the Diamond light source for data collection, but these crystals showed no diffraction.

10.4.4 Further study of Bd1483

Further study could be undertaken to obtain crystals that diffract. This would yield an opportunity to determine the structure of the vWA containing protein, and with this structure it may be possible to suggest what Bd1483 binds to, and whether or not it may be of prey or *Bdellovibrio* origin. As well as the continuation of crystallographic studies it would be interesting to characterise what Bd1483 binds to. This could be undertaken using histag pull-downs with *Bdellovibrio* and *E. coli* lysates. If Bd1483 was found to bind proteins, when eluted of an IMAC column, mass spectrometry could be used to identify the co-purified partners. This would be interesting to see if Bd1483 binds prey or native proteins, which could help place this protein in the model for prey recognition leading to invasion.

11.0 Conclusion

We have shown that Bd3100 is insoluble upon overexpression in *E. coli*, even when additives known to improve solubility are added, but shock refolding of denatured inclusion material in 0.1M sodium acetate supplemented with β -ME proved to yield soluble product. This remains to be optimised, with improvement to Bd3100 stability and purity needed. Bd1996 has been shown to be the first soluble protein that contains both the DUF4339 GYF-like and PilZ domains. Bd2538 remains to be cloned but a new forwards primer was shown to improve primary PCR amplification of the *bd2538* gene. Bd1483 has been shown to overexpress as a soluble protein and crystalized readily. Although this also remains to be optimised, for crystals that will diffract. While this study has not been able to conclusively place any of the studied proteins into the prey recognition/invasion pathway it has laid the basis for further study into how these proteins control prey recognition, as well as how C-di-GMP is involved in this signal. With this information a model for how this interesting, and possibly medically relevant, bacterium undergoes predation and how C-di-GMP controls this could be described.

Bibliography

Alderwick, L.J., Dover, L.G., Veerapen, N., *et al.* (2008) Expression, purification and characterisation of soluble GfT and the identification of a novel galactofuranosyltransferase Rv3782 involved in priming GfT-mediated galactan polymerisation in *Mycobacterium tuberculosis*. **Protein Expression and Purification**, 58 (2): 332-341.

Amikam, D. and Galperin, M.Y. (2006) PilZ domain is part of the bacterial C-di-GMP binding protein. **Bioinformatics (Oxford, England)**, 22 (1): 3-6.

Atterbury, R.J., Hopley, L., Till, R., *et al.* (2011) Effects of orally administered *Bdellovibrio bacteriovorus* on the well-being and *Salmonella* colonization of young chicks. **Applied and Environmental Microbiology**, 77 (16): 5794-5803.

Balaji, S. and Aravind, L. (2007) The RAGNYA fold: a novel fold with multiple topological variants found in functionally diverse nucleic acid, nucleotide and peptide-binding proteins. **Nucleic Acids Research**, 35 (17): 5658-5671.

Baneyx, F. and Mujacic, M. (2004) Recombinant protein folding and misfolding in *Escherichia coli*. **Nature Biotechnology**, 22 (11): 1399-1408.

Beck, S., Schwudke, D., Strauch, E., *et al.* (2004) *Bdellovibrio bacteriovorus* strains produce a novel major outer membrane protein during predacious growth in the periplasm of prey bacteria. **Journal of Bacteriology**, 186 (9): 2766-2773.

Bellini, D., Caly, D.L., McCarthy, Y., *et al.* (2014) Crystal structure of an HD-GYP domain cyclic-di-GMP phosphodiesterase reveals an enzyme with a novel trinuclear catalytic iron centre. **Molecular Microbiology**, 91 (1): 26-38.

Bergelson, J. and Hemler, M. (1995) Integrin-Ligand Binding: Do integrins use a 'MIDAS touch' to grasp an Asp? **Current Biology**, 5 (6): 615-617.

Burgess, R.R. (1996) Purification of overproduced *Escherichia coli* RNA polymerase sigma factors by solubilizing inclusion bodies and refolding from Sarkosyl. **Methods in Enzymology**, 273 (A): 145-149.

Capeness, M.J., Lambert, C., Lovering, A.L., *et al.* (2013) Activity of *Bdellovibrio* Hit Locus Proteins, Bd0108 and Bd0109, Links Type IVa Pilus Extrusion/Retraction Status to Prey-Independent Growth Signalling. **PLoS One**, 8 (11): e79759.

Chester, N. and Marshak, D.R. (1993) Dimethyl Sulfoxide-Mediated Primer *Tm* Reduction: A Method for Analyzing the Role of Renaturation Temperature in the Polymerase Chain Reaction. **Analytical Biochemistry**, 209 (2): 284-290.

Cotter, T.W. and Thomashow, M.F. (1992) Identification of a *Bdellovibrio bacteriovorus* genetic locus, hit, associated with the host-independent phenotype. **Journal of Bacteriology**, 174 (19): 6018-6024.

Craig, L., Pique, M.E. and Tainer, J.A. (2004) Type IV pilus structure and bacterial pathogenicity. **Nature Reviews Microbiology**, 2 (5): 363-378.

Dori-Bachash, M., Dassa, B., Pietrokovski, S., *et al.* (2008) Proteome-based comparative analyses of growth stages reveal new cell cycle-dependent functions in

the predatory bacterium *Bdellovibrio bacteriovorus*. **Applied and Environmental Microbiology**, 74 (23): 7152-7162.

Dwidar, M. and Mitchell, R.J. (2012) The dual probiotic and antibiotic nature of *Bdellovibrio bacteriovorus*. **Biochemistry and Molecular Biology Reports**, 45 (2): 71-78.

Evans, K.J., Lambert, C. and Sockett, R.E. (2007) Predation by *Bdellovibrio bacteriovorus* HD100 requires type IV pili. **Journal of Bacteriology**, 189 (13): 4850-4859.

Fitzgerald, J.R., Foster, T.J. and Cox, D. (2006) The interaction of bacterial pathogens with platelets. **Nature Reviews Microbiology**, 4 (6): 445-457.

Ghosh, S., Rasheedi, S., Rahim, S.S., *et al.* (2004) Method for enhancing solubility of the expressed recombinant proteins in *Escherichia coli*. **BioTechniques**, 37 418-423.

Hobley, L., Fung, R.K., Lambert, C., *et al.* (2012) Discrete cyclic di-GMP-dependent control of bacterial predation versus axenic growth in *Bdellovibrio bacteriovorus*. **PLoS Pathogens**, 8 (2): e1002493.

Iebba, V., Santangelo, F., Totino, V., *et al.* (2013) Higher prevalence and abundance of *Bdellovibrio bacteriovorus* in the human gut of healthy subjects. **PloS One**, 8 (4): e61608.

Jenal, U. and Malone, J. (2006) Mechanisms of cyclic-di-GMP signaling in bacteria. **Annual Review Genetics**, 40 385-407.

Jensen, M.A., Fukushima, M. and Davis, R.W. (2010) DMSO and betaine greatly improve amplification of GC-rich constructs in de novo synthesis. **PLoS One**, 5 (6): e11024.

Kadouri, D.E., To, K., Shanks, R.M., *et al.* (2013) Predatory Bacteria: A potential ally against multidrug-resistant Gram-negative pathogens. **PloS One**, 8 (5): e63397.

Kofler, M.M. and Freund, C. (2006) The GYF domain. **FEBS Journal**, 273 (2): 245-256.

Kofler, M., Motzny, K. and Freund, C. (2005) GYF domain proteomics reveals interaction sites in known and novel target proteins. **Molecular & Cellular Proteomics**, 4 (11): 1797-1811.

Kopec, K., Alva, V. and Lupas, A. (2011) Bioinformatics of the TULIP domain superfamily. **Biochemical Society Transactions**, 39 (4): 1033.

Kopec, K.O., Alva, V. and Lupas, A.N. (2010) Homology of SMP domains to the TULIP superfamily of lipid-binding proteins provides a structural basis for lipid exchange between ER and mitochondria. **Bioinformatics**, 26 (16): 1927-1931.

Krasteva, P.V., Giglio, K.M. and Sondermann, H. (2012) Sensing the messenger: The diverse ways that bacteria signal through c-di-GMP. **Protein Science**, 21 (7): 929-948.

LaMarre, A.G., Straley, S.C. and Conti, S.F. (1977) Chemotaxis toward amino acids by *Bdellovibrio bacteriovorus*. **Journal of Bacteriology**, 131 (1): 201-207.

Lambert, C., Chang, C., Capeness, M.J., *et al.* (2010) The first bite—profiling the predatosome in the bacterial pathogen *Bdellovibrio*. **PLoS One**, 5 (1): e8599.

Lambert, C., Fenton, A.K., Hogley, L., *et al.* (2011) Predatory *Bdellovibrio* bacteria use gliding motility to scout for prey on surfaces. **Journal of Bacteriology**, 193 (12): 3139-3141.

Lerner, T.R., Lovering, A.L., Bui, N.K., *et al.* (2012) Specialized peptidoglycan hydrolases sculpt the intra-bacterial niche of predatory *Bdellovibrio* and increase population fitness. **PLoS Pathogens**, 8 (2): e1002524.

Lovering, A.L., Capeness, M.J., Lambert, C., *et al.* (2011) The structure of an unconventional HD-GYP protein from *Bdellovibrio* reveals the roles of conserved residues in this class of cyclic-di-GMP phosphodiesterases. **mBio**, 2 (5): 10.1128/mBio.00163-11. Print 2011.

Luciano, J., Agrebi, R., Le Gall, A.V., *et al.* (2011) Emergence and modular evolution of a novel motility machinery in bacteria. **PLoS Genetics**, 7 (9): e1002268.

Medina, A.A., Shanks, R.M. and Kadouri, D.E. (2008) Development of a novel system for isolating genes involved in predator-prey interactions using host independent derivatives of *Bdellovibrio bacteriovorus* 109J. **BMC Microbiology**, 8 (33) doi:10.1186/1471-2180-8-33.

Milner, D.S., Till, R., Cadby, I., *et al.* (2014) Ras GTPase-Like Protein MglA, a Controller of Bacterial Social-Motility in Myxobacteria, Has Evolved to Control Bacterial Predation by *Bdellovibrio*. **PLoS Genetics**, 10 (4): e1004253.

Monera, O.D., Kay, C.M. and Hodges, R.S. (2008) Protein denaturation with guanidine hydrochloride or urea provides a different estimate of stability depending on the contributions of electrostatic interactions. **Protein Science**, 3 (11): 1984-1991.

Nishihara, K., Kanemori, M., Kitagawa, M., *et al.* (1998) Chaperone Coexpression Plasmids: Differential and Synergistic Roles of DnaK-DnaJ-GrpE and GroEL-GroES in Assisting Folding of an Allergen of Japanese Cedar Pollen, Cryj2, in *Escherichia coli*. **Applied and Environmental Microbiology**, 64 (5): 1694-1699.

Pallen, M., Chaudhuri, R. and Khan, A. (2002) Bacterial FHA domains: neglected players in the phospho-threonine signalling game? **Trends in Microbiology**, 10 (12): 556-563.

Rendulic, S., Jagtap, P., Rosinus, A., *et al.* (2004) A predator unmasked: life cycle of *Bdellovibrio bacteriovorus* from a genomic perspective. **Science**, 303 (5658): 689-692.

Römling, U. and Amikam, D. (2006) Cyclic di-GMP as a second messenger. **Current Opinion in Microbiology**, 9 (2): 218-228.

Römling, U., Gomelsky, M. and Galperin, M.Y. (2005) C-di-GMP: the dawning of a novel bacterial signaling system. **Molecular Microbiology**, 57 (3): 629-639.

Sacchi, L., Bigliardi, E., Corona, S., *et al.* (2004) A symbiont of the tick *Ixodes ricinus* invades and consumes mitochondria in a mode similar to that of the parasitic bacterium *Bdellovibrio bacteriovorus*. **Tissue and Cell**, 36 (1): 43-53.

- Schauder, C.M., Wu, X., Saheki, Y., *et al.* (2014) Structure of a lipid-bound extended synaptotagmin indicates a role in lipid transfer. **Nature**, 510 (7506): 552-555.
- Schirmer, T. and Jenal, U. (2009) Structural and mechanistic determinants of C-di-GMP signalling. **Nature Reviews Microbiology**, 7 (10): 724-735.
- Selkig, J., Mosbahi, K., Webb, C.T., *et al.* (2012) Discovery of an archetypal protein transport system in bacterial outer membranes. **Nature structural & molecular biology**, 19 (5): 506-510.
- Sockett, R.E. and Lambert, C. (2004) *Bdellovibrio* as therapeutic agents: a predatory renaissance? **Nature Reviews Microbiology**, 2 (8): 669-675.
- Sockett, R.E. (2009) Predatory lifestyle of *Bdellovibrio bacteriovorus*. **Annual Review of Microbiology**, 63: 523-539.
- Song, G., Koksal, A.C., Lu, C., *et al.* (2012) Shape change in the receptor for gliding motility in *Plasmodium* sporozoites. **Proceedings of the National Academy of Sciences of the United States of America**, 109 (52): 21420-21425.
- Springer, T.A. (2006) Complement and the multifaceted functions of VWA and integrin I domains. **Structure**, 14 (11): 1611-1616.
- Stolp, H. and Starr, M. (1963) *Bdellovibrio bacteriovorus* gen. et sp. n., a predatory, ectoparasitic, and bacteriolytic microorganism. **Antonie van Leeuwenhoek**, 29 (1): 217-248.

Van Den Ent, F. and Löwe, J. (2006) RF cloning: a restriction-free method for inserting target genes into plasmids. **Journal of Biochemical and Biophysical Methods**, 67 (1): 67-74.

Varon, M. and Shil, M. (1968) Interaction of *Bdellovibrio bacteriovorus* and host bacteria. I. Kinetic studies of attachment and invasion of *Escherichia coli* B by *Bdellovibrio bacteriovorus*. **Journal of Bacteriology**, 95 (3): 744-753.

Vagenende, V., Yap, M.G. and Trout, B.L. (2009) Mechanisms of protein stabilization and prevention of protein aggregation by glycerol. **Biochemistry**, 48 (46): 11084-11096.

Vincentelli R, Canaan S, Campanacci V, *et al.* (2004) High-throughput automated refolding screening of inclusion bodies. **Protein Science: A Publication of the Protein Society**, 13 (10): 2782-2792.

Whittaker, C.A. and Hynes, R.O. (2002) Distribution and evolution of von Willebrand/integrin A domains: widely dispersed domains with roles in cell adhesion and elsewhere. **Molecular Biology of the Cell**, 13 (10): 3369-3387.

Xu, L., Wu, D., Liu, L., *et al.* (2014) Characterization of mycobacterial UDP-N-acetylglucosamine enolpyruvate transferase (MurA). **Research in Microbiology**, 165 (13): 91-101.

Yan, X., Hu, S., Guan, Y., *et al.* (2012) Coexpression of chaperonin GroEL/GroES markedly enhanced soluble and functional expression of recombinant human

interferon-gamma in *Escherichia coli*. **Applied Microbiology and Biotechnology**,
93 (3):1065-1074